Diese Arbeit wurde vorgelegt am
Lehr- und Forschungsgebiet Theorie der hybriden Systeme

Optimierte Speicherstrategie für hybride konzentrierte Solar - Photovoltaik Kraftwerken

Optimal Storage Strategy for Hybrid Concentrated Solar Power - Photovoltaic Plants

Masterarbeit
Software Systems Engineering

Juli 2019

Vorgelegt von Presented by	Stella Coumbassa Rütscher Str. 165 52072 Aachen Matrikelnummer: 373594 stella.coumbassa@rwth-aachen.de
Erstprüfer First examiner	Prof. Dr. rer. nat. Erika Ábrahám Lehr- und Forschungsgebiet: Theorie der hybriden Systeme RWTH Aachen University
Zweitprüfer Second examiner	Prof. Dr. Christina Büsing Lehrstuhl II für Mathematik RWTH Aachen University
Externer Betreuer External supervisor	Dr. rer. nat. Pascal Richter Steinbuch Centre for Computing Karlsruhe Institute of Technology

Eigenständigkeitserklärung

Hiermit versichere ich, dass ich diese Masterarbeit selbständig verfasst und keine anderen als die angegebenen Quellen und Hilfsmittel benutzt habe. Die Stellen meiner Arbeit, die dem Wortlaut oder dem Sinn nach anderen Werken entnommen sind, habe ich in jedem Fall unter Angabe der Quelle als Entlehnung kenntlich gemacht. Dasselbe gilt sinngemäß für Tabellen und Abbildungen. Diese Arbeit hat in dieser oder einer ähnlichen Form noch nicht im Rahmen einer anderen Prüfung vorgelegen.

Aachen, im Juli 2019

Stella Coumbassa

I would first like to thank my thesis advisor Dr. Pascal Richter for all the support and guidance during the creation of this thesis. I deeply appreciate all the encouragement, revision of my work and patience for answering my various questions.
Furthermore, I would like to thank Dr. Torsten Trimborn for his advice and suggestions that were truly helpful in the creation of this work, as well as the company TSK Flagsol and Yibekal Gedle for assistance in the test case part of this thesis.
Lastly, I wish to thank my friends and family for their constant support, friendship and love throughout these years. Without you this work would not be possible. You made this journey truly memorable and worthwhile. Thank you.

Contents

1 Introduction **1**
- 1.1 State of the art . . . 1
  - 1.1.1 Modeling storage system . . . 1
  - 1.1.2 Storage strategies . . . 2
  - 1.1.3 Hybrid CSP-PV plant . . . 3
- 1.2 Outline . . . 4

2 Solar Thermal Power Plants **5**
- 2.1 CSP plant model . . . 6
- 2.2 Solar block . . . 7
- 2.3 Power block . . . 8
- 2.4 Storage block . . . 11
- 2.5 Economic model . . . 15
  - 2.5.1 Economic evaluation . . . 16

3 Storage strategy **17**
- 3.1 Buffer strategy . . . 17
- 3.2 Model predictive control . . . 20
  - 3.2.1 Model predictive control using Pontryagin's maximum principle 20
  - 3.2.2 Model predictive control using Mixed-Integer Linear Programming 27

4 Hybrid CSP-PV plant **29**
- 4.1 CSP-PV plant model . . . 30
- 4.2 Photovoltaic model . . . 32
- 4.3 Economic model . . . 36

5 Hybrid storage strategy **38**
- 5.1 Buffer strategy . . . 38
- 5.2 Model predictive control using Pontryagin's maximum principle . . . 40
- 5.3 Model Predictive Control using Mixed-Integer Linear Programming . . 43

6 Realistic test case of a hybrid CSP-PV plant **44**
- 6.1 Hybrid CSP-PV power plant . . . 44
- 6.2 Plant optimization . . . 49
  - 6.2.1 PV collector parameters . . . 49
  - 6.2.2 Storage strategies for CSP plant . . . 53
  - 6.2.3 Storage strategies for hybrid CSP-PV plant . . . 61
  - 6.2.4 Comparison of a CSP and hybrid CSP-PV plant . . . 68
  - 6.2.5 Hybrid CSP-PV size optimization . . . 68

7 Conclusion **74**
- 7.1 Outlook . . . 75

References **77**

1 Introduction

Extensive usage of conventional energy technologies in a form of fossil fuels, a non-renewable and finite energy source, has been known to produce negative effects on the environment, resulting in a rapid climate change. With the rise of population on Earth, energy consumption has rapidly increased, therefore causing the decline in the amount of available resources. To confront and possibly reverse this negative environmental impact there has been a rapid growth in interest in use of renewable energies.

The sun is one of the most sustainable and abundant renewable energy sources, capable of satisfying the global energy demand. Solar energy thus represents one of the greatest opportunities to maximize energy production in a sustainable way [1].

In this work we are regarding two different ways of producing electrical power from solar energy. Firstly, we consider concentrating solar power (CSP) plants, a technology that uses the solar irradiance to produce electricity, with the possibility of integrating a cost effective thermal energy storage (TES) system [2].

As solar irradiance is available only with the existence of sun, the storage system enables us to use solar energy even when the external conditions are not optimal (i.e. cloudy weather or at night). Hence, a CSP plant becomes a more reliable source of energy that also provides us with the possibility to shift the power production from times when the demand is low to periods of higher demand. The periods of higher demand are usually characterized by higher electricity prices, therefore a storage system is what makes a CSP plant more profitable [3].

Beside the concentrating solar power plants, photovoltaic (PV) plants represent another popular way of utilizing renewable energy. To take advantage of both types of plants (CSP and PV), a CSP-PV hybrid plant can be used. The electric power is produced by both components of the plant, while the storage system of the CSP plant proves useful for storing the power for later production.

1.1 State of the art

In this subsection we will shortly give a brief overview of the current state of research on the storage modeling and storage strategies, followed by the hybrid power plants and plant optimization.

1.1.1 Modeling storage system

Currently, there exist various ways of modeling a storage system. In the context of concentrated solar power plants Kuravi et al. [4] published a review of thermal energy storage system design methodologies and the factors that need to be considered when designing concentrating solar power plants with storage. In their work they focus both on the storage system design and its integration into the power plant. Furthermore, they compared the two most common storage systems, the two-tank and thermocline systems. The presented analysis uses oil as a heat transfer fluid. In their model they also consider the storage effiency and account for heat losses.

Cirocco et al. [5] present a simple CSP system model with storage constraints optimizing the plant control strategy to maximize the revenue. They model the system by considering the power flows in the system and also introduce a simple way to calculate the revenue, which is used in this work.

Powell and Edgar [6] described a thermodynamic model of the power plant with a two-tank storage system. For modeling the storage they used dynamic mass and energy balances, while taking into account the heat losses to the environment.

This thesis regards the storage system both from energetic and economic perspective. Works of Heiming [7], Morin [8], Flueckiger et al. [9] and Nithyanandam and Pitchumani [10] present economic models for CSP plants and were therefore used for designing a cost model of a CSP plant.

1.1.2 Storage strategies

There have been different approaches to the constructing storage strategies. Dynamic programming and mixed-integer programming have been some of the prevalent methods used for designing an optimal strategy. The focus of the strategies is usually on maximization of plant revenue or minimization of plant costs.

Power plant operation strategy has particularly been the focus in works of Cirocco et al. [11, 5]. While the former work considers the storage system with an infinite capacity and only three distinct control modes of operation, the latter presents an expanded analysis and more realistic storage case with additional constraints, including the limited storage capacity and four modes of operation. Cirocco et al. use Pontraygin's maximum principle to determine the optimal strategy for maximising revenue. This method will also be used as one of the strategy optimization methods in this work.

Guédez et al. [12] consider the integration of thermal energy storage system from two perspectives that take into account the market role of concentrating solar power plants. Namely, they differentiate between the continuous power production where the goal is to produce electricity during all 24 hours of the day and the peaking power production where the goal is to shift power production to times when it is needed the most (i.e. usually when the market prices of electricity are higher). Therefore, Guédez et al. present an instant-dispatch and peaking operation strategy. Similarly to the works of Cirocco et al. they differentiate between four different control modes. The difference is, however, that they do not consider directly using collected power from the sun for generation and also take into account plant being offline (i.e., not generating any power) at certain times. If there is any input power from the solar field it is directly stored to the storage or in case of excess power from the solar field or peaking prices they use the energy from the storage for power generation. The energy from the solar field thus always passes through the storage.

Usaola [13] also focus on maximizing the plant revenue, while taking into account daily electricity prices. They model the strategy as a mixed linear integer problem and demonstrate the one-day and two-day strategy optimization.

Casella et al. [14] focus on optimal control of the plant, while optimizing each month

of the operation. Casella et al. demonstrate the influence a storage size can have on the overall performance, as it determines the quantity of production that can be deferred [14].

Wittmann et al. [15] present the optimization of a price-driven operation strategy using dynamic programming, while taking into account the physical (e.g. storage capacity) and technical (e.g maximum overload situations) constraints, as well as solar forecasts. The strategy is mostly determined only by the direct solar irradiation forecast, while price fluctuations in the market are not taken into account.

Camacho et al. [16] and Camacho and Gallego [17] introduce the optimal scheduling for energy production using model predictive control. However, they do not consider tariffs for energy production in their work, and focus on the optimization for determining the amount of energy that needs to be released from the solar block.

On the other hand Vasallo and Bravo [18] introduce a model predictive control with mixed-integer programming for optimal generation scheduling in CSP plants, and consider the market in their model. Thus, their model was used as a reference for the model predictive control model introduced in this thesis.

1.1.3 Hybrid CSP-PV plant

With regards to the hybrid CSP-PV plant, the research normally focuses on the usage of batteries for storing the power produced by the photovoltaic (PV) component of the plant. On the other hand, this work considers a cheaper alternative to the battery, namely the shared usage of the CSP thermal storage by both CSP and PV plants. To the knowledge of the author this way of storing PV power in the hybrid plants has not yet been studied.

Dominio [19] expresses the problem of battery usage in hybrid CSP-PV plants. A CSP plant is often located in the environment that is not optimal for usage of batteries associated with PV plants [19]. This represents yet another encouragement to use the thermal storage.

Zhai et al. [20] optimize the hybrid CSP-PV plant design by using the genetic algorithm. The plant design is optimized with respect to the PV-capacity, PV battery capacity and CSP thermal storage capacity, while taking into account a fixed CSP capacity and plant costs. On the contrary, in this work the optimization of the design is done with regards to the CSP capacity, thermal storage capacity and PV capacity. Furthermore, Casella et al. [14] presented optimum plant configurations for both PV and CSP plants. In their work it was demonstrated that with a similar capacity of both plants, the combined CSP-PV systems can become an attractive investment. The PVs however, have the drawback of not allowing the integration of any cost-effective energy storage system, making the conventional battery systems for large PV plants rather unprofitable [14].

1.2 Outline

This thesis focuses on integration of the storage system in a solar thermal power plant, as well as combining the CSP and PV plants into a hybrid CSP-PV plant to produce electricity. To demonstrate the power production, it considers various storage strategies both from energetic and economic perspectives.

We start off this work by modeling a solar thermal power plant and demonstrating how a plant revenue is calculated in Section 2. Section 3 describes how to operate a plant with a storage system by using different storage strategies.

In Section 4 we extend the existing CSP plant by connecting it with a PV plant into a hybrid CSP-PV plant. The PV plant model is thus briefly introduced, along with a simplified hybrid CSP-PV plant model. Section 5 focuses on developing the strategies for the hybrid plant. The strategies presented in Section 3 are extended to correspond to the new extended plant.

Finally, in Section 6 we demonstrate the operation of the plant and its optimization based on the realistic data provided by the company TSK Flagsol[1]. Furthermore, we compare the usage of CSP plant to hybrid CSP-PV plant and consider the optimal design of the hybrid plant components (e.g. CSP solar field, PV output power and storage size).

[1]TSK Flagsol, Anna-Schneider-Steig 10, 50678 Köln, Germany, `http://www.flagsol.com`

2 Solar Thermal Power Plants

A typical solar thermal power plant can be divided into three main parts: solar block, power block and storage block.

The overview of two typical power plants and the three blocks they consist of is given in Figure 1.

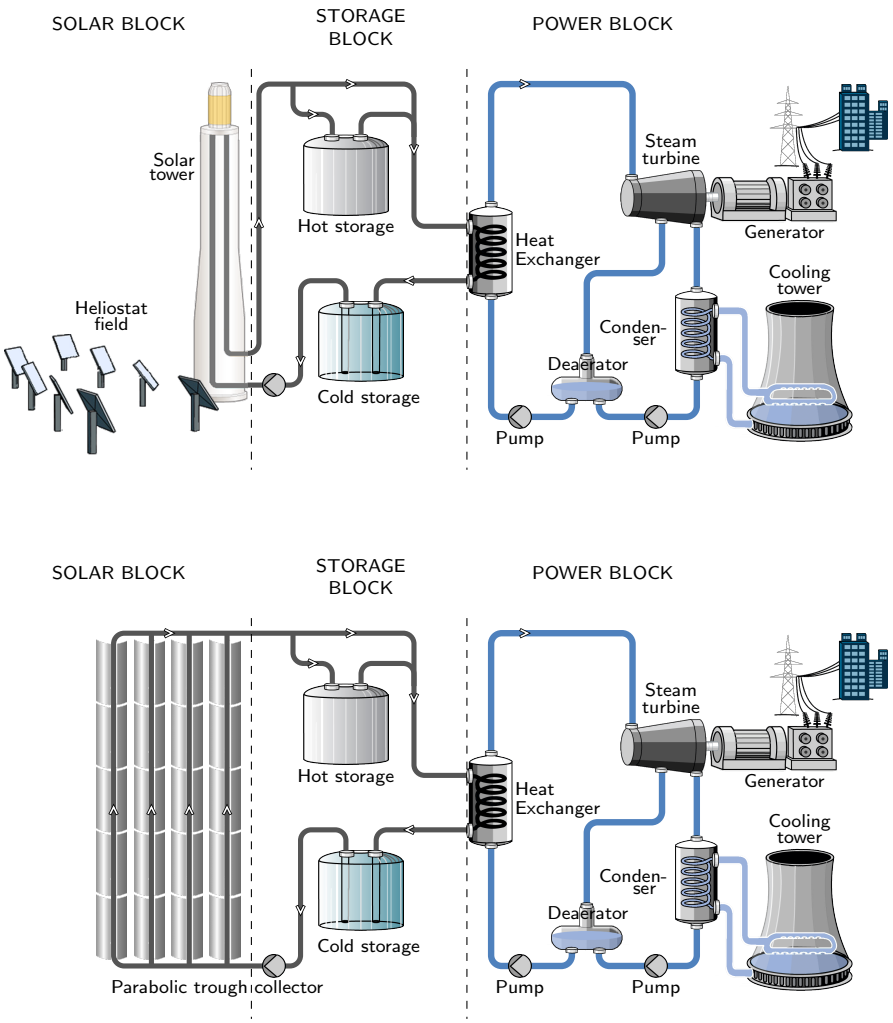

Figure 1: Overview of two concentrated solar power plants with thermal energy storage: solar tower power plant (upper) and parabolic trough plant (lower). Plants are divided into three main parts: solar block, storage block and power block. The main difference between the plants is in the solar block receiver technology. Solar block in solar tower power plant consists of a heliostat field with solar tower, while solar block in a parabolic trough plant contains parabolic trough as a receiver. The power block consists of the heat exchanger, steam turbine, generator and a cooling system. The storage block contains two storage tanks for storing thermal power. Furthermore, a direct line bypasses the storage to connect the solar block directly to the power block. Arrows indicate heat transfer fluid flows through the system.

The solar block is used for concentrating the rays of sunlight with a central receiver system and converting the solar irradiance from the rays into thermal power. Collected thermal power is then transferred via heat transfer fluid to the storage or directly to the power block. The power block consists of a steam turbine and a generator that converts thermal power into electricity [7].

The storage is limited in the amount of energy it can store, while the power block is limited in the amount of power it can process. Thus, in the event where solar block produces excessive amount of energy, we discard this energy from the system by defocusing the receiver.

Accordingly, we describe each of the blocks and connect them into a model described in Section 2.1, see also Figure 2.

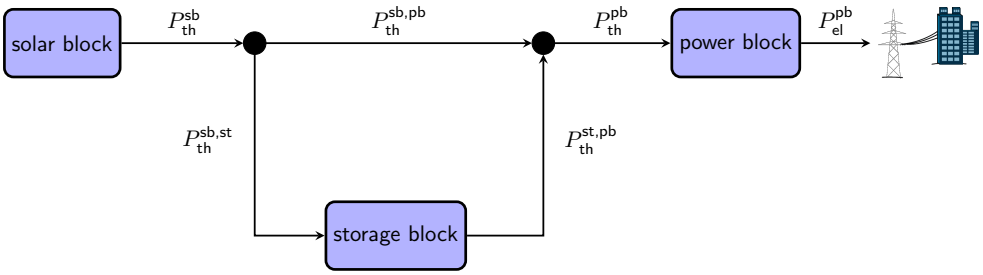

Figure 2: Overview of a CSP plant model with three blocks: solar block, power block and storage block. Solar block converts the solar irradiance to thermal power $P_{\text{th}}^{\text{sb}}$, which is sent directly to the power block via $P_{\text{th}}^{\text{sb,pb}}$ or stored in storage, $P_{\text{th}}^{\text{sb,st}}$. Stored energy can be drawn from storage and sent to the power block, $P_{\text{th}}^{\text{st,pb}}$. The power block converts the received thermal power from solar block and storage block, $P_{\text{th}}^{\text{pb}}$, to electricity $P_{\text{el}}^{\text{pb}}$,which is sent to the grid.

2.1 CSP plant model

We connect the three blocks in a CSP plant model by describing the thermal power transferred through the system, see Figure 3. The given model is based on the simplified CSP model with limited storage originally presented in Cirocco et al. [5].

The thermal power first appears as the output from the solar block $P_{\text{th}}^{\text{sb}}$, where it either goes directly to the power block as $P_{\text{th}}^{\text{sb,pb}}$ or it is stored in the storage via $P_{\text{th}}^{\text{sb,st}}$. Any additional energy that cannot be processed by the system is discarded by reducing the received thermal power in the receiver via defocusing of mirrors. This is described by the modeling parameter $P_{\text{th}}^{\text{excess}}$.

The relation between the described power flows is given by

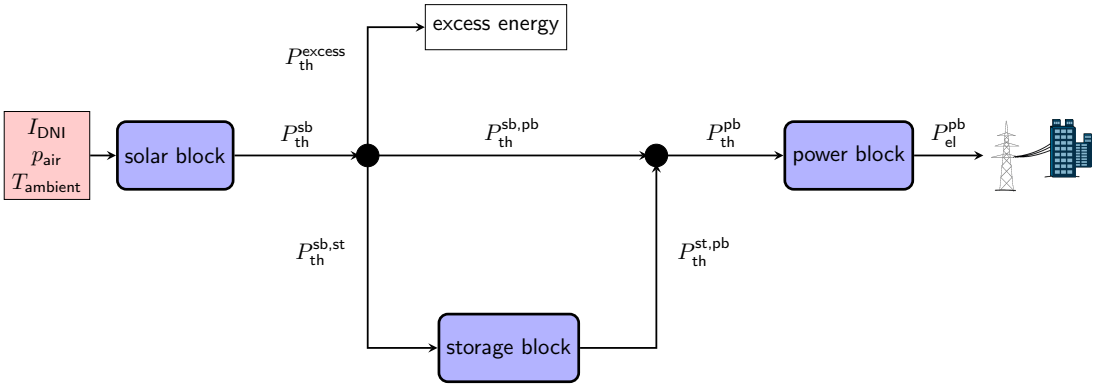

Figure 3: Simplified CSP plant model, containing the three main blocks. The entry point in the system is the input data in the solar block, while the exit point is the electrical power that goes to the grid. The blocks are connected by the power flows between them. The excess energy branch represents the energy that is discarded when it cannot be stored or used for power generation.

$$P_{\text{th}}^{\text{sb}} = P_{\text{th}}^{\text{sb,pb}} + P_{\text{th}}^{\text{sb,st}} + P_{\text{th}}^{\text{excess}}. \tag{1}$$

The power block can receive the power for generation $P_{\text{th}}^{\text{pb}}$ from the solar block and storage,

$$P_{\text{th}}^{\text{pb}} = P_{\text{th}}^{\text{sb,pb}} + P_{\text{th}}^{\text{st,pb}}. \tag{2}$$

2.2 Solar block

The solar block represents the first contact point of the power plant system. It retrieves the solar irradiance by focusing sun rays on the receiver. The receiver is either a line-focusing or a point-focusing system. In line-focusing systems we focus the rays on a single line and use a single tracking axis [7]. A commonly used line-focusing system is the parabolic trough (Figure 4a), where the irradiation is focused on the pipe that runs down the trough.

In point-focusing system we direct the sun rays to a point. A prevalent implementation of this approach is the solar tower with a heliostat field (Figure 4b). The heliostat field consists of mirrors that focus sun rays on the tower.

Once the sun rays are focused on the receiver, the irradiance is converted into thermal power by heating up the heat transfer fluid (HTF) that arrives to the receiver from the cold storage tank. For the HTF we only consider the molten salt, commonly used in CSP plants.

The heat transfer fluid goes from the receiver either directly to the power block via a heat exchanger or to the storage system. The flow of heat transfer fluid for solar

(a) Parabolic trough (b) Solar tower

Figure 4: Most common solar collector systems representing two different ray focusing approaches: (a) Line-focusing in parabolic trough receiver. (b) Point-focusing concentrating system implemented as a solar tower system with a heliostat field.

tower plants and parabolic trough is depicted in Figure 1.

We are regarding the solar block as a black box, as the detailed process of conversion from solar irradiance to thermal power is beyond the scope of this work. This means we only focus on its input and output parameters, which may be given by any tool. Specifically, for calculation of thermal output power in this work, the STRAL tool developed by DLR was used [21].

The input of our model includes solar irradiance, ambient temperature and air pressure. The output is the thermal power $P_{\text{th}}^{\text{sb}} \geq 0$, obtained by heating up the molten salt and used by the rest of the system, see Figure 5.

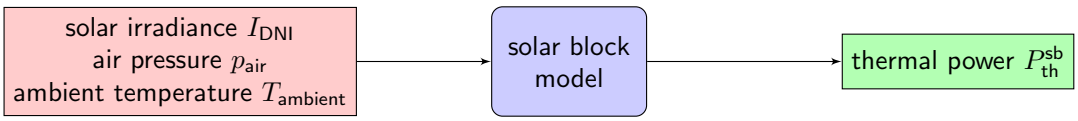

Figure 5: Solar block model with solar irradiance, air pressure and ambient temperature as input, and thermal power as output data. Solar irradiance is converted to thermal power by heating up the molten salt. The obtained thermal power further depends on the air pressure and ambient temperature at a given point in time.

All input parameters that illustrate weather conditions at a certain point in time are presented in Table 1. The solar block output in the form of thermal energy is presented in Table 2.

2.3 Power block

The power block is used for generating electricity from thermal power and corresponds to the power block of a conventional thermal power plant [7]. It consists of the heat exchanger (i.e. steam generator), steam turbine, generator and the cooling system, see Figure 1.

Symbol	Parameter	Unit
I_{DNI}	direct solar irradiance	W/m^2
p_{air}	air pressure	Pa
T_{ambient}	ambient temperature	°C

Table 1: Solar block input parameters: solar irradiance (for heating up the molten salt), air pressure and ambient temperature.

Symbol	Parameter	Unit
$P_{\text{th}}^{\text{sb}}$	thermal power	MW_{th}

Table 2: Solar block output data: thermal power attained by heating up the molten salt

Thermal power arrives as a heated molten salt to the power block either directly from the solar block or from the thermal storage. The salt enters the heat exchanger where it heats up the water from the cooling system. The water converts into steam, which is then used to run the steam turbine and generator to produce electricity. The salt is cooled down and directed to the cold tank.

Similarly to the solar block, we regard the entire power block as a black box, see Figure 6. Thus, instead of modeling each of its components separately, we model the entire block with a simple lookup table shown in Table 3. The data for this power block model was provided by TSK Flagsol [7].

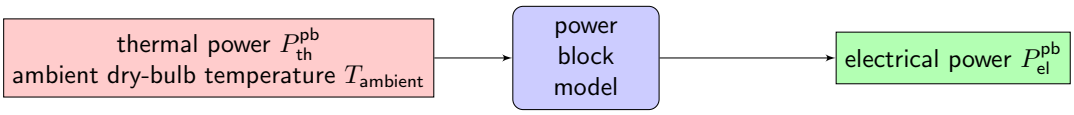

Figure 6: Power block model with input and output data. Thermal power is received from the solar block and storage, converted to electrical power and released to the grid. The amount of power received in the power block is limited by its turbine size $P_{\text{th}}^{\text{pb_max}}$.

At a certain point in time we consider the thermal power $P_{\text{th}}^{\text{pb}}$ that enters the power block, as well as the ambient temperature T_{ambient}. The turbine in the power block can receive a limited amount of power $P_{\text{th}}^{\text{pb_max}}$, defined by its size (3). The fraction of this maximum power the turbine receives at a specific moment, defines its current load (4). Thus, if received power is equal to maximal power $P_{\text{th}}^{\text{pb_max}}$, we say the turbine is operating at its full or 100% load.

$$P_{\text{th}}^{\text{pb_min}} \leq P_{\text{th}}^{\text{pb}}(t) \leq P_{\text{th}}^{\text{pb_max}} \tag{3}$$

$$\ell(t) = \frac{P_{\text{th}}^{\text{pb}}(t)}{P_{\text{th}}^{\text{pb_max}}} \tag{4}$$

Symbol	Parameter	Unit
$P_{\text{th}}^{\text{pb}}$	thermal power	MW_{th}
T_{ambient}	ambient temperature	°C

Table 3: Power block input data: thermal power received from the solar block and storage, and ambient temperature.

Symbol	Parameter	Unit
$P_{\text{el}}^{\text{pb}}$	electrical power	MW_{el}

Table 4: Power block output: electrical power released to the grid. This power is obtained via efficiency of the power block and received thermal power.

Power block efficiency The power block efficiency η_{pb} determines the electric power produced by the power plant,

$$P_{\text{el}}^{\text{pb}}(t) = \eta_{\text{pb}}\left(T_{\text{ambient}}, \ell\right) \cdot P_{\text{th}}^{\text{pb}}(t) \tag{5}$$

It depends on the turbine load and the ambient temperature, as illustrated in Figure 7 presented in Heiming [7].

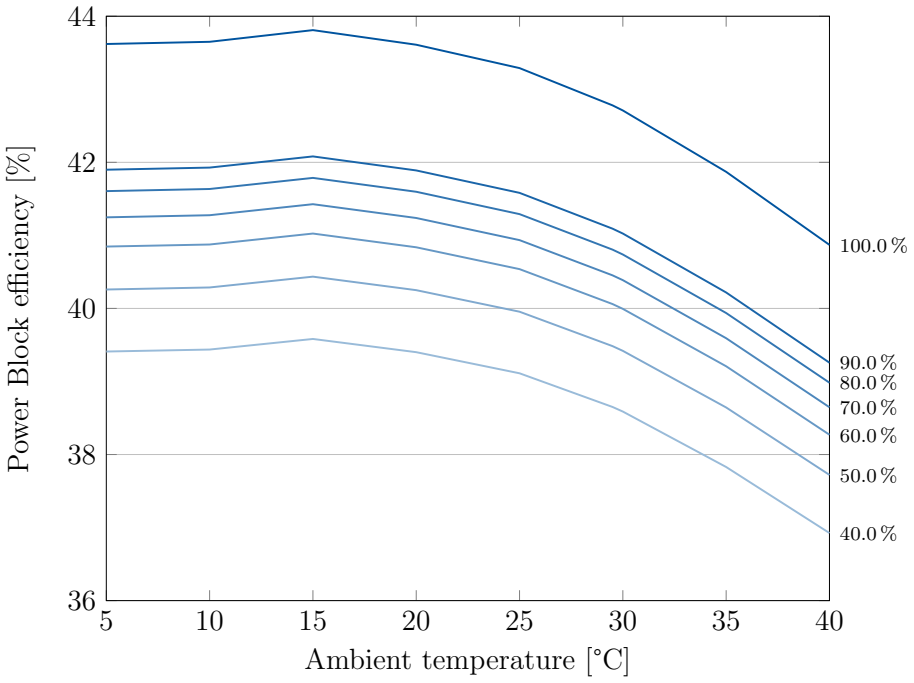

Figure 7: Characteristic Diagram of a $100\,\text{MW}_{\text{th}}$ power conversion unit. The lines represent the temperature-dependent efficiencies for different loads. Source: Heiming [7]

For a specific temperature and load the efficiency is approximated as

$$\begin{aligned}\eta_{\text{pb}}\left(T_{\text{ambient}}, \ell\right) = a_{3,0} \cdot T_{\text{ambient}}^3 + a_{0,3} \cdot \ell^3 \\ + a_{2,1} \cdot T_{\text{ambient}}^2 \cdot \ell + a_{1,2} \cdot T_{\text{ambient}} \cdot \ell^2 \\ + a_{0,2} \cdot \ell^2 + a_{2,0} \cdot T_{\text{ambient}}^2 + a_{1,1} \cdot T_{\text{ambient}} \cdot \ell \\ + a_{1,0} \cdot T_{\text{ambient}} + a_{0,1} \cdot \ell + a_{0,0}\end{aligned} \tag{6}$$

with coefficient values expressed in Table 5. The approximation was implemented using a least-squares method in MATLAB and is depicted in Figure 8. The coefficients are described as $a_{\text{x,y}}$, where x describes the order of temperature T_{ambient} and y describes the order of load in the approximation.

Coefficient	Constant	Cubic
$a_{0,0}$	39.8262	31.56
$a_{1,0}$	0	0.05034
$a_{0,1}$	0	0.338
$a_{1,1}$	0	0.0001051
$a_{2,0}$	0	-0.001244
$a_{0,2}$	0	-0.004598
$a_{2,1}$	0	$-6.617 \cdot 10^{-6}$
$a_{1,2}$	0	$5.802 \cdot 10^{-7}$
$a_{3,0}$	0	$-3.168 \cdot 10^{-5}$
$a_{0,3}$	0	$2.368 \cdot 10^{-5}$

Table 5: Power block efficiency approximations. The coefficients are depicted for constant and cubic approximations. The coefficient index equals to the order of temperature or load in the curve.

To keep our models used in optimization linear, the constant (mean) efficiency was used, while the cubic approximation was applied to the expected output power.

2.4 Storage block

The storage block consists of a thermal energy storage (TES) system used for storing collected heat. While there exist different types of storage, within this thesis we focus on direct active storage systems.

Direct active storage systems are characterized by containing a liquid storage medium, and using the same medium as a heat transfer fluid. This eliminates the need for an additional heat exchanger between the solar block and storage, while reducing the heat losses caused by the heat exchange between different liquids [4]. The storage medium we consider is the HITEC molten salt.

Two commonly used direct active TES systems are:

- Two-tank storage: includes a hot and a cold storage tank. An example of a direct two tank storage system is shown in Figure 1 and will be used in the context of this work.

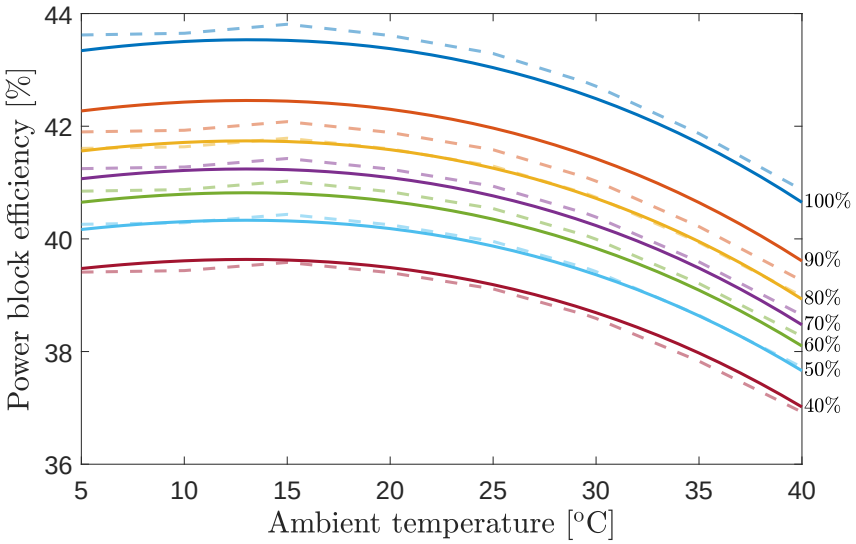

Figure 8: Power block load curve cubic approximation.

We store the energy in the hot tank by filling it with heated molten salt in a process known as charging. The salt is taken from the hot tank in the process of discharging, and used for power generation in the power block. When heated molten salt enters the heat exchanger (i.e., an entry point to the power block), it is cools down and goes to the cold tank. From there it is extracted for again collecting the thermal power in the solar block.

- Thermocline storage: a single tank system, where hot and cold salt are stored in the same tank. The fluids are separated as a result of a thermal gradient in the tank [4]. Usage of such a TES has the potential to reduce investment costs associated with tank construction materials [2].

In order to describe our storage model, we first define entry and exit points of the system.

As an entry point we consider the first point after the receiver where we use heated molten salt. With no heat exchanger before the storage, the entry point can be placed between the receiver and the hot storage tank. Examples of direct two-tank storage systems and their defined entry and exit points are illustrated in Figures 9 and 10.

Thermal power from solar block is an input to our storage model, while thermal power going to the power block represents the output, see Figure 11.

The cold tank is not regarded in this model, as it is not intended for storing the thermal energy used for power generation.

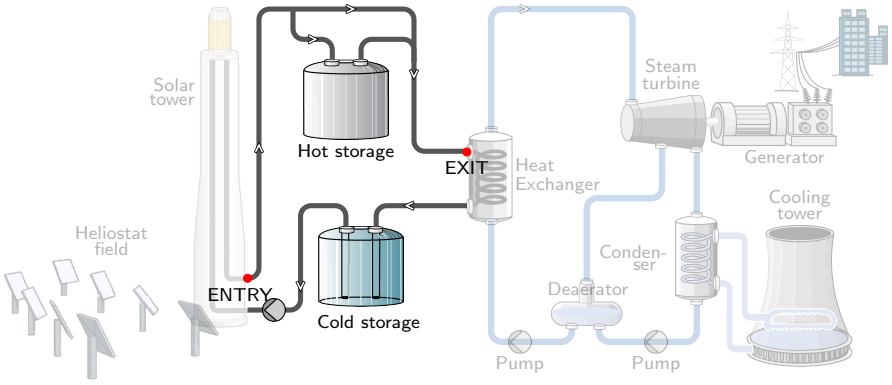

Figure 9: Solar tower plant storage system entry and exit points. The entry point is placed between the receiver and the hot storage tank. The exit point is placed on the heat exchanger where hot salt heats up the water from the power block.

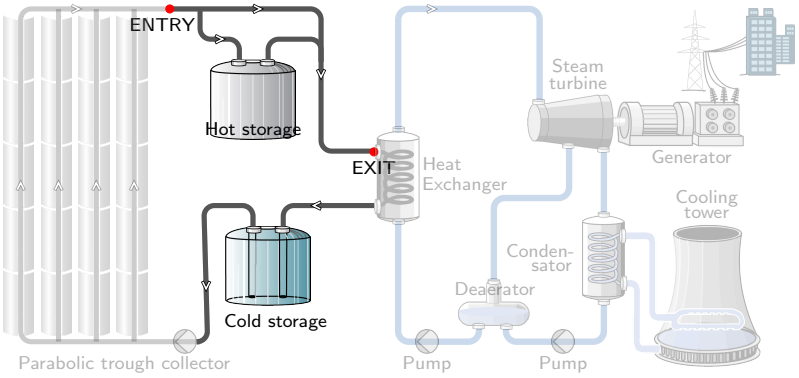

Figure 10: Parabolic trough plant storage entry and exit points defined at the end of the parabolic trough receiver and at the heat exchanger, respectively.

Stored energy We define the amount of currently stored thermal energy as $Q_{\text{th}}^{\text{st}}$. The stored energy increases by charging the storage with the incoming power from the solar block $P_{\text{th}}^{\text{sb,st}}$, during the time period delta Δt, which amounts to $P_{\text{th}}^{\text{sb,st}} \cdot \Delta t$ thermal energy increase. Similarly, the stored energy decreases by discharging, when, during the time period Δt, we send thermal power to the power block via $P_{\text{th}}^{\text{st,pb}}$ and thus decrease the total stored energy by $P_{\text{th}}^{\text{st,pb}} \cdot \Delta t$ (8). The time period Δt, can be described as

$$\Delta t = t_{\text{n}} - t_{\text{n-1}}, \tag{7}$$

where t_{n} and $t_{\text{n-1}}$ represent specific consecutive points in time.

We also consider the storage charging efficiency $\eta_{\text{st_in}}$ and discharging efficiency $\eta_{\text{st_out}}$ [13], describing the power losses in charging and discharging processes. The heat loss from the storage tank to the environment $P_{\text{th}}^{\text{loss}}$ is also considered [13]. The stored thermal energy is thus given by

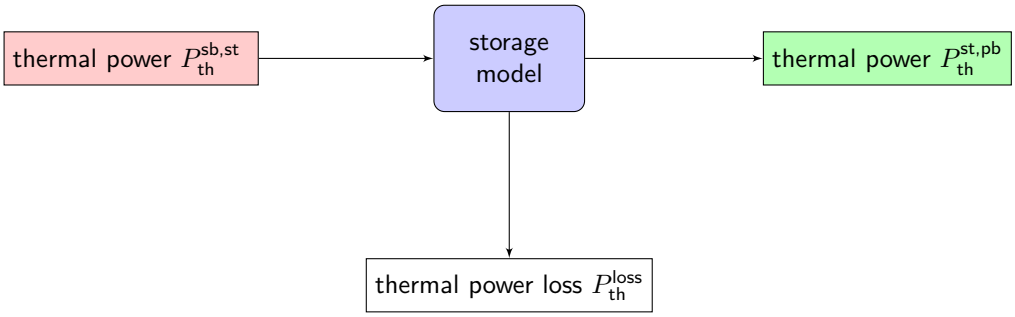

Figure 11: Storage block with input and output, in the form of thermal power from the solar block and thermal power to the power block, respectively. The heat loss from hot tank to the environment is also considered.

$$Q_{\text{th}}^{\text{st}}(t+\Delta t) = Q_{\text{th}}^{\text{st}}(t) + (\eta_{\text{st_in}} P_{\text{th}}^{\text{sb,st}}(t) - \eta_{\text{st_out}}^{-1} P_{\text{th}}^{\text{st,pb}}(t) - P_{\text{th}}^{\text{loss}}(t)) \cdot \Delta t, \tag{8}$$

with heat loss

$$P_{\text{th}}^{\text{loss}}(t) = Q_{\text{th}}^{\text{st}}(t) \cdot \xi_{\text{loss}}. \tag{9}$$

The heat loss depends on the amount of stored energy and the heat loss factor ξ_{loss} [%/h], which defines the percentage of stored heat lost per hour.

Storage capacity The storage system has a limited capacity for storing thermal energy, $Q_{\text{th}}^{\text{st_max}}$,

$$Q_{\text{th}}^{\text{st_min}} \leq Q_{\text{th}}^{\text{st}} \leq Q_{\text{th}}^{\text{st_max}}. \tag{10}$$

The capacity typically ranges between hundreds of kWh to several MWh [22].

Alternatively, storage size is defined in hours, where it presents the additional hours of full power electrical generation (in power block) [11]. Furthermore, for storage system we also consider the minimum amount of stored energy $Q_{\text{th}}^{\text{st_min}}$ required to prevent solidification of stored molten salts [13].

Maximum charging and discharging power We derive the maximum charging $P_{\text{th}}^{\text{max_in}}$ and discharging $P_{\text{th}}^{\text{max_out}}$ power within one time step as

$$P_{\text{th}}^{\text{st,max_in}}(t) = \eta_{\text{st_in}}^{-1} \cdot \left(\frac{Q_{\text{th}}^{\text{st_max}} - Q_{\text{th}}^{\text{st}}(t-1)}{\Delta t} + \eta_{\text{st_out}} P_{\text{th}}^{\text{st,pb}}(t) - P_{\text{th}}^{\text{loss}}(t) \right) \tag{11}$$

$$P_{\text{th}}^{\text{st,max_out}}(t) = \eta_{\text{st_out}} \cdot \left(\eta_{\text{st_in}} P_{\text{th}}^{\text{sb,st}}(t) - P_{\text{th}}^{\text{loss}}(t) + \frac{Q_{\text{th}}^{\text{st}}(t-1) - Q_{\text{th}}^{\text{st_min}}}{\Delta t} \right). \tag{12}$$

Furthermore, the maximal charging and discharging power is limited by the amount of power that can be transferred through the pipes and pumps in the system [6], but this limit will not be considered in this model.

2.5 Economic model

In our economic model we focus on the plant revenue. The revenue depends on the produced electrical power $P_{\text{el}}^{\text{pb}}$ and tariff for energy production π, see Figure 12. Additionally, we consider the remaining energy in the storage at the end of the observed time horizon. We describe our input data in Table 6 and output data in Table 7.

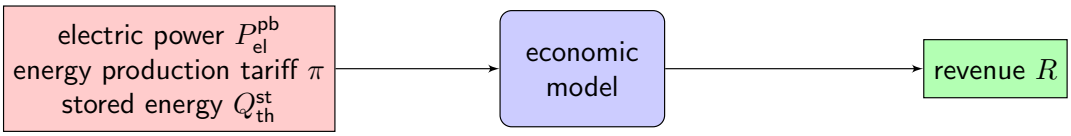

Figure 12: Economic model that focuses on plant revenue and takes electric power and energy tariff as an input, while also considering the remaining stored energy.

Symbol	Parameter	Unit
$P_{\text{el}}^{\text{pb}}$	electric power	MW_{el}
π	tariff for energy production	€/MW_{el}h

Table 6: Economic model input data

Symbol	Parameter	Unit
R	revenue	€

Table 7: Economic model output: plant revenue

We define the available electrical energy from electrical power P_{el} for each time step t as

$$E_{\text{el}}(t) = P_{\text{el}}^{\text{pb}}(t) \cdot \Delta t. \tag{13}$$

The tariff for energy production is time-dependent, and varies according to the time of the day, with a higher tariff normally occurring at night. In this work two values of tariff are considered.

With reference to Cirocco et al. [11], we describe the total revenue for the time period t_{end} as

$$\begin{aligned} R &= \sum_{t=t_0}^{t_{\text{end}}} \pi(t) E_{\text{el}}(t) + R_{\text{st}} \\ &= \sum_{t=t_0}^{t_{\text{end}}} \pi(t) \cdot P_{\text{el}}^{\text{pb}}(t) \cdot \Delta t + \pi_{\text{res}} \cdot Q_{\text{th}}^{\text{st}}(t_{\text{end}}) \end{aligned} \tag{14}$$

where π is the tariff for energy production, E_{el} is the produced electric energy and R_{st} represents the additional revenue from storage or the residual.

The amount of stored energy contributes to the future revenue of the plant. We define the revenue from storage R_{st} as

$$R_{\text{st}} = \pi_{\text{res}} \cdot Q_{\text{th}}^{\text{st}}(t_{\text{end}}), \tag{15}$$

with π_{res} as the residual tariff for energy production, and $Q_{\text{th}}^{\text{st}}(t_{\text{end}})$ as the storage state at the end of the observed time horizon. Furthermore, prospective storage heat losses for the remaining stored energy are not considered.

2.5.1 Economic evaluation

For economic evaluation of a plant several measures are considered.

Gain rate The gain rate takes into account the amount of revenue the plant had during its lifetime period (i.e. its gain) and its total costs for the said period. It is calculated as:

$$i_{\text{gain}} = \frac{R_{\text{lifetime}} - (C_{\text{invest}} + C_{\text{O\&M}})}{C_{\text{invest}} + C_{\text{O\&M}}}, \tag{16}$$

with R_{lifetime} as the revenue during for the plant lifetime, C_{invest} as the investment costs for the plant lifetime and $C_{\text{O\&M}}$ as the operation and maintenance costs.

Net present value The net present value represents the sum of all investments and values of all incomes and expenses over the project lifetime, which is the incomes and expenses of each year, while considering the interest rate [7]. It represents the total profit of a plant, taken from Augsburger, Heiming [23, 7]:

$$NPV = \frac{1}{f_{\text{annuity}}} \left(R_{\text{annual}} - \frac{C_{\text{O\&M}}}{N} \right) - \frac{C_{\text{invest}}}{N}, \tag{17}$$

with R_{annual} as the annual revenue, f_{annuity} as the annuity factor and N as the lifetime.

$$f_{\text{annuity}} = \frac{(1+i)^N \cdot i}{(i+1)^N - 1}, \tag{18}$$

with i as an interest rate.

3 Storage strategy

In this section different storage strategies are considered. A storage strategy is used to define how a storage system is integrated into the power plant to achieve its optimal performance with respect to the produced energy and revenue. We start by defining a simple buffer strategy.

3.1 Buffer strategy

The goal of the buffer strategy is to generate as much power as possible at each time interval. This means that all the available thermal power from the solar block and from the storage is sent to the power block in order to achieve a full load on the turbine,

$$P_{\text{th}}^{\text{pb}} = \max P_{\text{th}}^{\text{pb}}(t), \forall t, \tag{19}$$

while considering constraints defined in (3).

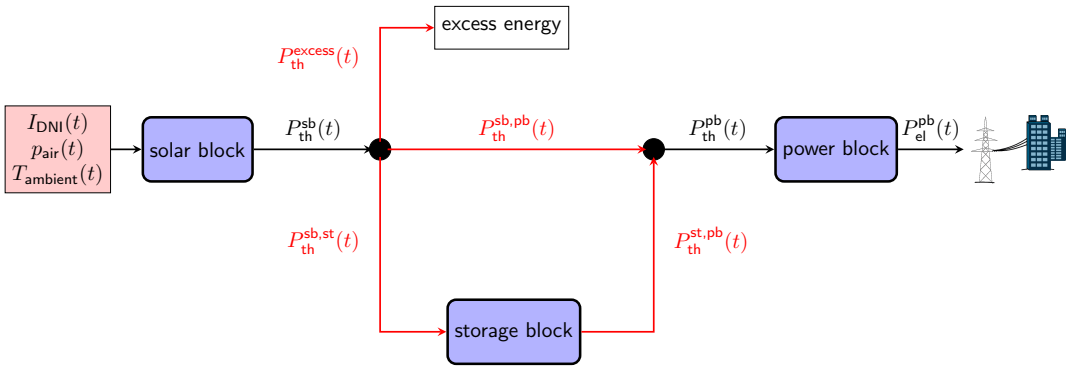

Figure 13: CSP plant model. In red: power flows whose values are determined by the buffer strategy. Solar block power $P_{\text{th}}^{\text{sb}}$ values are known in advance, while total power entering the power block $P_{\text{th}}^{\text{pb}}$ is calculated in relation to the remainder of the power flows, as described in (2).

We start the strategy by directing the maximum possible amount of solar block thermal power $P_{\text{th}}^{\text{sb}}$, to the power block,

$$P_{\text{th}}^{\text{sb,pb}} := \min\left(P_{\text{th}}^{\text{sb}}, P_{\text{th}}^{\text{pb_max}}\right), \tag{20}$$

while using the storage for storing or delivering thermal power, as needed. Bearing in mind that both power block and storage are limited in their capacity, any power that cannot be used or stored is discarded from the system ($P_{\text{th}}^{\text{excess}}$).

With reference to the storage strategy introduced in Cirocco et al. [5], we specify two modes of operation:

- *Generate mode*: The power from the solar block does not exceed the maximal power capacity on the turbine, $P_{\text{th}}^{\text{sb}} \leq P_{\text{th}}^{\text{pb_max}}$. There is no thermal power flowing to the storage ($P_{\text{th}}^{\text{sb,st}} := 0$) and no excess thermal power ($P_{\text{th}}^{\text{excess}} := 0$), as all the available power from the solar block is directed to the power block,

$$P_{\text{th}}^{\text{sb,pb}} := P_{\text{th}}^{\text{sb}}. \tag{21}$$

  Any additional power that can be processed by the turbine is drawn from the storage:

$$P_{\text{th}}^{\text{st,pb}} := \min\left(P_{\text{th}}^{\text{pb_max}} - P_{\text{th}}^{\text{sb,pb}},\ \ P_{\text{th}}^{\text{st,max_out}}\right). \tag{22}$$

- *Surplus mode*: The power from the solar block exceeds the maximal turbine capacity, $P_{\text{th}}^{\text{sb}} > P_{\text{th}}^{\text{pb_max}}$. We limit the power directed from the solar block to the power block capacity,

$$P_{\text{th}}^{\text{sb,pb}} := P_{\text{th}}^{\text{pb_max}}, \tag{23}$$

  store as much as possible in the storage system,

$$P_{\text{th}}^{\text{sb,st}} := \min\left(P_{\text{th}}^{\text{sb}} - P_{\text{th}}^{\text{sb,pb}},\ \ P_{\text{th}}^{\text{st,max_in}}\right), \tag{24}$$

  and discard the remaining power

$$P_{\text{th}}^{\text{excess}} := \max\left(0,\ \ P_{\text{th}}^{\text{sb}} - P_{\text{th}}^{\text{sb,pb}} - P_{\text{th}}^{\text{sb,st}}\right). \tag{25}$$

  No thermal power is drawn from the storage, $P_{\text{th}}^{\text{st,pb}} := 0$.

The strategy is depicted in Figure 14, where the input is the solar block thermal power $P_{\text{th}}^{\text{sb}}$ over a limited time horizon and the power limit on the power block $P_{\text{th}}^{\text{pb_max}}$. At each time step, based on the received thermal power in the solar block, one of the two modes (generate or surplus) is applied to the system. From the resulting power in the power block $P_{\text{th}}^{\text{pb}}$ the produced electric power P_{el} for the respective time step is calculated (13). Once the produced electric power for the observed time horizon has been obtained, the strategy is concluded by calculating the total revenue, as described in (14).

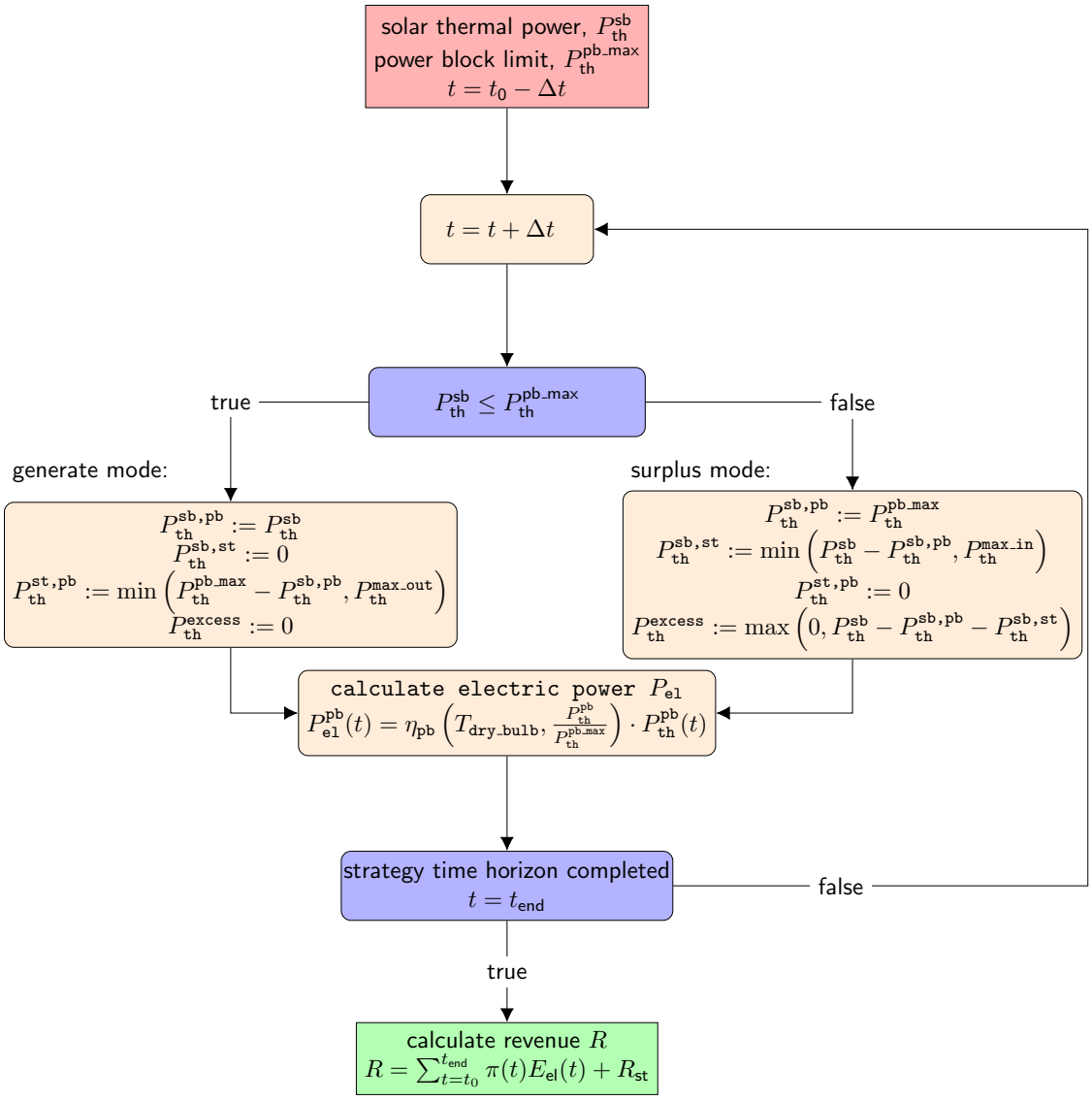

Figure 14: Buffer storage strategy with generate and surplus control modes. We send the maximal possible amount of solar block thermal power $P_{\text{th}}^{\text{sb}}$, to the power block. In generate mode we draw any additionally needed power for generation from the storage, while in surplus mode we store any left-over power from the solar block in the storage or discard it from the system. For each time step, we calculate electric power that exits the system and complete the strategy by calculating the total revenue for the time horizon.

3.2 Model predictive control

Model predictive control uses numerical optimization to define an optimal control sequence for a limited future time window, also known as the horizon, beginning from the current state [24]. By applying the receding horizon strategy, at every time instance we shift the horizon one time step toward the future [25], and apply only the first element of calculated optimal control to the system [17].

Specifically, in this work the optimal strategy is designed with the goal of optimizing the plant revenue, while taking into account the constraints of the plant model [25]. As optimization methods, we demonstrate the usage of Pontryagin's maximum principle and mixed integer programming (MIP) with a linear problem formulation.

3.2.1 Model predictive control using Pontryagin's maximum principle

The Pontryagin's maximum principle is applied to the system with reference to Cirocco et al. [5].

Pontryagin's maximum principle Pontryagin's maximum principle considers the optimal control problem with state constraints, expressed as:

$$J = \int_{t_0}^{t_{\text{end}}} g(\mathbf{x}(t), \mathbf{u}(t), t)dt + h(\mathbf{x}(t_{\text{end}}), t_{\text{end}}) \rightarrow \max, \tag{26}$$

$$\dot{\mathbf{x}}(t) = a(\mathbf{x}(t), \mathbf{u}(t), t), \quad \mathbf{x}(0) = \mathbf{x}_0, \tag{27}$$

$$c(\mathbf{x}(t), \mathbf{u}(t), t) \geq 0, \tag{28}$$

$$f(\mathbf{x}(t), t) \geq 0, \tag{29}$$

where $\mathbf{x}(t)$ represents the system state, while $\mathbf{u}(t)$ represents the control that influences the system [26][27]. The objective function to be optimized is represented in (26), while (27) describes the state behavior of the system. Furthermore, the constraints on the system controls and state are described in (28) and (29), respectively.

The goal of the Pontryagin's maximum principle is to find the admissible optimal control $\mathbf{u}^*(t)$, that will maximize the objective function (26) [26].

For this purpose, we first introduce the Hamiltonian as:

$$H(\mathbf{x}(t), \mathbf{u}(t), \boldsymbol{\lambda}(t), t) = g(\mathbf{x}(t), \mathbf{u}(t), t) + \boldsymbol{\lambda}^{\mathbf{T}}(t) \cdot a(\mathbf{x}(t), \mathbf{u}(t), t), \tag{30}$$

with $\boldsymbol{\lambda}(t)$ as the adjoint coefficient [26].

According to the Pontryagin's maximum principle, we find the optimal control $\mathbf{u}^*(t)$ through the set of conditions that should be satisfied as necessary, but not sufficient conditions [28]. The set of necessary conditions is:

$$\dot{\boldsymbol{\lambda}}^*(t) = -\frac{\partial H}{\partial \mathbf{x}}(\mathbf{x}^*(t), \mathbf{u}^*(t), \boldsymbol{\lambda}^*(t), t) \tag{31}$$

$$\boldsymbol{\lambda}(t_{\text{end}}) = h_{\text{x}}^*(t_{\text{end}}) \tag{32}$$

$$\dot{\mathbf{x}}^*(t) = \frac{\partial H}{\partial \boldsymbol{\lambda}}(\mathbf{x}^*(t), \mathbf{u}^*(t), \boldsymbol{\lambda}^*(t), t) \tag{33}$$

$$H(\mathbf{x}^*(t), \mathbf{u}^*(t), \boldsymbol{\lambda}^*(t), t) \geq H(\mathbf{x}^*(t), \mathbf{u}(t), \boldsymbol{\lambda}^*(t), t), \quad \text{for all admissible } \mathbf{u}(\mathrm{t}) \tag{34}$$

for all $t \in [t_0, t_{\mathrm{end}}]$ [26].

To accommodate the state constraint a new variable (additional state behavior) is defined [26]:

$$\dot{\mathrm{x}}_{\mathrm{n+1}}(t) = [f_1(\mathbf{x}(t), t)]^2 \, \mathcal{H}(-f_1) + [f_2(\mathbf{x}(t), t)]^2 \, \mathcal{H}(-f_2) + ... + [f_l(\mathbf{x}(t), t)]^2 \, \mathcal{H}(-f_l), \tag{35}$$

with $\mathcal{H}(-f_i)$ as a unit Heaviside step function:

$$\mathcal{H}(-f_i) = \begin{cases} 0, & \text{for} \quad f_i(\mathbf{x}(t) \geq 0 \\ 1, & \text{for} \quad f_i(\mathbf{x}(t) < 0, \end{cases} \tag{36}$$

for $i = 1, 2, ..., l$ [26]. An extra adjoint coefficient with new state behavior is added to the Hamiltonian, while the necessary optimality conditions are extended with:

$$\dot{\lambda}^*_{\mathrm{n+1}}(t) = -\frac{\partial H}{\partial \mathrm{x}_{\mathrm{n+1}}}(\mathbf{x}^*(t), \mathbf{u}^*(t), \boldsymbol{\lambda}^*(t), t) = 0 \tag{37}$$

$$\dot{\mathrm{x}}^*_{\mathrm{n+1}}(t) = \frac{\partial H}{\partial \lambda_{\mathrm{n+1}}}(\mathbf{x}^*(t), \mathbf{u}^*(t), \boldsymbol{\lambda}^*(t), t) = a_{\mathrm{n+1}}(\mathbf{x}^*(t), t). \tag{38}$$

Maximum principle for the CSP plant model For the purpose of this strategy, continuous formulations of the models described in the previous section are introduced.

The plant revenue described in (14) represents the objective function of this optimization problem. To directly account for the power flows in the objective function we express it as

$$\begin{aligned} R &= \int_{t_0}^{t_{\mathrm{end}}} \pi(t) \cdot \eta_{\mathrm{pb}} \cdot P_{\mathrm{th}}^{\mathrm{pb}}(t) \mathrm{d}t + R_{\mathrm{st}}(t_{\mathrm{end}}) \\ &= \int_{t_0}^{t_{\mathrm{end}}} \pi(t) \cdot \eta_{\mathrm{pb}} \cdot \left(P_{\mathrm{th}}^{\mathrm{sb}}(t) - P_{\mathrm{th}}^{\mathrm{sb,st}}(t) + P_{\mathrm{th}}^{\mathrm{st,\,pb}}(t) - P_{\mathrm{th}}^{\mathrm{excess}}(t) \right) \mathrm{d}t + \pi_{\mathrm{res}} \cdot Q_{\mathrm{th}}^{\mathrm{st}}(t_{\mathrm{end}}) \end{aligned} \tag{39}$$

This objective function corresponds to the objective function of the Pontryagin's maximum principle formulation defined in (26).

The strategy decisions on when to store and when to generate power are based on the current tariff $\pi(t)$ for energy production, as well as the currently available thermal power from the solar block $P_{\mathrm{th}}^{\mathrm{sb}}$ and storage $P_{\mathrm{th}}^{\mathrm{st,max_out}}$.

The stored energy is now defined as an ordinary differential equation,

$$\frac{\mathrm{d}Q}{\mathrm{d}t} = \eta_{\mathrm{st_in}} P_{\mathrm{th}}^{\mathrm{sb,st}}(t) - \eta_{\mathrm{st_out}}^{-1} P_{\mathrm{th}}^{\mathrm{st,pb}}(t) - \xi_{\mathrm{loss}} \cdot Q_{\mathrm{th}}^{\mathrm{st}}(t), \tag{40}$$

and corresponds to the state behavior equation introduced in (27).

The power flows $P_{\text{th}}^{\text{sb,st}}$ and $P_{\text{th}}^{\text{st,pb}}$ represent the controls of the system ($\mathbf{u}(t)$), while the currently stored thermal energy $Q_{\text{th}}^{\text{st}}$ describes its state ($\mathbf{x}(t)$). For Pontryagin's maximum principle we consider the following constraints on the power flows:

- All the power flows in the system are considered as non-negative
- The power flow to the power block is limited by the maximum amount of power the turbine can receive, $P_{\text{th}}^{\text{st,pb_max}}$, as described in (3)
- The relation between the power flows in the system is taken from (1) and with the specified constraints from above limits the power flows as follows:

$$\begin{aligned} &P_{\text{th}}^{\text{sb}} - P_{\text{th}}^{\text{sb,st}} + P_{\text{th}}^{\text{st, pb}} - P_{\text{th}}^{\text{excess}} \geq 0 \\ &P_{\text{th}}^{\text{pb_max}} - (P_{\text{th}}^{\text{sb}} - P_{\text{th}}^{\text{sb,st}} + P_{\text{th}}^{\text{st,pb}} - P_{\text{th}}^{\text{excess}}) \geq 0 \end{aligned} \tag{41}$$

Furthermore, the constraints on the storage as defined in (8) and (10) are considered.

According to the Pontryagin's principle, the control that maximizes the revenue, also maximizes the Hamiltonian [11].

Applied to this problem, the Hamiltonian is defined as

$$\begin{aligned} H(Q_{\text{th}}^{\text{st}}, P_{\text{th}}^{\text{sb,st}}, P_{\text{th}}^{\text{st,pb}}, P_{\text{th}}^{\text{excess}}, \lambda, t) &= \pi(t) \cdot \eta_{\text{pb}}\left(T_{\text{dry_bulb}}, \text{Load}\right) \cdot P_{\text{th}}^{\text{pb}}(t) \\ &+ \lambda_1(t) \cdot \left(\eta_{\text{st_in}} P_{\text{th}}^{\text{sb,st}}(t) - \eta_{\text{st_out}}^{-1} P_{\text{th}}^{\text{st,pb}}(t) - \xi_{\text{loss}} Q_{\text{th}}^{\text{st}}\right) \\ &+ \lambda_2(t)\{\left[Q_{\text{th}}^{\text{st_max}} - Q_{\text{th}}^{\text{st}}(t)\right]^2 \mathcal{H}(-Q_{\text{th}}^{\text{st_max}} + Q_{\text{th}}^{\text{st}}(t)) \\ &\quad + \left[Q_{\text{th}}^{\text{st}}(t) - Q_{\text{th}}^{\text{st_min}}\right]^2 \mathcal{H}(-Q_{\text{th}}^{\text{st}}(t) + Q_{\text{th}}^{\text{st_min}})\} \end{aligned} \tag{42}$$

From the Hamiltonian the necessary conditions for optimality are derived.

Necessary conditions for optimality The necessary conditions for optimality are:

$$\begin{aligned} \dot{\lambda}_1 = -\frac{\partial H}{\partial Q_{\text{th}}^{\text{st}}} &= \lambda_1(t)\xi_{\text{loss}} + 2\lambda_2(t)\left[Q_{\text{th}}^{\text{st_max}} - Q_{\text{th}}^{\text{st}}(t)\right]\mathcal{H}(-Q_{\text{th}}^{\text{st_max}} + Q_{\text{th}}^{\text{st}}(t)) \\ &\quad - 2\lambda_2(t)\left[Q_{\text{th}}^{\text{st}}(t) - Q_{\text{th}}^{\text{st_min}}\right]\mathcal{H}(-Q_{\text{th}}^{\text{st}}(t) + Q_{\text{th}}^{\text{st_min}}) \end{aligned} \tag{43}$$

$$\lambda_1(t_{\text{end}}) = R'_{\text{st}}(Q_{\text{th}}^{\text{st}}) = \pi_{\text{res}} \tag{44}$$

$$\frac{\partial H}{\partial P_{\text{th}}^{\text{sb,st}}} \stackrel{!}{=} 0 \tag{45}$$

$$\frac{\partial H}{\partial P_{\text{th}}^{\text{st,pb}}} \stackrel{!}{=} 0. \tag{46}$$

These conditions are however not necessarily sufficient. The constraints on the controls and state of the system are directly considered when applying the strategy. Thus,

the necessary conditions derived for the state constraint will be removed from future problem formulations. Therefore, the Hamiltonian will be:

$$
\begin{aligned}
&H(Q_{\text{th}}^{\text{st}}, P_{\text{th}}^{\text{sb,st}}, P_{\text{th}}^{\text{st,pb}}, P_{\text{th}}^{\text{excess}}, \lambda, t) \\
&\quad = \pi(t) \cdot \eta_{\text{pb}}\left(T_{\text{dry_bulb}}, \text{Load}\right) \cdot P_{\text{th}}^{\text{pb}}(t) \\
&\qquad + \lambda(t) \cdot \left(\eta_{\text{st_in}} P_{\text{th}}^{\text{sb,st}}(t) - \eta_{\text{st_out}}^{-1} P_{\text{th}}^{\text{st,pb}}(t) - \xi_{\text{loss}} Q_{\text{th}}^{\text{st}}\right) \\
&\quad = \pi(t) \cdot \eta_{\text{pb}}\left(T_{\text{dry_bulb}}, \text{Load}\right) \cdot P_{\text{th}}^{\text{sb}}(t) \\
&\qquad + \left(\lambda(t)\eta_{\text{st_in}} - \pi(t) \cdot \eta_{\text{pb}}\left(T_{\text{dry_bulb}}, \text{Load}\right)\right) P_{\text{th}}^{\text{sb,st}}(t) \\
&\qquad - \left(\lambda(t)\eta_{\text{st_out}}^{-1} - \pi(t) \cdot \eta_{\text{pb}}\left(T_{\text{dry_bulb}}, \text{Load}\right)\right) P_{\text{th}}^{\text{st,pb}}(t) \\
&\qquad - \pi(t) \cdot \eta_{\text{pb}}\left(T_{\text{dry_bulb}}, \text{Load}\right) P_{\text{th}}^{\text{excess}}(t) \\
&\qquad - \lambda(t) Q_{\text{th}}^{\text{st}}(t) \xi_{\text{loss}})
\end{aligned}
\tag{47}
$$

Constant efficiency When expressed with a constant mean efficiency, the necessary conditions for optimality become:

$$\dot{\lambda} = -\frac{\partial H}{\partial Q_{\text{th}}^{\text{st}}} = \lambda(t)\xi_{\text{loss}} \tag{48}$$

$$\lambda(t_{\text{end}}) = R'_{\text{st}}(Q_{\text{th}}^{\text{st}}) = \pi_{\text{res}} \tag{49}$$

$$\frac{\partial H}{\partial P_{\text{th}}^{\text{sb,st}}} = \lambda(t)\eta_{\text{st_in}} - \pi(t)\eta_{\text{pb}} \stackrel{!}{=} 0 \tag{50}$$

$$\frac{\partial H}{\partial P_{\text{th}}^{\text{st,pb}}} = \lambda(t)\eta_{\text{st_out}}^{-1} - \pi(t)\eta_{\text{pb}} \stackrel{!}{=} 0 \tag{51}$$

The Hamiltonian is linear in the control variable and the conditions do not depend on the controls (i.e. the flows to and from the storage), but rather only on the value of the tariff for energy production at time t. This leads to the so-called bang-bang control, where the controls are at their lower or upper bound, depending on the value of their coefficients [29].

Thus from (50) and (51) the price boundaries for controls are derived. They determine when electricity production is profitable.

The *storage price* π_{s} represents the lower price threshold. Below this threshold no electricity is generated, as it is not profitable to do so. It is defined as:

$$\pi_{\text{s}}(t) := \frac{\lambda(t)\eta_{\text{st_in}}}{\eta_{\text{pb}}}. \tag{52}$$

The *generation price* π_{g} is the upper price threshold. Above this price we aim to produce maximal amount of electric power with the goal to achieve a full load on the turbine. Generation price is defined as:

$$\pi_{\text{g}}(t) := \frac{\lambda(t)}{\eta_{\text{pb}}\eta_{\text{st_out}}}, \tag{53}$$

as described in Cirocco et al. [5].

Based on the current generation price, we enter one of the three operation modes:

- *Store mode*: Current tariff for electricity production is lower than the storage price, $\pi \leq \pi_s$. Therefore, it is not profitable to produce electricity in the power block. Thus, we store all incoming solar power, not exceeding the storage capacity.

$$P_{th}^{sb,st} := \min\left(P_{th}^{sb},\ P_{th}^{max_in}\right) \tag{54}$$

  In case of full storage, we first send the remaining power to the power block and remove the excess thermal power from the system. Sending the excess power out of the system minimizes the Hamiltonian. Therefore, the power is sent out of the system only when it cannot be used by the system.

$$P_{th}^{excess} := \max\left(0,\ P_{th}^{sb} - P_{th}^{sb,st}\right) \tag{55}$$

- *Solar mode*: Tariff for energy production is between the storage and generation price, $\pi_s \leq \pi \leq \pi_g$, which makes it profitable to generate electric power. However, the price is not high enough to draw any power from the storage, and we therefore use the storage only for storing any additional power from the solar block. We generate electricity using only the thermal power from the solar block. Furthermore, the power flows in the system depend on the incoming solar power and thus we introduce two submodes to accommodate the constraints in the system.

  Solar mode (a): The incoming solar power is less than the limit on the power block ($P_{th}^{sb} \leq P_{th}^{pb_max}$), and all the solar block power is sent to the power block,

$$P_{th}^{sb,pb} := P_{th}^{sb}. \tag{56}$$

  Solar mode (b): The thermal power from the solar block exceeds the power block limit ($P_{th}^{sb} > P_{th}^{pb_max}$), thus we generate electricity at full load, while storing and discarding any surplus power. This is analogue to the surplus mode presented in the buffer strategy (see Section 3.1), with the power flows described by (23), (24) and (25).

- *Generate mode*: Tariff for electricity generation is higher than the generation price, $\pi_g \leq \pi$. We generate at maximum turbine load using both solar block thermal power and stored power. This is analogue to the generation mode in the buffer strategy, therefore power flows are defined by (21) and (22).

The optimal control is constructed by finding the optimal generation price, π_g [5]. The value of adjoint coefficiend λ is necessary to obtain this value.

As the adjoint coefficient final value $\lambda(t_{\text{end}})$ is defined by the residual tariff (49), the values of λ for every time step Δt can be calculated based on (48). The chosen value for the residual tariff thus greatly influences the behavior of the strategy and should be chosen carefully. The control modes dependent on the current tariff for energy production are depicted in Figure 15.

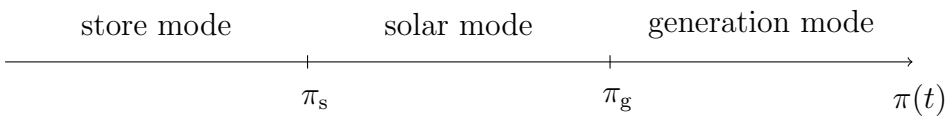

Figure 15: Dependency of the current control mode of the optimal control strategy on the tariff for energy production $\pi(t)$. The store mode, solar mode and generation mode are defined by the storage price π_{s} and the generation price π_{g}. Thus, with the lowest tariff the store mode is used. Once the storage price π_{s} has been exceeded, we switch to the solar mode. Finally, for the tariff higher than the generation price π_{g}, we use generation mode.

The full optimal control is depicted in Figure 16.

An alternative to setting up the residual tariff is setting up the starting and final storage fill level. In this case, the value of λ is guessed and found by using a shooting method. That is, the optimal control is run for different values of the adjoint coefficient, until the resulting end state is within an acceptable range. The control still depends on the adjoint coefficient in the same way, but this coefficient is not predefined as in the case of the residual in the objective function and needs to be guessed.

Dynamic programming is an alternative approach to this strategy implementation. However, it would also result in a significant additional computation time [28], and is thus not considered in this work.

Model predictive control For applying Pontryagin's maximum principle in model predictive control, we apply the necessary conditions for optimality on the given horizon and apply first element of the calculated optimal control to the system. Then we shift the window for one time step and repeat the process.

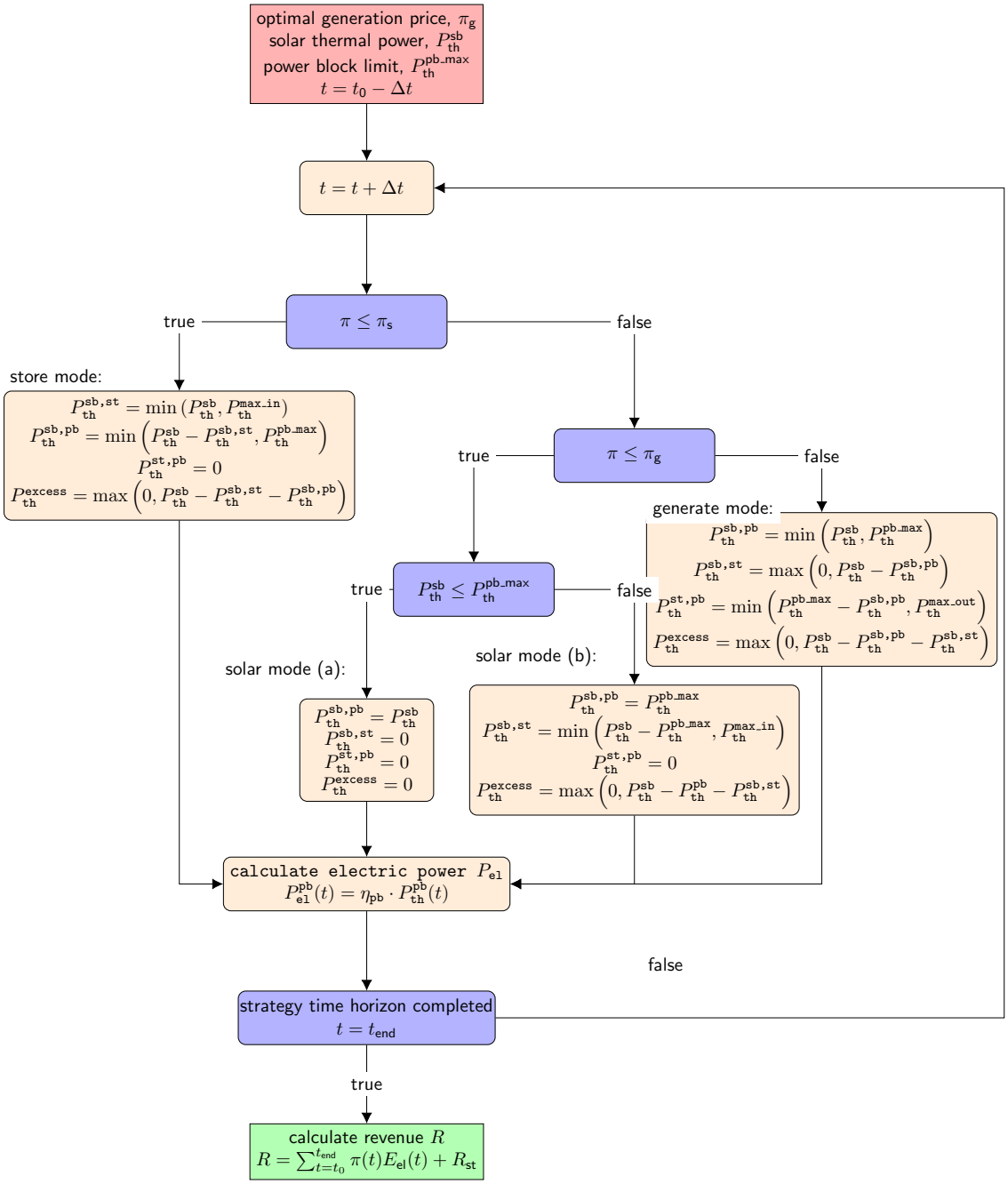

Figure 16: Optimal control storage strategy for constant efficiency in the power block. Three control modes are defined. We decide on the current control mode based on the current electricity price π and incoming thermal power $P_{\text{th}}^{\text{sb}}$. For each time step, we calculate electric power that exits the system and complete the strategy by calculating the total revenue for the time horizon.

3.2.2 Model predictive control using Mixed-Integer Linear Programming

A mixed-integer linear programming problem consists of a linear objective function with linear constraints and one or more integer decision variables [30]. Mixed integer linear programming guarantees globally-optimal solutions, compared to mixed-integer nonlinear programming which might result in local optima [24].

The power-block efficiency, earlier defined in our power block model, has a nonlinear dependency on the turbine load and ambient temperature. In order to keep the model linear, a mean value of all efficiencies defined in the load curve is considered.

Based on the MIP-MPC model from Vasallo and Bravo [18], the objective function is

$$\begin{aligned}\max R(t) = &\sum_{k=1}^{N} \pi(t+k\cdot\Delta t|t) P_{\mathrm{el}}^{\mathrm{pb}}(t+k\cdot\Delta t|t)\cdot\Delta t - l\cdot P_{\mathrm{th}}^{\mathrm{excess}}(t+k\cdot\Delta t|t)\Delta t \\ &+ \pi_{\mathrm{res}} Q_{\mathrm{th}}^{\mathrm{st}}(N),\end{aligned} \tag{57}$$

with k as the current time step in the horizon and N as the length of the horizon. An additional penalty has been added to the original revenue expression to avoid discarding excess thermal power instead of storing it in the storage ($l\cdot P_{\mathrm{th}}^{\mathrm{excess}}(t+k|t)$). The decision variables we considered are the storage charging $P_{\mathrm{th}}^{\mathrm{sb,st}}$ and discharging $P_{\mathrm{th}}^{\mathrm{st,pb}}$ heat flows.

The stored energy is defined as:

$$\begin{aligned}Q_{\mathrm{st}}(t+k\cdot\Delta t|t) = &\, Q_{\mathrm{st}}(t+(k-1)\cdot\Delta t|t) \\ &+ (\eta_{\mathrm{st_in}} P_{\mathrm{th}}^{\mathrm{sb,st}}(t+k\cdot\Delta t|t) - \eta_{\mathrm{st_out}}^{-1} P_{\mathrm{th}}^{\mathrm{st,pb}}(t+k\cdot\Delta t|t))\cdot\Delta t \\ &- P_{\mathrm{th}}^{\mathrm{loss}}(t+k\cdot\Delta t|t)\cdot\Delta t,\end{aligned} \tag{58}$$

with a constraint on the storage

$$Q_{\mathrm{th}}^{\mathrm{st_min}} \le Q_{\mathrm{th}}^{\mathrm{st}}(t+k\cdot\Delta t|t) \le Q_{\mathrm{th}}^{\mathrm{st_max}}. \tag{59}$$

The relation between the heat flows between the blocks is defined as

$$P_{\mathrm{th}}^{\mathrm{sb}}(t+k\cdot\Delta t|t) = P_{\mathrm{th}}^{\mathrm{sb,pb}}(t+k\cdot\Delta t|t) + P_{\mathrm{th}}^{\mathrm{sb,st}}(t+k\cdot\Delta t|t) + P_{\mathrm{th}}^{\mathrm{excess}}(t+k\cdot\Delta t|t), \tag{60}$$

with the upper constraints on power flows as described in Section 2, and the power flows considered as non-negative.

The electric power remains:

$$P_{\mathrm{el}}^{\mathrm{pb}}(t+k\cdot\Delta t|t) = \eta_{\mathrm{pb}}\cdot P_{\mathrm{th}}^{\mathrm{pb}}(t+k\cdot\Delta t|t), \tag{61}$$

with a constant efficiency applied, as to keep the model linear.

Direct flow from the solar block is always preferred to redirecting the power through the storage, as to avoid the heat losses caused by storing the thermal energy. Simultaneous charging and discharging creates a flow through storage instead of utilizing the

direct flow from solar block to the storage block. We prevent this by expanding the MIP-MPC model and applying two binary variables $\alpha(t + k \cdot \Delta t|t)$ and $\beta(t + k \cdot \Delta t|t)$ to the power flows $P_{\text{th}}^{\text{sb,st}}$ and $P_{\text{th}}^{\text{st,pb}}$ in the model as

$$\begin{aligned} 0 \leq P_{\text{th}}^{\text{sb,st}}(t + k \cdot \Delta t|t) \leq \alpha(t + k \cdot \Delta t|t) P^{\text{max_in}} \\ 0 \leq P_{\text{th}}^{\text{st,pb}}(t + k \cdot \Delta t|t) \leq \beta(t + k \cdot \Delta t|t) P^{\text{max_out}}, \end{aligned} \tag{62}$$

with

$$\begin{aligned} P_{\text{th}}^{\text{max_in}} &= \eta_{\text{st_in}}^{-1} \frac{Q_{\text{th}}^{\text{st_max}} - Q_{\text{th}}^{\text{st_min}}}{\Delta t} \\ P_{\text{th}}^{\text{max_out}} &= P_{\text{th}}^{\text{pb_max}} \end{aligned} \tag{63}$$

and

$$\alpha(t + k \cdot \Delta t|t) + \beta(t + k \cdot \Delta t|t) \leq 1 \tag{64}$$

An additional binary variable $\gamma(t + k \cdot \Delta t|t)$ is added to the model to account for the lower limit on the power block turbine,

$$P_{\text{th}}^{\text{pb}}(t + k \cdot \Delta t|t) = \gamma(t + k \cdot \Delta t|t) \cdot P_{\text{th}}^{\text{pb}}(t + k \cdot \Delta t|t). \tag{65}$$

This ensures that no thermal power is sent to the power block when the total flow to the power block is not sufficient (i.e. below the minimum power block power threshold).

This mixed-integer linear programming formulation was solved using the Gurobi[2] solver.

[2]Gurobi optimization, `https://www.gurobi.com/`

4 Hybrid CSP-PV plant

Photovoltaic systems represent the most common way of producing electricity from solar energy. While concentrated solar power plants convert solar irradiance to thermal power, photovoltaic power plants implement a direct conversion of sunlight into electricity [31]. However, due to a relatively high price of photovoltaic energy storage systems, the usage of a storage system has mostly been considered in concentrated solar power plants [20].

In order to utilize the benefits of electricity production from both CSP and PV plants, this work focuses on a hybrid CSP-PV power plant (see Figure 17), which is created by coupling a CSP and PV plant via a storage system.

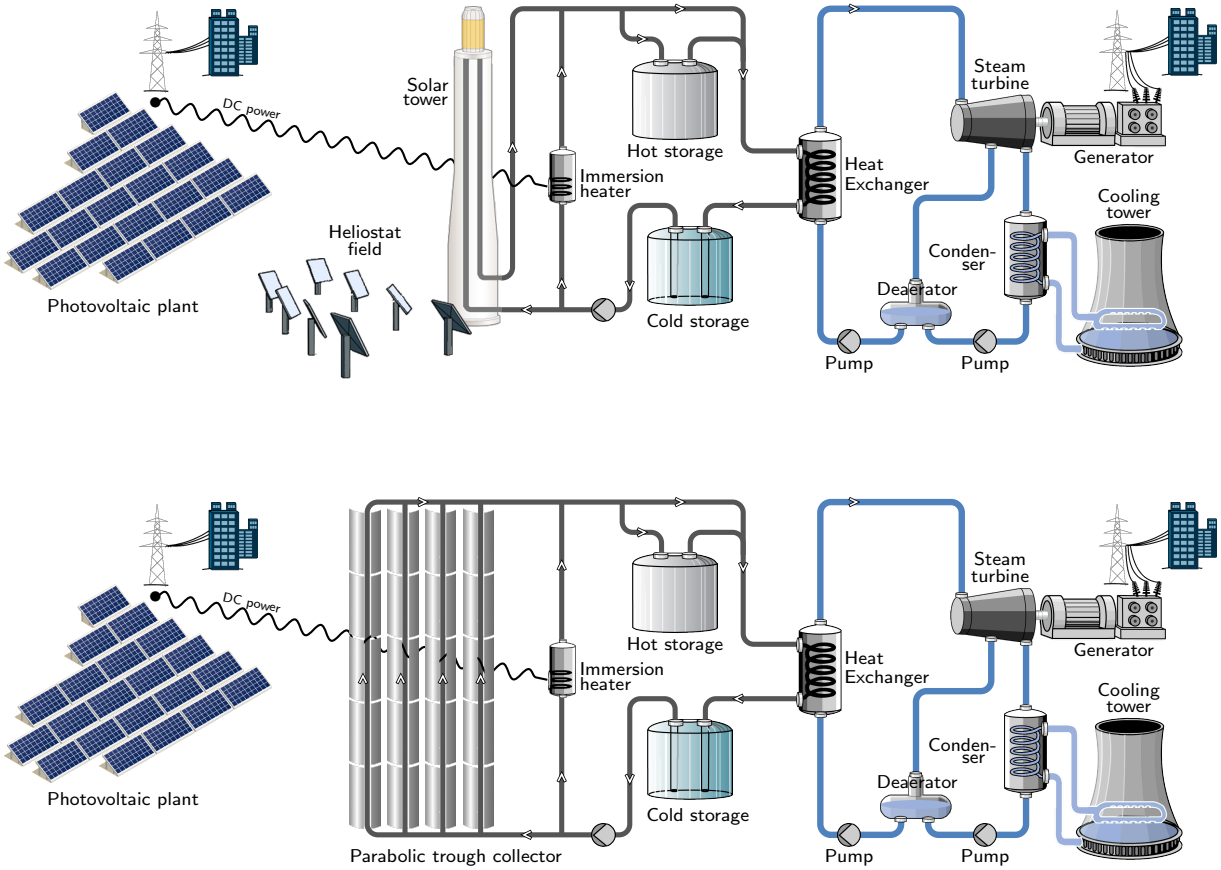

Figure 17: Overview of two hybrid concentrated solar power - photovoltaic (CSP-PV) plants with thermal energy storage. The concentrated solar power plants use the solar tower (upper) or the parabolic trough (lower) as the receiver. The CSP and PV plants are connected through the immersion heater. CSP operates as previously described in this work. The PV component converts the solar power into electric DC power. The electric DC power is converted into electric AC power and sent to the grid, or directly sent to the immersion heater where it is heats up the molten salt and stores it into the thermal storage system as thermal energy.

The CSP plant component still operates as previously described in this work. The PV plant component converts the solar irradiance into electric DC power. The produced electric DC power is converted into electric AC power and sent to the grid or sent to the immersion heater where it heats up the molten salt from the cold storage tank and stores it into the hot storage tank as thermal energy. An extension of the simple model introduced in Figure 2 is depicted in Figure 18.

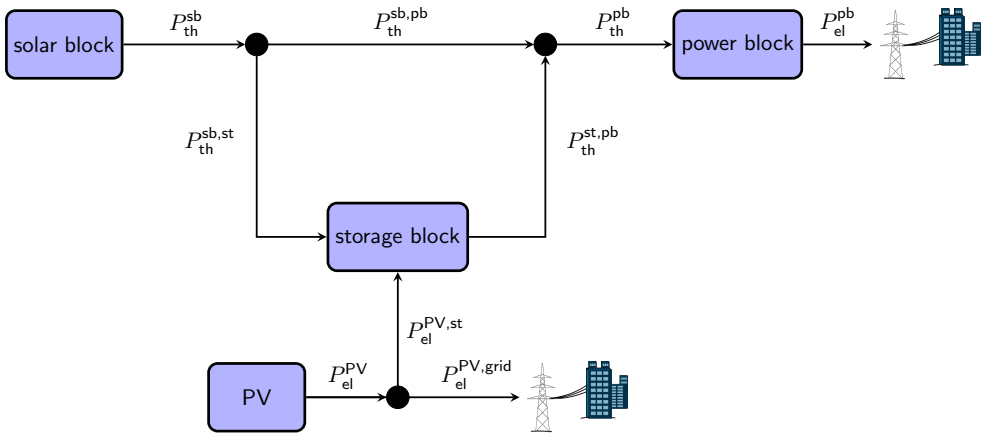

Figure 18: Overview of a hybrid CSP-PV plant model. The model is an extension of an existing simplified CSP model from Figure 2. A PV block is added to the model. The PV produces electric DC power $P_{\text{el}}^{\text{PV}}$. This power is then converted into electric AC power and forwarded to the grid via $P_{\text{el}}^{\text{PV,grid}}$ or sent into the thermal storage via $P_{\text{el}}^{\text{PV,st}}$ and converted into thermal power.

4.1 CSP-PV plant model

The CSP model introduced in Figure 3 is extended into a simplified hybrid CSP-PV plant model.

The extension of the CSP plant with the PV plant is considered from the perspective of the heat storage system. That is, the electric power produced by the PV is either sent directly to the grid or used for storing the thermal energy in storage system of the CSP plant,

$$P_{\text{el}}^{\text{PV}} = P_{\text{el}}^{\text{PV,st}} + \eta_{\text{inv}}^{-1} P_{\text{el}}^{\text{PV,grid}}, \tag{66}$$

with η_{inv} as inverter efficiency accounting for power losses induced by the conversion from DC electric produced by the PV to AC electric power required by the grid.

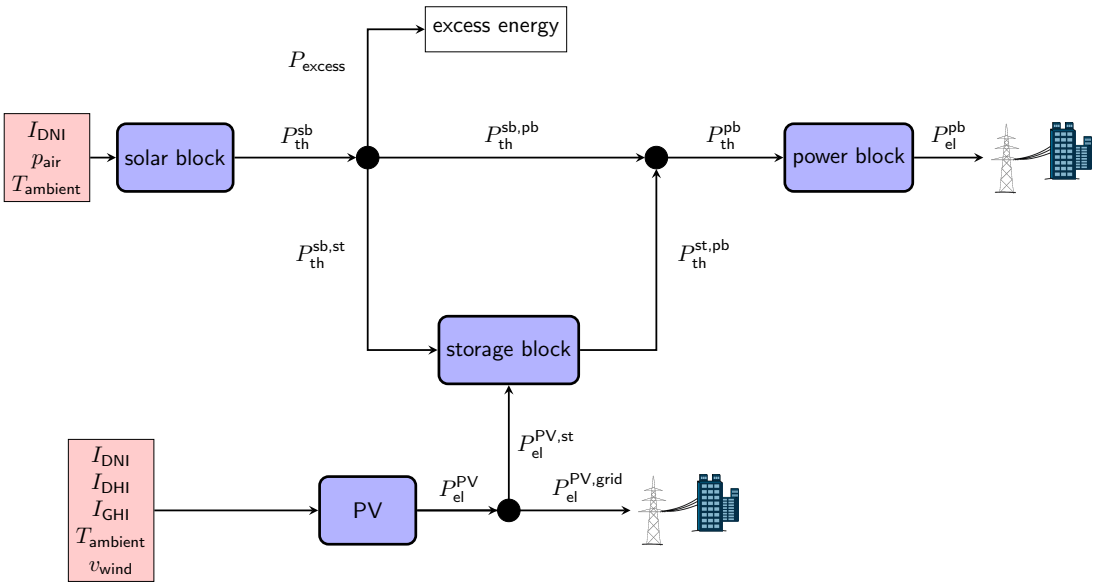

Figure 19: Simplified hybrid CSP-PV model, containing the three CSP blocks and a PV model component. The entry points in the system are the input data in the solar block and input data into the PV. The exit point is the electric power released from the CSP component and PV component into the grid. The blocks are connected by the power flows between them. The excess energy branch represents the energy that is discarded from the system when it cannot be stored or used for power generation.

The electric DC power from PV is converted to thermal power by heating up the molten salt from the cold tank in the immersion heater. The salt is stored in the hot storage tank. To account for the power loss caused by the conversion from electric DC to thermal power we consider the conversion efficiency η_{PVth}. Therefore, the thermal power sent to the storage is

$$P_{\mathrm{th}}^{\mathrm{PV,st}} = \eta_{\mathrm{PVth}} P_{\mathrm{el}}^{\mathrm{PV,st}} \tag{67}$$

The thermal power from PV now contributes to the state of the storage system. Thus the power flow $P_{\mathrm{th}}^{\mathrm{PV,st}}$ is added to the original formulation 8 for stored thermal energy,

$$Q_{\mathrm{th}}^{\mathrm{st}}(t+\Delta t) = Q_{\mathrm{th}}^{\mathrm{st}}(t) + \left[\eta_{\mathrm{st_in}}(P_{\mathrm{th}}^{\mathrm{sb,st}}(t) + P_{\mathrm{th}}^{\mathrm{PV,st}}(t)) - \eta_{\mathrm{st_out}}^{-1} P_{\mathrm{th}}^{\mathrm{st,pb}}(t) - P_{\mathrm{th}}^{\mathrm{loss}}(t)\right] \cdot \Delta t \tag{68}$$

The heat flows from the CSP storage block and PV are both influenced by the storage charging efficiency.

Both CSP and PV components of the hybrid plant are contributing to the total electric power output to the grid,

$$P_{\mathrm{el}}^{\mathrm{grid}} = P_{\mathrm{el}}^{\mathrm{pb}} + P_{\mathrm{el}}^{\mathrm{PV,grid}} \tag{69}$$

. The power electric power produced by the grid limited as

$$P_{\mathrm{el}}^{\mathrm{grid}} \leq P_{\mathrm{el}}^{\mathrm{grid_max}}. \tag{70}$$

4.2 Photovoltaic model

The PV system includes PV array and an inverter subsystem. The PV array can further be divided into subarrays that contain multiple PV modules. Each PV subarray contains the inverter to convert the DC current produced by the PV into the AC current required by the grid [20].

The PV model receives the total solar irradiance and converts it to electricity. Similarly to the CSP model, in this model the power output from the PV plant is considered. The electric power is directed either directly to the grid or stored in the thermal storage of the CSP plant.

The conversion of the DC electric power to the AC electric power relevant for the grid is done only when the electric power is sent to the grid. This power conversion is left out when storing the energy in the CSP storage to avoid the losses induced by the conversion. Thus, the DC electric power to be stored in the tanks from the PV is converted to the thermal energy and sent to the storage.

PV electric DC output power The produced electric power depends on the total solar irradiance and PV panel temperature. It is calculated in reference to the model presented in [20].

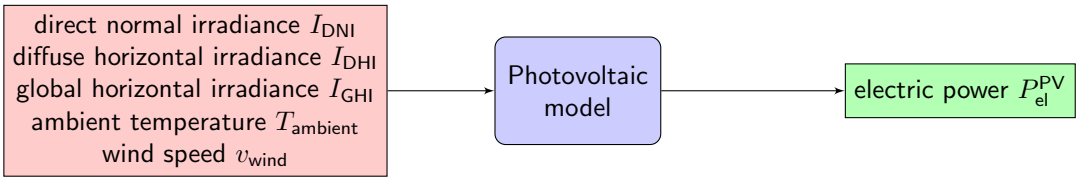

Figure 20: PV model with input and output data. Direct normal irradiance, diffuse horizontal irradiance, global horizontal irradiance, ambient temperature and wind are considered in the calculation of the output electrical power $P_{\text{el}}^{\text{PV}}$.

Symbol	Parameter	Unit
I_{DNI}	direct solar irradiance	W/m^2
I_{DHI}	diffuse horizontal irradiance	W/m^2
I_{GHI}	global horizontal irradiance	W/m^2
v_{wind}	wind speed	m/s
T_{ambient}	ambient temperature	°C

Table 8: PV model input parameters: direct solar irradiance, diffuse horizontal irradiance and global horizontal irradiance, ambient temperature and wind speed.

Firstly, the operating temperature of PV panels is calculated, while considering the current ambient temperature, global irradiance and rated heat transfer factor [20], as

$$T_{\text{pv}} = T_{\text{ambient}} + (T_{\text{nominal}} - T_{\text{ambient,nominal}}) \cdot \frac{I}{I_{\text{nominal}}} \cdot \frac{U_{\text{nominal}}}{U} \left[1 - \frac{\eta_{\text{PV}}}{\tau\alpha}\right], \tag{71}$$

where T_{nominal} (46 °C) represents a nominal operating cell temperature and $T_{\text{ambient,nominal}}$ (20 °C) the ambient temperature for nominal operating cell temperature [20, 32].

I_{nominal} is nominal solar irradiance with the assumed value of 800 W/m^2, while U_{nominal} is the rated heat transfer factor with a value of 9.5. The actual heat transfer factor U is estimated as

$$U = 5.7 + 3.8 v_{\text{wind}}, \tag{72}$$

with v_{wind} as the wind speed [20, 32].

The efficiency of a PV panel is represented as

$$\eta_{\text{PV}} = \eta_{\text{PV,nominal}} \left[1 + \gamma (T_{\text{pv}} - T_{\text{pv,ref}})\right] \tag{73}$$

with $\eta_{\text{PV,nominal}}$ as the nominal PV panel efficiency, γ as the temperature factor and $T_{\text{pv,ref}}$ as the module temperature under standard test conditions.

Finally, the resulting output electrical power is expressed as

$$P_{\text{el}}^{\text{PV}} = A \cdot I \cdot \eta_{\text{PV}} \cdot f_{\text{PV}}, \tag{74}$$

with A representing the panel area, I as total solar irradiance on the panels, η_{PV} as PV panel efficiency [20]. Furthermore, the derating factor f_{PV} is added to account for soiling of the panels, wiring losses, shading, snow cover, aging, and other secondary losses [20].

Symbol	Parameter	Unit
$P_{\text{el}}^{\text{PV}}$	electrical DC power	MW_{el}

Table 9: PV output: electric DC power, sent to the grid or directed to the storage.

Total solar irradiance, I The total solar irradiance I (74) depends on the setup of PV collectors. Namely, the collectors are usually either permanently placed at a certain tilt angle ψ and surface azimuth angle ϕ, or they use a tracking system. With the help of a tracking system collectors move in a way to minimize the angle of incidence and maximize the direct beam irradiance and thus also the total irradiance on the surface [32]. The tracking is implemented as a one-axis or two-axis tracking. The calculation of total irradiance for all three settings, as well as the relevant solar angles presented in the following paragraphs is taken from Masters [33].

For the purpose of total irradiance we introduce the relevant solar angles and how they are calculated..

The solar irradiance I on a PV collector consists of a direct (beam) solar irradiance I_{BC}, diffuse solar irradiance I_{DC} and reflected solar irradiance I_{RC}, as described in (75) [33].

$$I = I_{\text{BC}} + I_{\text{DC}} + I_{\text{RC}} \tag{75}$$

For all three PV collector configurations, the direct beam irradiance I_{BC} is calculated as

$$I_{\text{BC}} = I_{\text{DNI}} \cdot \cos\theta, \tag{76}$$

where θ is the incidence angle between the collector and the sun beam [33]. The diffuse solar irradiance and reflected solar irradiance are obtained based on the measured values of diffuse horizontal irradiance I_{DHI} and global horizontal irradiance I_{GHI}, respectively.

Fixed collectors Fixed collectors are attached at a tilt angle ψ and surface azimuth angle ϕ_{c}.

For the given tilt angle and surface azimuth we obtain the angle of incidence θ as

$$\cos\theta = \cos\beta\cos(\phi_{\text{s}} - \phi_{\text{c}})\sin\psi + \sin\beta\cos\psi, \tag{77}$$

where β is the solar altitude angle and ϕ_{s} is the solar azimuth angle [33].

The solar altitude angle β depends on the PV plant location latitude L, solar declination angle δ and the hour angle H, as

$$\sin\beta = \cos L\cos\delta\cos H + \sin L\sin\delta. \tag{78}$$

The solar declination represents the angle between the sun and the equator, calculated as

$$\delta = 23.45\sin\left(\frac{360}{365}(n-81)\right), \tag{79}$$

with n representing the day number in the year. The hour angle H (80) represents the number of degrees the earth must rotate before the sun will be directly over the longitude of the PV plant location [33].

$$H = (15^\circ) \cdot (12 - st), \tag{80}$$

$$st = ct - \frac{\text{longitude}}{15^\circ} + \frac{E}{60} \tag{81}$$

$$E = 9.78 \sin 2B - 7.53 \cos B - 1.5 \sin B \tag{82}$$

$$B = \frac{360}{364}(n - 81) \tag{83}$$

The hour angle depends on the solar time st, which is calculated based on the current clock time ct, and the location longitude of the plant, as well as the current day of the year n.

Furthermore, the solar azimuth ϕ_s (77) is

$$\begin{aligned} \sin \phi_s &= \frac{\cos \delta \sin H}{\cos \beta}, \\ \text{with} \quad |\phi_s| &\leq 90^\circ \quad \text{when} \quad \cos H \geq \frac{\tan \delta}{\tan L} \quad \text{and} \\ |\phi_s| &> 90^\circ \quad \text{otherwise.} \end{aligned} \tag{84}$$

In fixed collector the diffuse and reflected irradiance depend on the tilt angle ψ. Thus, the diffuse solar irradiance of a collector is

$$I_{\text{DC}} = I_{\text{DHI}} \left(\frac{1 + \cos \psi}{2} \right), \tag{85}$$

while reflected solar irradiance is

$$I_{\text{RC}} = \rho I_{\text{GHI}} \left(\frac{1 - \cos \psi}{2} \right), \tag{86}$$

with ρ as the ground reflectance.

One-axis tracking For one-axis tracking in this work we consider only the commonly used horizontal single-axis tracker that rotates around the horizontal axis with the tilt angle of the collectors changing based on the sun position. The tracker is moving (i.e. the tilt angle is changing) in a way to minimize the angle of incidence θ (77). The angle of incidence for a fixed collector azimuth ϕ_c becomes

$$\cos \theta = \sqrt{1 - (\cos \beta \sin(\phi_s - \phi_c))^2}. \tag{87}$$

,

The diffuse solar irradiance is

$$I_{\mathrm{DC}} = I_{\mathrm{DHI}} \left(\frac{1 + (\sin\beta / \cos\theta)}{2} \right), \tag{88}$$

and the reflected solar irradiance is

$$I_{\mathrm{RC}} = \rho I_{\mathrm{GHI}} \left(\frac{1 - (\sin\beta / \cos\theta)}{2} \right). \tag{89}$$

Two-axis tracking In case of two-axis tracking the collector is always facing the sun, with the angle of incidence equal to zero [33],

$$\cos\theta = 1. \tag{90}$$

The diffuse solar irradiance (91) and the reflected solar irradiance (92) now depend only on the solar altitude angle β.

$$I_{\mathrm{DC}} = I_{\mathrm{DHI}} \left(\frac{1 + \sin\beta}{2} \right) \tag{91}$$

$$I_{\mathrm{RC}} = \rho I_{\mathrm{GHI}} \left(\frac{1 - \sin\beta}{2} \right) \tag{92}$$

4.3 Economic model

The economic model considers the total electric power released to the grid (from CSP plant and PV plant), as well as the tariff for energy production with the energy in the storage system, see Figure 21.

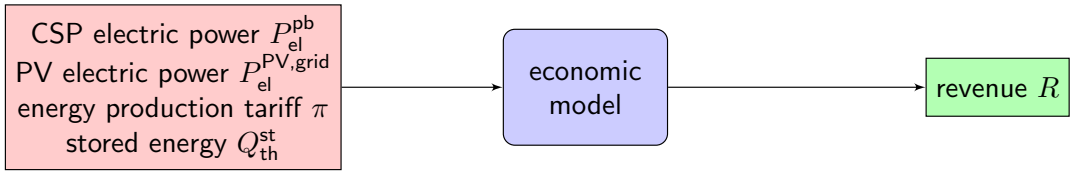

Figure 21: Economic model that focuses on plant revenue and takes electric power produced by the CSP and PV, with energy tariff as an input, while also considering the remaining energy in the storage.

Symbol	Parameter	Unit
$P_{\mathrm{el}}^{\mathrm{pb}}$	CSP electric power	$\mathrm{MW_{el}}$
$P_{\mathrm{el}}^{\mathrm{PV,grid}}$	PV electric power	$\mathrm{MW_{el}}$
π	tariff for energy production	€/$\mathrm{MW_{el}h}$

Table 10: Hybrid CSP-PV economic model input data

Symbol	Parameter	Unit
R	revenue	€

Table 11: Hybrid CSP-PV economic model output: plant revenue

Existing economic model is extended by adding an additional term to the total electric power output

$$E_{\mathrm{el}}(t) = P_{\mathrm{el}}^{\mathrm{pb}}(t) \cdot \Delta t + P_{\mathrm{el}}^{\mathrm{PV,grid}}(t) \cdot \Delta t. \tag{93}$$

The revenue is calculated with reference to the calculation described in Section 2.5,

$$\begin{aligned} R &= \sum_{t=t_0}^{t_{\mathrm{end}}} \pi(t) E_{\mathrm{el}}(t) + R_{\mathrm{st}} \\ &= \sum_{t=t_0}^{t_{\mathrm{end}}} \left(P_{\mathrm{el}}^{\mathrm{pb}}(t) + P_{\mathrm{el}}^{\mathrm{PV,grid}}(t) \right) \cdot \Delta t + \pi_{\mathrm{res}} \cdot Q_{\mathrm{th}}^{\mathrm{st}}(t_{\mathrm{end}}). \end{aligned} \tag{94}$$

The storage at the end of the calculation window is now also influenced by the power flow from the PV.

The plant evaluation factors (i.e. gain rate, net present value) remain the same as described in Section 2.5.

5 Hybrid storage strategy

5.1 Buffer strategy

Like the original buffer strategy, the extended buffer strategy aims to maximize the plant power output at any time.

As there is an upper limit on how much power can be sent to the grid from the hybrid plant, the PV counterpart uses the storage only when the power available from the plant is larger than the grid limit. Thus, at every time step t we separately consider the outputs from both plants.

When the joint output is below the grid limit, the flow from the PV to the storage is $P_{\mathrm{el}}^{\mathrm{PV,st}} = 0$. The power sent to the grid is $P_{\mathrm{el}}^{\mathrm{PV,grid}} = \eta_{\mathrm{inv}} P_{\mathrm{el}}^{\mathrm{PV}}$, while the total electric energy of the plant is calculated as defined in (93), with CSP power flows as defined in Section 3.1.

In case the joint output is above the limit, the excess power from the PV is sent to the CSP storage or discarded when there is no storage space left. Therefore, the PV output power is

$$P_{\mathrm{el}}^{\mathrm{PV,grid}} := P_{\mathrm{el}}^{\mathrm{grid_max}} - P_{\mathrm{el}}^{\mathrm{pb}}, \tag{95}$$

while the flow from the PV to the storage is,

$$P_{\mathrm{el}}^{\mathrm{PV,st}} := \min\left(P_{\mathrm{el}}^{\mathrm{PV}} - \eta_{\mathrm{inv}}^{-1} P_{\mathrm{el}}^{\mathrm{PV,grid}},\ \ \eta_{\mathrm{PVth}}^{-1} P_{\mathrm{th}}^{\mathrm{st,max_in}}\right). \tag{96}$$

The excess power power is

$$P_{\mathrm{el}}^{\mathrm{PV,excess}} := \max\left(0, P_{\mathrm{el}}^{\mathrm{PV}} - P_{\mathrm{el}}^{\mathrm{PV,st}} - \eta_{\mathrm{inv}}^{-1} P_{\mathrm{el}}^{\mathrm{PV,grid}}\right). \tag{97}$$

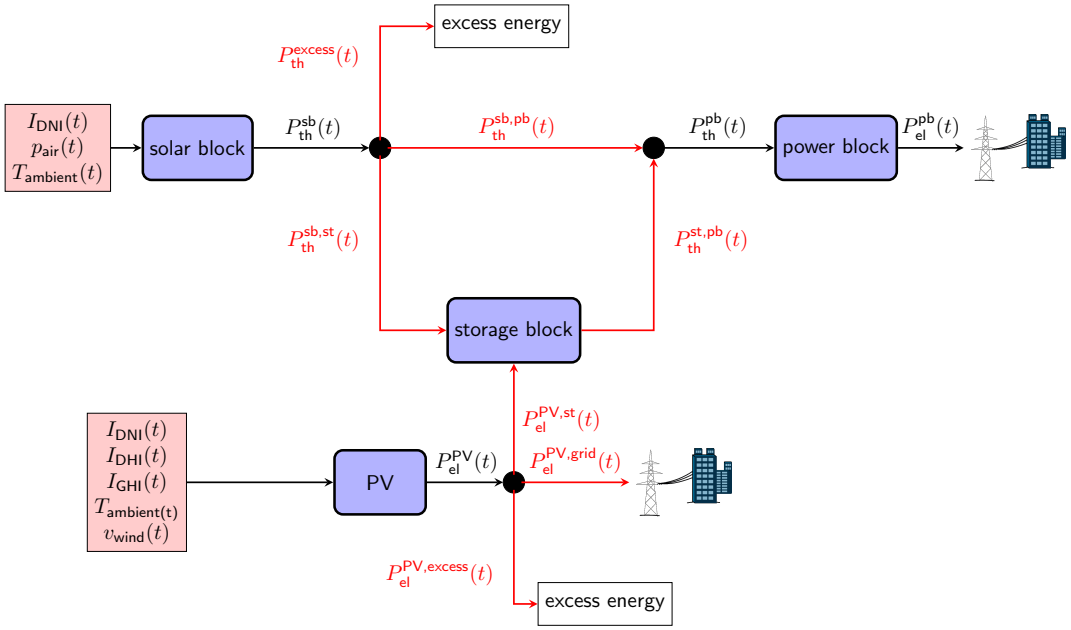

Figure 22: Hybrid CSP-PV plant model, with power flows as used in the buffer strategy. The buffer strategy aims to maximize the plant power production. Therefore, the flow from the PV to storage is ignored, and all the power produced by the PV is used directly in the grid.

5.2 Model predictive control using Pontryagin's maximum principle

When applying Pontryagin's maximum principle to the hybrid CSP-PV model, additional flows need to be considered. That is, the flow from the PV to the storage influences the state (storage) variable, which is now modified as,

$$\frac{\mathrm{d}Q}{\mathrm{d}t} = \eta_{\mathrm{st_in}}(P_{\mathrm{th}}^{\mathrm{sb,st}}(t) + P_{\mathrm{th}}^{\mathrm{PV,st}}(t)) - \eta_{\mathrm{st_out}}^{-1} P_{\mathrm{th}}^{\mathrm{st,pb}}(t) - \xi_{\mathrm{loss}} \cdot Q_{\mathrm{th}}^{\mathrm{st}}(t). \tag{98}$$

Furthermore, the extended objective function considers the flow of PV electric power to the grid,

$$\begin{aligned} R &= \int_{t_0}^{t_{\mathrm{end}}} \pi(t) \cdot (\eta_{\mathrm{pb}} \cdot P_{\mathrm{th}}^{\mathrm{pb}}(t) + P_{\mathrm{el}}^{\mathrm{PV,grid}}(t))\mathrm{d}t + R_{\mathrm{st}}(t_{\mathrm{end}}) \\ &= \int_{t_0}^{t_{\mathrm{end}}} \pi(t) \cdot \eta_{\mathrm{pb}} \cdot \left(P_{\mathrm{th}}^{\mathrm{sb}}(t) - P_{\mathrm{th}}^{\mathrm{sb,st}}(t) + P_{\mathrm{th}}^{\mathrm{st,pb}}(t) - P_{\mathrm{th}}^{\mathrm{excess}}(t)\right) \mathrm{d}t \\ &\quad + \pi(t) \cdot \eta_{\mathrm{inv}} \cdot (P_{\mathrm{el}}^{\mathrm{PV}}(t) - P_{\mathrm{el}}^{\mathrm{PV,st}}(t))\mathrm{d}t + \pi_{\mathrm{res}} \cdot Q_{\mathrm{th}}^{\mathrm{st}}(t_{\mathrm{end}}) \end{aligned} \tag{99}$$

The storage state is still considered as the only state variable in the formulation, while the power flow from PV to the storage $P_{\mathrm{el}}^{\mathrm{PV,st}}(t)$ is added as an additional control variable. This power flow is considered as non-negative. The constraint on the output electric power is considered as described in (70). Furthermore, the remaining constraints on the power flows and storage state remain the same as in the original strategy.

The new Hamiltonian is defined as:

$$\begin{aligned} &H(Q_{\mathrm{th}}^{\mathrm{st}}, P_{\mathrm{th}}^{\mathrm{sb,st}}, P_{\mathrm{th}}^{\mathrm{st,pb}}, P_{\mathrm{th}}^{\mathrm{excess}}, \lambda, t) \\ &\quad = \pi(t) \cdot \eta_{\mathrm{pb}}\left(T_{\mathrm{dry_bulb}}, \mathrm{Load}\right) \cdot P_{\mathrm{th}}^{\mathrm{pb}}(t) \\ &\qquad + \pi(t) \cdot P_{\mathrm{el}}^{\mathrm{PV,grid}}(t) \\ &\qquad + \lambda(t) \cdot \left(\eta_{\mathrm{st_in}} P_{\mathrm{th}}^{\mathrm{sb,st}}(t) + \eta_{\mathrm{st_in}}\eta_{\mathrm{PV,th}} P_{\mathrm{el}}^{\mathrm{PV,st}}(t) - \eta_{\mathrm{st_out}}^{-1} P_{\mathrm{th}}^{\mathrm{st,pb}}(t) - \xi_{\mathrm{loss}} Q_{\mathrm{th}}^{\mathrm{st}}\right) \\ &\quad = \pi(t) \cdot \eta_{\mathrm{pb}}\left(T_{\mathrm{dry_bulb}}, \mathrm{Load}\right) \cdot P_{\mathrm{th}}^{\mathrm{sb}}(t) \\ &\qquad + \left(\lambda(t)\eta_{\mathrm{st_in}} - \pi(t) \cdot \eta_{\mathrm{pb}}\left(T_{\mathrm{dry_bulb}}, \mathrm{Load}\right)\right) P_{\mathrm{th}}^{\mathrm{sb,st}}(t) \\ &\qquad - \left(\lambda(t)\eta_{\mathrm{st_out}}^{-1} - \pi(t) \cdot \eta_{\mathrm{pb}}\left(T_{\mathrm{dry_bulb}}, \mathrm{Load}\right)\right) P_{\mathrm{th}}^{\mathrm{st,pb}}(t) \\ &\qquad - \pi(t) \cdot \eta_{\mathrm{pb}}\left(T_{\mathrm{dry_bulb}}, \mathrm{Load}\right) P_{\mathrm{th}}^{\mathrm{excess}}(t) \\ &\qquad + \pi(t) \cdot \eta_{\mathrm{inv}} \cdot P_{\mathrm{el}}^{\mathrm{PV}}(t) \\ &\qquad + (\lambda(t)\eta_{\mathrm{st_in}}\eta_{\mathrm{PV,th}} - \pi(t) \cdot \eta_{\mathrm{inv}}) P_{\mathrm{el}}^{\mathrm{PV,st}}(t) \\ &\qquad - \lambda(t) Q_{\mathrm{th}}^{\mathrm{st}}(t)\xi_{\mathrm{loss}}) \end{aligned} \tag{100}$$

Necessary conditions for optimality The necessary conditions for optimality are defined as:

$$\dot{\lambda} = -\frac{\partial H}{\partial Q_{\mathrm{th}}^{\mathrm{st}}} = \lambda(t)\xi_{\mathrm{loss}} \tag{101}$$

$$\lambda(t_{\mathrm{end}}) = R'_{\mathrm{st}}(Q_{\mathrm{th}}^{\mathrm{st}}) = \pi_{\mathrm{res}} \tag{102}$$

$$\frac{\partial H}{\partial P_{\mathrm{th}}^{\mathrm{sb,st}}} \stackrel{!}{=} 0 \tag{103}$$

$$\frac{\partial H}{\partial P_{\mathrm{th}}^{\mathrm{st,pb}}} \stackrel{!}{=} 0 \tag{104}$$

$$\frac{\partial H}{\partial P_{\mathrm{el}}^{\mathrm{PV,st}}} \stackrel{!}{=} 0 \tag{105}$$

The constraints on the adjoint coefficient λ remain the same, with its final value equal to the residual tariff. An additional condition (105) is added for the new control $P_{\mathrm{el}}^{\mathrm{PV,st}}$.

Constant efficiency When expressed with a constant mean efficiency, the necessary conditions for optimality are:

$$\dot{\lambda} = -\frac{\partial H}{\partial Q_{\mathrm{th}}^{\mathrm{st}}} = \lambda(t)\xi_{\mathrm{loss}} \tag{106}$$

$$\lambda(t_{\mathrm{end}}) = R'_{\mathrm{st}}(Q_{\mathrm{th}}^{\mathrm{st}}) = \pi_{\mathrm{res}} \tag{107}$$

$$\frac{\partial H}{\partial P_{\mathrm{th}}^{\mathrm{sb,st}}} = \lambda(t)\eta_{\mathrm{st_in}} - \pi(t)\eta_{\mathrm{pb}} \stackrel{!}{=} 0 \tag{108}$$

$$\frac{\partial H}{\partial P_{\mathrm{th}}^{\mathrm{st,pb}}} = \lambda(t)\eta_{\mathrm{st_out}}^{-1} - \pi(t)\eta_{\mathrm{pb}} \stackrel{!}{=} 0 \tag{109}$$

$$\frac{\partial H}{\partial P_{\mathrm{el}}^{\mathrm{PV,st}}} = \lambda(t)\eta_{\mathrm{st_in}}\eta_{\mathrm{PV,th}} - \pi(t)\eta_{\mathrm{inv}} \stackrel{!}{=} 0 \tag{110}$$

The Hamiltonian remains linear in the control variable and the introduced formulation is still only dependent on the current value of the tariff for energy production. This again leads to the bang-bang control of the system [29].

A new price threshold is introduced as PV price π_{pv},

$$\pi_{\mathrm{pv}}(t) := \frac{\lambda(t)\eta_{\mathrm{st_in}}\eta_{\mathrm{PV,th}}}{\eta_{\mathrm{inv}}}. \tag{111}$$

Below this threshold a portion of electric power from the PV is stored in the storage system. Storage and generation price remain as defined in (52) and (53) respectively. With PV inverter efficiency η_{inv} typically having a higher value than the power block efficiency η_{pb}, the PV power will be stored only when current tariff is low enough.

An additional operation mode is introduced to the control - *PV store mode*. This mode is called when the tariff value is lower than the pv price, $\pi \leq \pi_{\mathrm{pv}}$.

The price thresholds depend on adjoint coefficient λ, with the choice of residual price becoming even more important.

The control modes dependent on the current tariff for energy production are depicted in Figure 23.

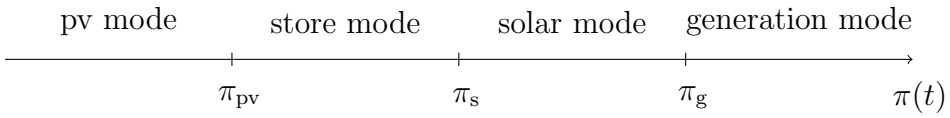

Figure 23: Dependency of the current control mode of the optimal control strategy on the tariff for energy production $\pi(t)$. The pv mode, store mode, solar mode and generation mode are defined by the PV price π_{pv}, storage price π_{s} and the generation price π_{g}. Thus, with the lowest tariff the pv mode is used, followed by the store mode above the pv price π_{pv}. Once, the storage price π_{s} has been exceeded, we switch to the solar mode. Finally, for the tariff higher than the generation price π_{g}, we use generation mode.

The strategy behavior depends heavily on the tariff for electricity production, with lower tariff encouraging the storing of the energy and higher tariff the power production. Another factor that influences the flows in this system is the limitation on the output power to the grid. The PV component of the plant often produces more power than the grid can take. In such a case, the excess power can either be discarded or stored. As throwing the power away always decreases the Hamiltonian more, it is preferred to store the excess electric power as long as the storage can accommodate this need. In this case the power flow from PV to storage is the same as for the buffer strategy.

5.3 Model Predictive Control using Mixed-Integer Linear Programming

An extended model is considered. The MIP-MPC model used in optimization remains similar to the model introduced in Section 3.2.2.

The objective function is extended with additional term for the PV electric output to the grid, as

$$\begin{aligned}\max R(t) = &\sum_{k=1}^{N} \pi(t+k\cdot\Delta t|t) P_{\mathrm{el}}^{\mathrm{pb}}(t+k\cdot\Delta t|t)\cdot\Delta t \\ &+ \pi(t+k\cdot\Delta t|t) P_{\mathrm{el}}^{\mathrm{PV,grid}}(t+k\cdot\Delta t|t)\Delta t \\ &- l\cdot P_{\mathrm{th}}^{\mathrm{excess}}(t+k\cdot\Delta t|t)\Delta t + \pi_{\mathrm{res}} Q_{\mathrm{th}}^{\mathrm{st}}(N).\end{aligned} \tag{112}$$

The constraints on the flows and storage introduced earlier stay the same. The stored energy expression now considers the additional flow from PV to storage as

$$\begin{aligned}Q_{\mathrm{st}}(t+k\cdot\Delta t|t) = &Q_{\mathrm{st}}(t+(k-1)\cdot\Delta t|t) \\ &+ (\eta_{\mathrm{st_in}} P_{\mathrm{th}}^{\mathrm{sb,st}}(t+k\cdot\Delta t|t) + \eta_{\mathrm{st_in}}\eta_{\mathrm{PV,th}} P_{\mathrm{el}}^{\mathrm{PV,st}}(t+k\cdot\Delta t|t) \\ &- \eta_{\mathrm{st_out}}^{-1} P_{\mathrm{th}}^{\mathrm{st,pb}}(t+k\cdot\Delta t|t))\cdot\Delta t \\ &- P_{\mathrm{th}}^{\mathrm{loss}}(t+k\cdot\Delta t|t)\cdot\Delta t.\end{aligned} \tag{113}$$

The new relation between the power flows is introduced:

$$P_{\mathrm{el}}^{\mathrm{PV}}(t+k\cdot\Delta t|t) = P_{\mathrm{el}}^{\mathrm{PV,st}}(t+k\cdot\Delta t|t) + \eta_{\mathrm{inv}}^{-1} P_{\mathrm{el}}^{\mathrm{PV,grid}}(t+k\cdot\Delta t|t) \tag{114}$$

An upper limit on the power that can be directed to the grid (70) is set as

$$P_{\mathrm{el}}^{\mathrm{grid}}(t+k\cdot\Delta t|t) \leq P_{\mathrm{el}}^{\mathrm{grid_max}}. \tag{115}$$

6 Realistic test case of a hybrid CSP-PV plant

The company TSK Flagsol has chosen a hypotetical location and a reference setting for a hybrid CSP-PV power plant in the MENA[3] region, see Table 12. Weather data (consisting of DNI, DHI, DIF, wind speed and ambient temperature) has been obtained for 365 days on an hourly basis. All parameters for the reference plant are presented in the following Subsection 6.1. Within a test case the CSP solar field size, PV area and storage size are optimized in Subsection 6.2.

6.1 Hybrid CSP-PV power plant

In the following, all parameters for the CSP plant, storage, and PV plant are presented. Furthermore, the weather data and economic parameters are drawn.

Parameter	Value
Latitude	32°N
Max power to grid	200 MW_{el}

Table 12: Location of the reference hybrid CSP-PV power plant and its contribution to the grid.

Power block parameters

The power block converts the obtained thermal power to electric power, which is calculated by considering the power block efficiency described in Table 13 and depicted in Figure 7. The electric power of the turbine ranges from 10 to 50 MW_{el}, see Table 14.

Load	5 °C	10 °C	15 °C	20 °C	25 °C	29.5 °C	30 °C	35 °C	40 °C
20%	37.076	37.101	37.237	37.067	36.795	36.362	36.303	35.589	34.739
30%	38.243	38.27	38.41	38.235	37.954	37.507	37.446	36.709	35.832
40%	39.41	39.437	39.582	39.401	39.112	38.651	38.588	37.829	36.925
50%	40.259	40.287	40.435	40.25	39.955	39.484	39.419	38.644	37.721
60%	40.847	40.875	41.025	40.837	40.538	40.06	39.994	39.208	38.271
70%	41.247	41.276	41.427	41.238	40.935	40.453	40.387	39.592	38.647
80%	41.606	41.635	41.787	41.597	41.291	40.805	40.738	39.937	38.983
90%	41.899	41.928	42.081	41.889	41.582	41.092	41.025	40.218	39.257
100%	43.62	43.65	43.81	43.61	43.29	42.78	42.71	41.87	40.87

Table 13: Power block load curve table, describing efficiencies (in %) for the given load on the turbine and ambient temperature.

[3]Middle East and North Africa

Parameter	Value
Maximal power block power	50 MW_{el}
Minimal power block power	10 MW_{el}

Table 14: Power block settings.

Solar field parameters

The size of solar field is considered, which correlates to the solar block thermal power provided by the CSP receiver on an hourly basis.

Storage block parameters

For the storage, the in Table 15 denoted parameters are used.

Parameter	Value
Storage charging efficiency	97 %
Storage discharging efficiency	97 %
Storage heat loss factor	0.05 %/h
Minimal storage fill	0 $MW_{th}h$

Table 15: Storage block static parameters.

PV plant parameters

The needed parameters for the PV model were taken from Duffie and Beckman [32] and Zhai et al. [20], see Table 16.

Parameter	Value
Nominal PV panel efficiency	0.149
Temperature coefficient of power	-0.0041 /°C
Nominal operating cell temperature (NOCT)	46 °C
Ambient temperature for NOCT	20 °C
Nominal solar irradiance	800 W/m^2
Rated heat transfer factor	9.5
Transmittance absorptance coefficient	0.8
PV module temperature under std. conditions	25 °C
Inverter nominal efficiency	97.8 %
PV derating factor	0.8
Electric to thermal power conversion efficiency	97.5 %
PV collector tilt angle	1-axis tracking
PV collector southern azimuth angle	-12°

Table 16: PV plant static parameters [32, 20].

The PV collector azimuth angle is optimized as described in Section 6.2.1.

Weather data

The direct normal irradiance(DNI), global horizontal irradiance (GHI) and DHI (diffuse horizontal irradiance) (see Figure 24) is given throughout the year. For the above settings we display the thermal power available in the CSP and electric power from the PV (Figure 24).

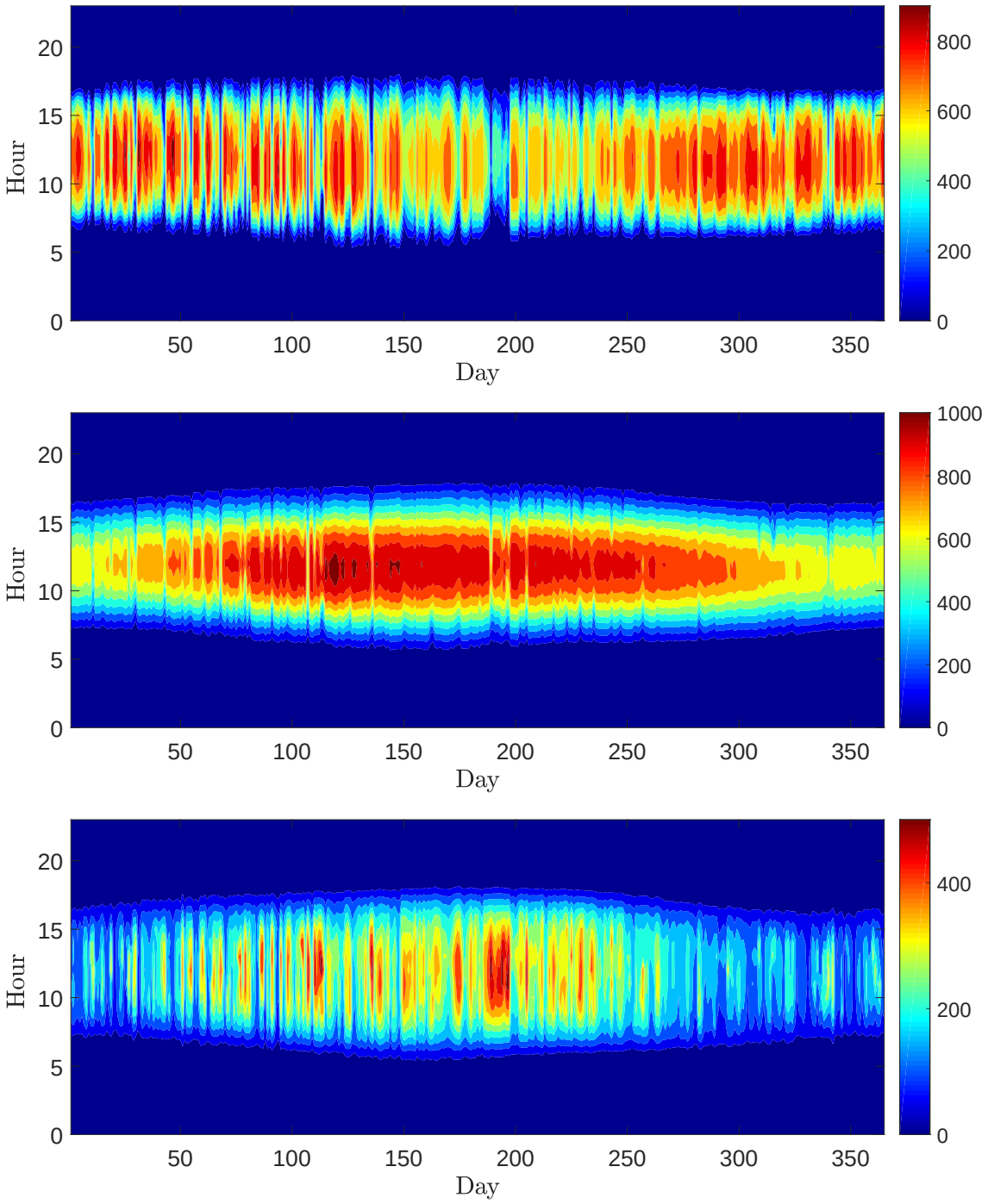

Figure 24: Hourly direct normal irradiance (DNI), global horizontal irradiance (GHI), and diffuse horizontal irradiance (DHI) in [W/m^2] for a whole year.

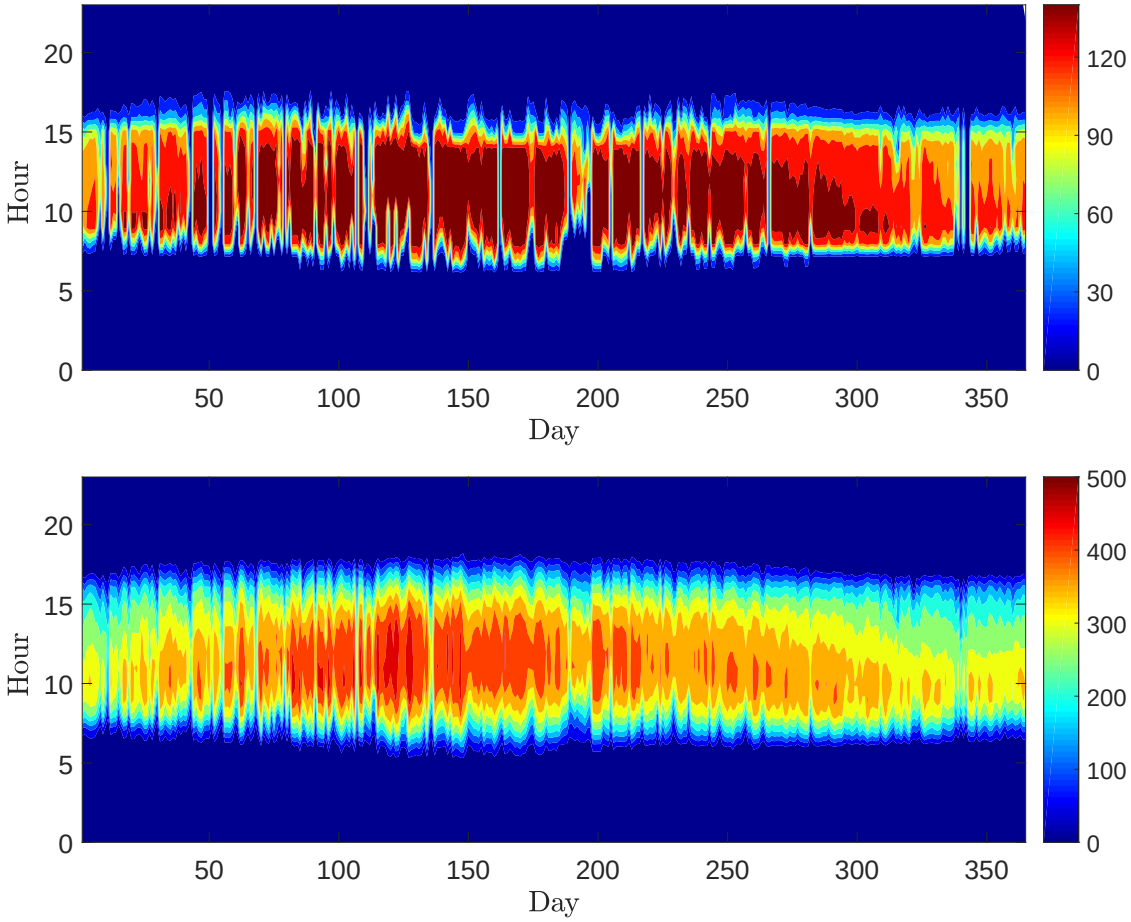

Figure 24: CSP solar block thermal output power in [MW] and PV electric DC output power in [MW] for the corresponding measured DNI, GHI and DHI throughout the year.

Economic parameters

The remuneration for the generated electricity depends on the daytime, see Table 17.

Parameter	Value
Day Tariff (7 to 17h)	100 €/$MW_{el}h$
Night Tariff (18 to 6h)	125 €/$MW_{el}h$
Plant lifetime	25 years
Interest rate	9%

Table 17: Economic parameters: two different remuneration rates during the day.

For the whole lifetime of the power plant the investment costs of the power block amount to 30 M€, the solar field to 85 M€, the storage cost to 44 M€, and the PV plant to 400 M€, see Table 18.

Parameter	Value	Cost
Power block capacity	125 MW_{th}	30 M€
CSP Solar field	150 MW_{th}	85 M€
Storage capacity	1200 $MW_{th}h$	44 M€
PV peak power	400 MW_p	400 M€

Table 18: Investment costs of the hybrid CSP plant for the whole lifetime.

For the test case, we assume a linear behavior for the costs if we increase the thermal power output of the solar field, the storage capacity and the peak power of the PV plant, see Figure 25. The reference values given in Table 18 are considered as the values at scaling factor 100%. The power block settings and its costs stay fixed.

Furthermore, for the economic evaluation of the plant the lifetime period of 25 years is considered. The investment costs for this period are introduced in Table 18, while the operation and maintenance (O&M) costs are expressed the percentage of total investment costs C_{invest} for the given period (see Table 19). The O&M costs are taken from Parrado et al. [34].

Plant	O&M costs
CSP	2 %
Hybrid CSP-PV	1.5 %

Table 19: Operations and maintenance (O&M) costs of CSP and PV plant for the period one year. The O&M costs for the hybrid plant are simply taken as the sum of O&M costs for CSP and PV plant. Source: Parrado et al. [34].

6.2 Plant optimization

6.2.1 PV collector parameters

The PV field parameters are optimized, namely the set-up of the PV panels. As demonstrated in Section 4.2, the PV collectors can be fixed, or tracking the sun by

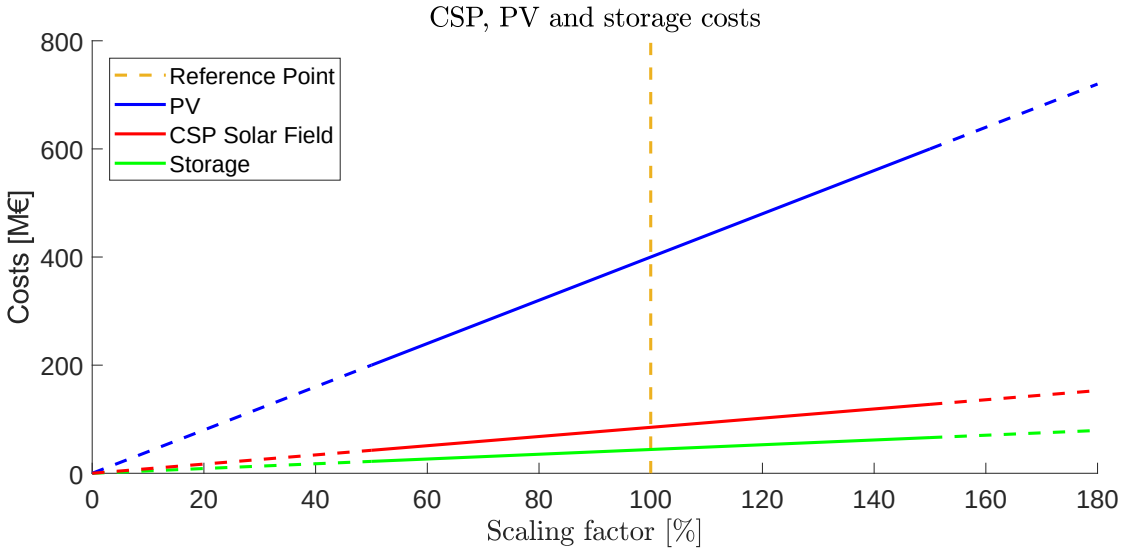

Figure 25: CSP solar field, storage and PV costs in dependency of their scaling with regard to the reference setting. from Table 18.

using a one-axis or two-axis tracking system. We compare the annual electric energy production for an area of 1 m^2 for all three possible set-ups.

The two-axis tracking is the set-up that collects the most solar power. For the given weather data, the annual collected optical energy and total DC electrical energy for the PV area of 1 m^2 are given in Table 20. As two-axis tracking produces the highest possible amount of energy a PV can produce, we set it up as the reference value.

Parameter	**Value**
Annual optical energy	2.80325 MWh
Annual DC electric energy	0.30809 $MW_{el}h$

Table 20: Total annual optical and DC electric energy collected by PV of area of 1 m^2, with a two-axis tracking system.

In the horizontal one-axis tracking system, we fix the value of an azimuth angle and change the tilt angle of the collector. The most common horizontal single-axis tracker is set-up either on the north-south or west-east axis. To get the highest possible amount of electric energy we first optimize this azimuth angle. The annual production for azimuth angles between -15° and 15° is shown in Figure 26. The annual energy is expressed as relative to the DC energy produced by the two-axis system, with the annual DC energy for two-axis system equal to 100 %.

For one-axis tracking, the produced electric DC energy for the period of one year is maximal at -10°, with the relative energy equal to 90.83277%.

When considering a fixed collector system, the goal is to find the optimal collector azimuth and tilt angles. The angles depend on the latitude of the plant [32, 33]. Firstly,

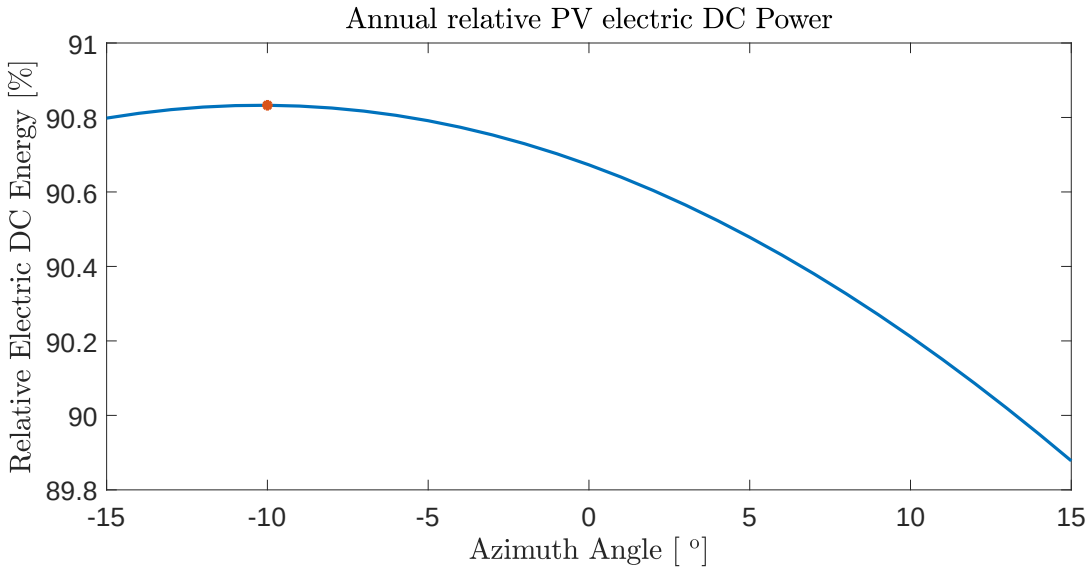

Figure 26: Annual relative DC electric energy for a single-axis tracking system. The DC electric energy is maximal at -10°.

the annual relative production of DC electric energy is demonstrated for different azimuth and tilt angles (see Figure 27).

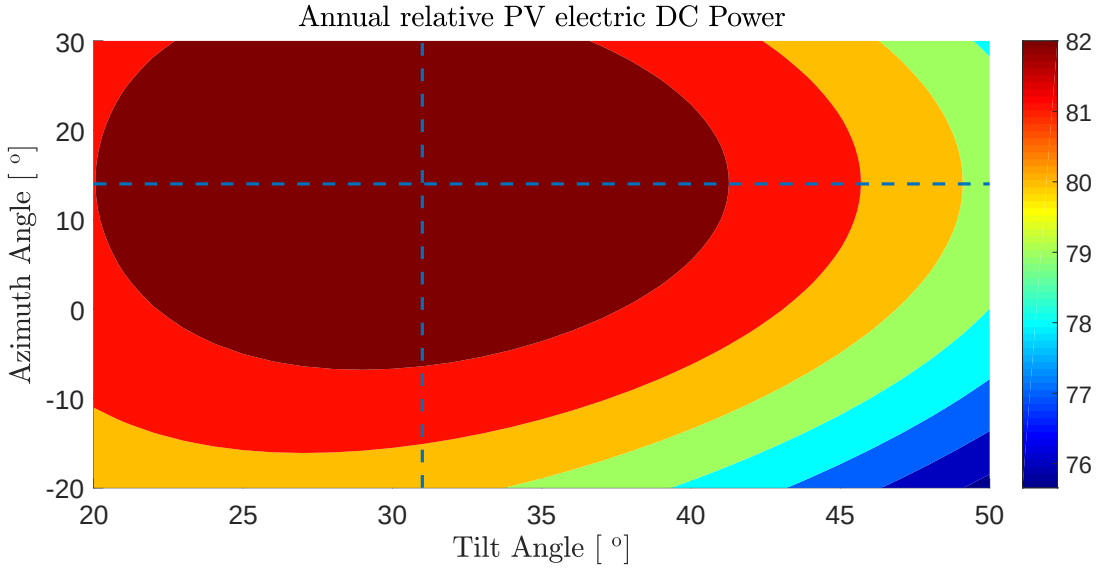

Figure 27: Annual relative DC electric energy for a fixed collector setting. The produced energy is maximal at an azimuth of 14° and tilt angle of 31 °.

For the optimal azimuth angle the relative annual production depending on the tilt angle is depicted in Figure 28a, while the relative annual production for an optimal tilt angle depending on different azimuth angles is depicted in Figure 28b.

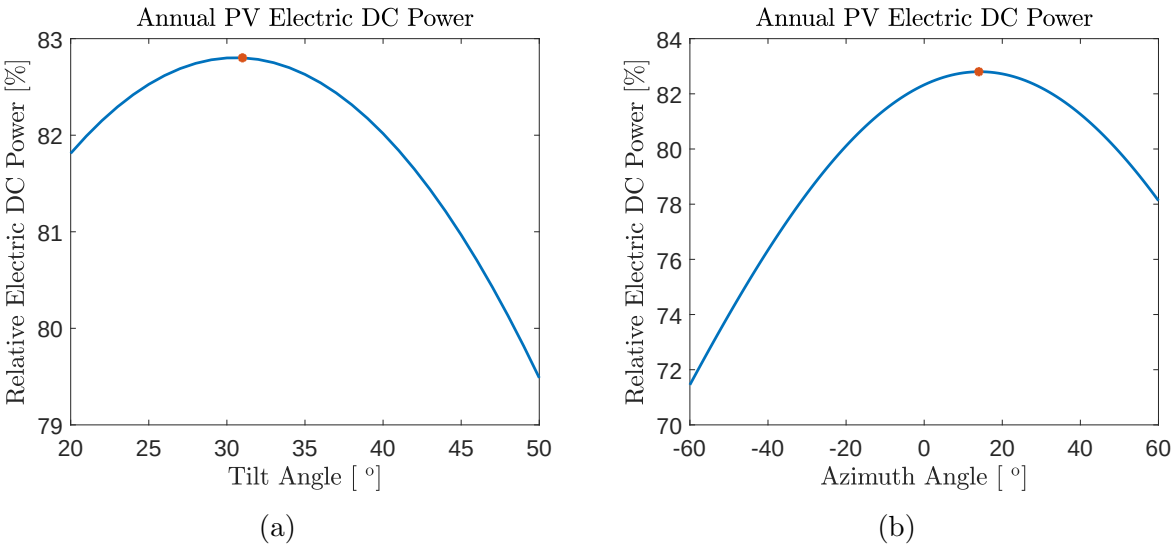

(a) (b)

Figure 28: Annual relative DC electric energy for a fixed collector setting: (a) annual energy as a result of different tilt angles for a fixed collector azimuth of 14°. (b) annual energy as a result of different azimuth angles for a fixed collector tilt angle of 31°. The produced energy is maximal at an azimuth of 14° and tilt angle of 31°. It equals 82.80148%.

The relation between the PV collector set-ups (tracking or fixed) is shown in Figure 29, with the annual DC electric energy produced by the PV with two-axis tracking system considered as 100%.

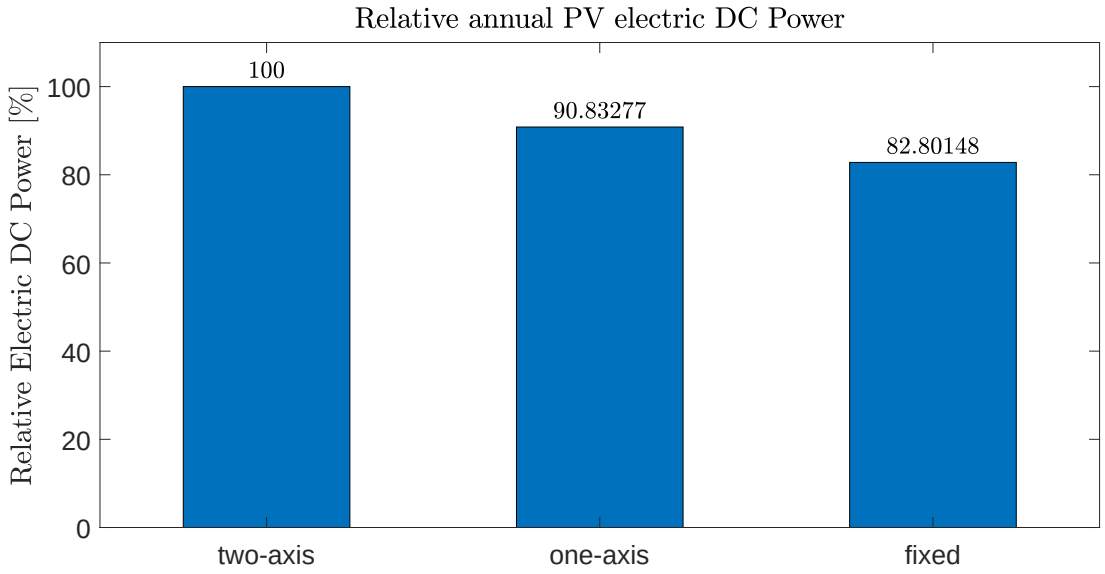

Figure 29: Comparison of annual DC electric energy production for two-axis, one-axis and fixed PV systems.

The test case considers the single-axis tracker, as described in the previous section.

6.2.2 Storage strategies for CSP plant

All three storage strategies described in Section 3 are applied to the reference data for the CSP plant presented at the beginning of this section.

Buffer strategy The buffer strategy is first applied to the reference data. It is concerned only with releasing as much power as possible to the grid. We demonstrate the output power to the grid, along with the storage fill level during a period of one year. Regarding the efficiency, since there is no importance of having a linearity with this strategy, the cubic approximation of the load curve is directly applied.

For a greater overview of the flows during the strategy, we depict the power block power output and the storage state for the obtained solar block power (Figure 30) during a period of five days (April 10th to April 14th, starting at 6 a.m.). This example demonstrates precisely the case when there is more power provided by the solar block than the turbine can process.

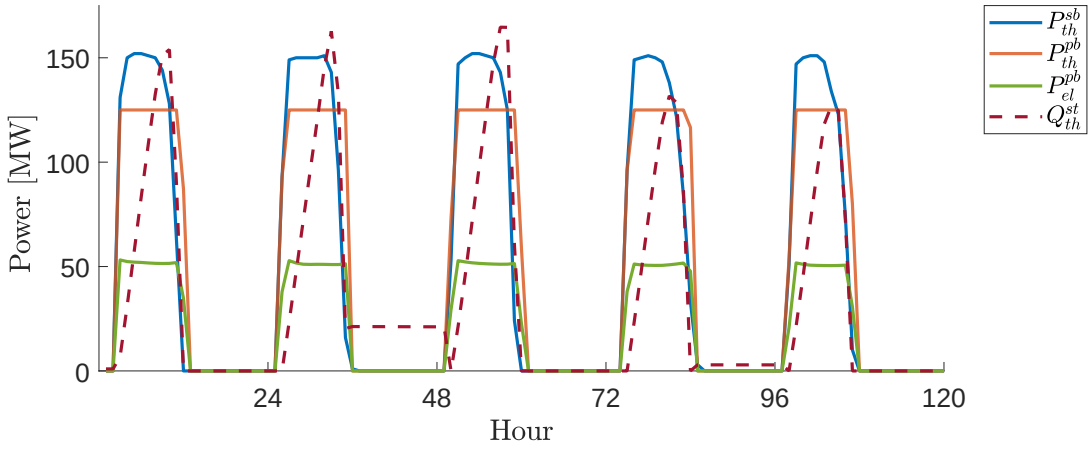

Figure 30: Buffer strategy power block output power and storage state based on the solar block power input. A period of 5 days, starting on day 100 at 6 a.m. is depicted.

We start with an empty storage and during the first 24 hours any excess power is directed to the storage, while the maximum power that the power block can accept is sent to the power block. The storage is also used for power production in the second half of the day, when there is no more power from the solar block, but storage is discharged and used for power production. However, if the power available for the power block is below the minimum (25 $\mathrm{MW_{th}}$) no power is used for generation. This is nicely demonstrated during the second 24 hours, where there is still some energy left in the storage, even though it could potentially be used.

Another example (Figure 31) depicts the period of 5 days (January 10th to January 14th) with a shortage of the solar block power.

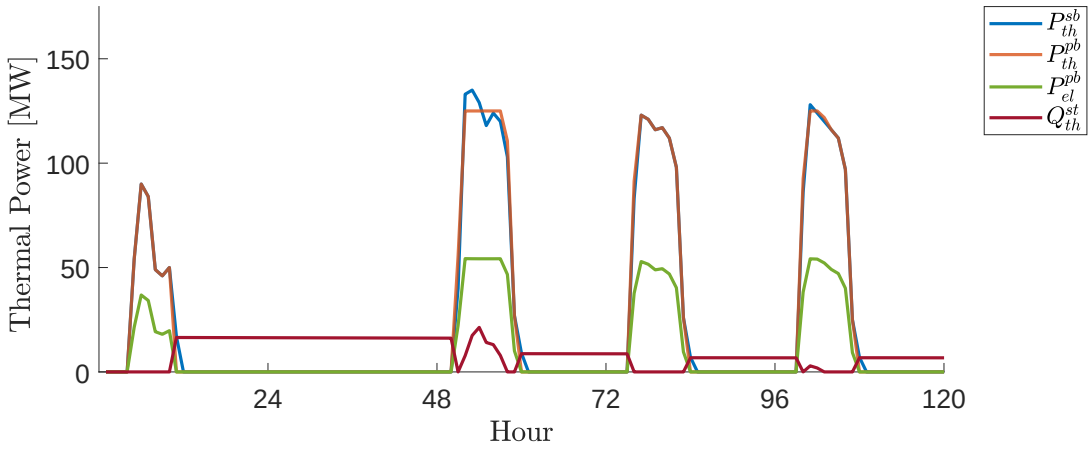

Figure 31: Buffer strategy power block output power and storage state based on the solar block power input. A period of 5 days, starting on day 10 at 6 a.m. is depicted. The solar block power input is mostly lower than the turbine limit.

During the first 24 hours all the power from solar block is sent to the power block. In case the amount of solar block power is less than the lower turbine limit, the power is sent to the storage. Therefore, at the evening of the first day the storage is not empty. However, with no power from the solar block in the next 24 hours, the power from the storage also cannot be used.

Both examples demonstrate the main drawback of using this simple strategy. It heavily depends on the available power from the sun and doesn't utilize the storage in an efficient way. During the night (when the tariff is higher, Table 17), there is mostly no power output. Therefore, while the power output is maximized, it does not solve the problem of days with a shortage of solar irradiance, nor does it consider releasing the power to the grid when the demand is higher.

Model predictive control using Pontryagin's maximum principle The Pontryagin's maximum principle is applied to the objective function presented in Section 3.2.1. The behavior of the strategy heavily depends on the residual tariff determined for the power remaining in the storage. According to (49), it sets the adjoint coefficient λ which is the determining factor for the decision on whether the incoming solar power should be stored or released to the grid. The behavior of λ during the horizon period is affected by the heat loss factor for the storage. The model predictive control was run with a horizon of 24 hours.

Because only two values of tariff are used, it becomes simple to define the residual tariff in an optimal way. An investigation was done for different values of residual tariff (and thus different values of λ) to determine the revenue (Table 21).

Residual tariff	Revenue without the residual	Revenue with the residual
35 €/MW_{el}h	14.646994 M€	14.646994 M€
40 €/MW_{el}h	14.951084 M€	14.951084 M€
45 €/MW_{el}h	16.963535 M€	16.961303 M€
50 €/MW_{el}h	12.984942 M€	13.044762 M€
55 €/MW_{el}h	12.984942 M€	13.050744 M€

Table 21: Comparison of a plant revenue for a period of one year, for different residual tariffs π_{res}.

The residual tariff of 45 €/MW_{el}h results in a maximum revenue. This particular revenue influences the strategy in a way that the energy is stored when the day tariff is running and generates power when the night tariff is actual. By lowering the residual tariff, there is an increased emphasis on energy generation, while higher residual tariff strives to store more energy.

The Pontryagin's maximum principle is thus applied with a residual tariff $\pi_{res} = 45$ €/MW_{el}h (Figure 32).

For a typical day with more solar power than the turbine can process, the power is stored during the day tariff and used for generation during the night tariff.

An example of a five days with lower solar irradiance is given (Figure 33). The power is sent to the power block during the night tariff. However, due to not enough power stored in the storage we again have longer time periods without power generation.

Because it is heavily dependent on the tariff, the Pontryagin's maximum principle proves efficient on the days with enough solar power. However, longer periods of suboptimal weather conditions remain problematic.

Furthermore, an optimization that considers the storage fill level was applied as an alternative to defining the residual tariff. Thus, instead of a defined final value of adjoint coefficient λ (through the residual tariff), we define the beginning and final storage state for the horizon. With reference to Cirocco et al. [5], a binary search was used to find the optimal adjoint coefficient λ. The shooting method was executed with different start and end storage fill level. An initial λ value was guessed and modified until the end value within an acceptable range was found.

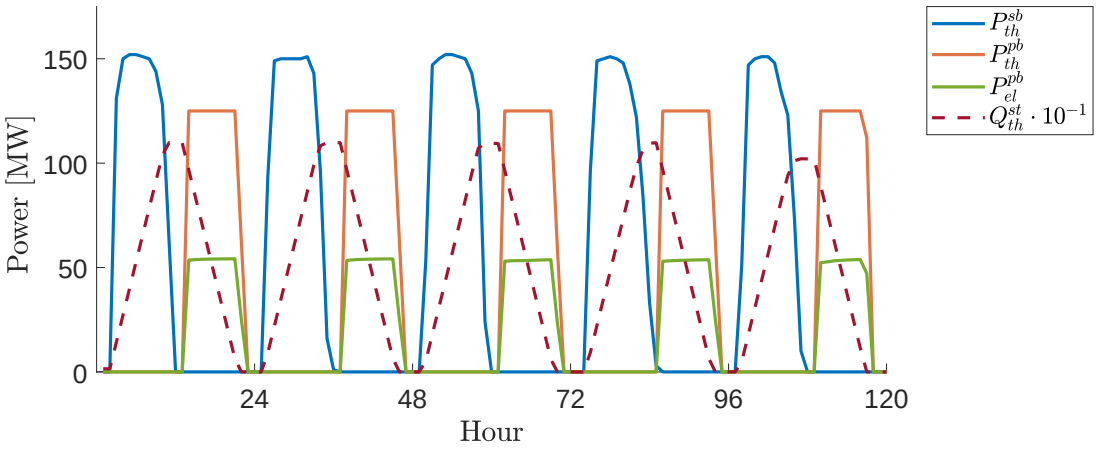

Figure 32: Power block output power and storage state based on the solar block power input under Pontryagin's maximum principle with a residual tariff $\pi_{\text{res}} = 45$ €/MW$_{\text{el}}$h. A period of 5 days, starting on day 100 at 6 a.m. is depicted.

The method proved most profitable for a half-full storage at the beginning and end of the optimization window. In order for the appropriate λ to be found, a difference of 100 MW between the starting and ending fill level was allowed. Also, the binary search had a limited number of iterations, after which this threshold was increased, so that the solution could be found. Compared to directly applying the residual tariff, the shooting method resulted in a slightly lower revenue (see Table 22).

Method	**Revenue without the residual**	**Revenue with the residual**
Residual tariff	16.963535 M€	16.961303 M€
Fill level	16.358728 M€	16.389557 M€

Table 22: Comparison of a plant revenue for a period of one year, for a predefined residual tariff π_{res} and fill level $Q_{\text{st}}^{\text{th}}$.

The behavior of the strategy for weather conditions with higher and lower solar irradiance days is displayed in Figures 34 and 35, respectively.

One can notice that compared to just the residual in the objective function, when optimizing with regards to the starting and final storage state, the storing and generating prices are not fixed. That is a new λ is defined for every step of model predictive control. With the residual tariff defined the adjoining coefficient is "reset" at every time-step of the control and behaves according to (48).

However, the drawback of using the storage start and end fill level instead of defining the residual tariff is the execution time that heavily increases (ca. 1430 s) compared to the execution time when the residual tariff is defined (ca. 156 s).

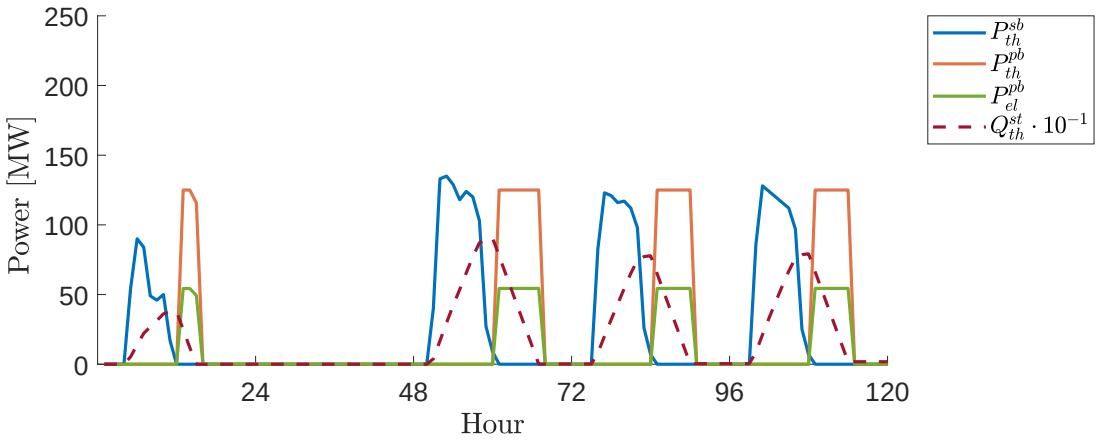

Figure 33: Power block output power and storage state based on the solar block power input under Pontryagin's maximum principle with a residual tariff $\pi_{\text{res}} = 45$ €/MW_{el}h. A period of 5 days, starting on day 10 at 6 a.m. is depicted. The solar block power input is mostly lower than the turbine limit.

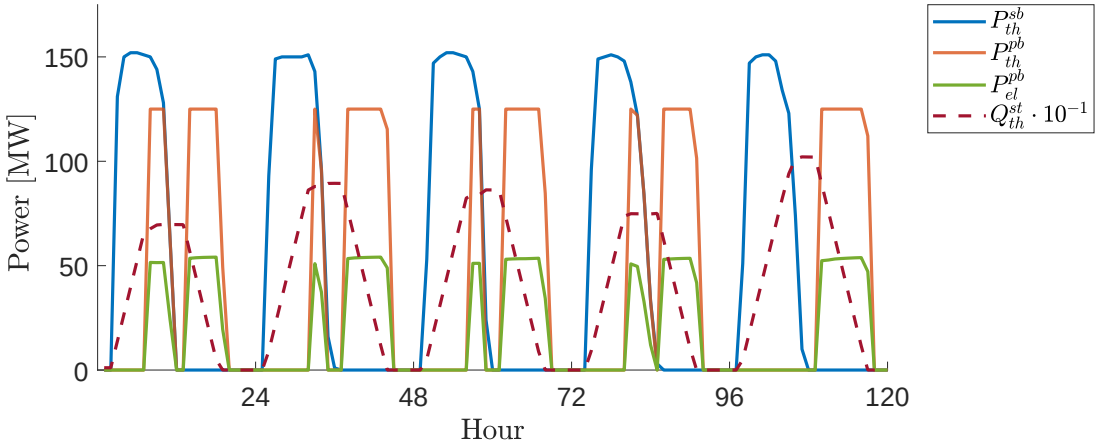

Figure 34: Power block output power and storage state based on the solar block power input under Pontryagin's maximum principle with a half-full storage at the start and end of model predictive control. A period of 5 days, starting on day 100 at 6 a.m. is depicted.

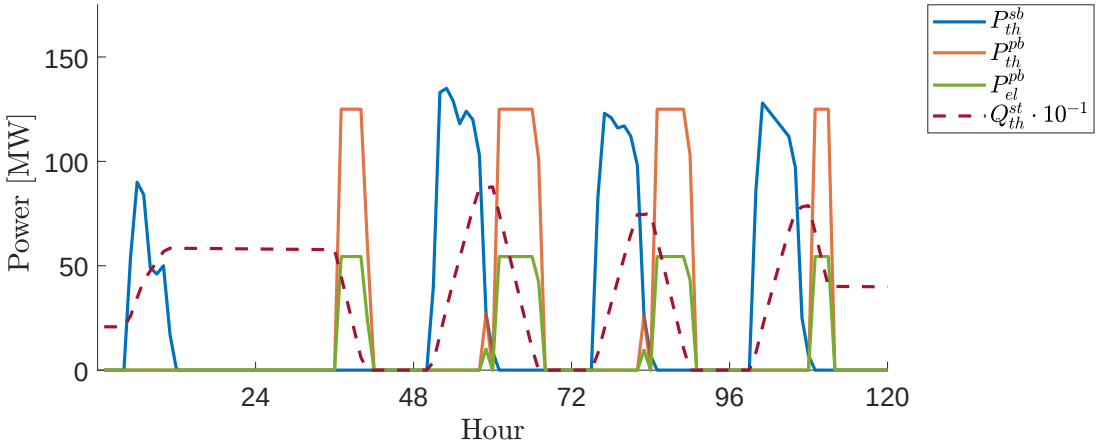

Figure 35: Power block output power and storage state based on the solar block power input under Pontryagin's maximum principle with a half-full storage at the start and end of model predictive control. A period of 5 days, starting on day 10 at 6 a.m. is depicted. The solar block power input is mostly lower than the turbine limit.

Model predictive control using Mixed-Integer Linear Programming The optimization horizon size is first considered when applying model predictive control with a mixed-integer linear programming formulation. The revenue has been tested for horizon sizes between 12 and 72 hours (see Figure 36) during the period of 30 days.

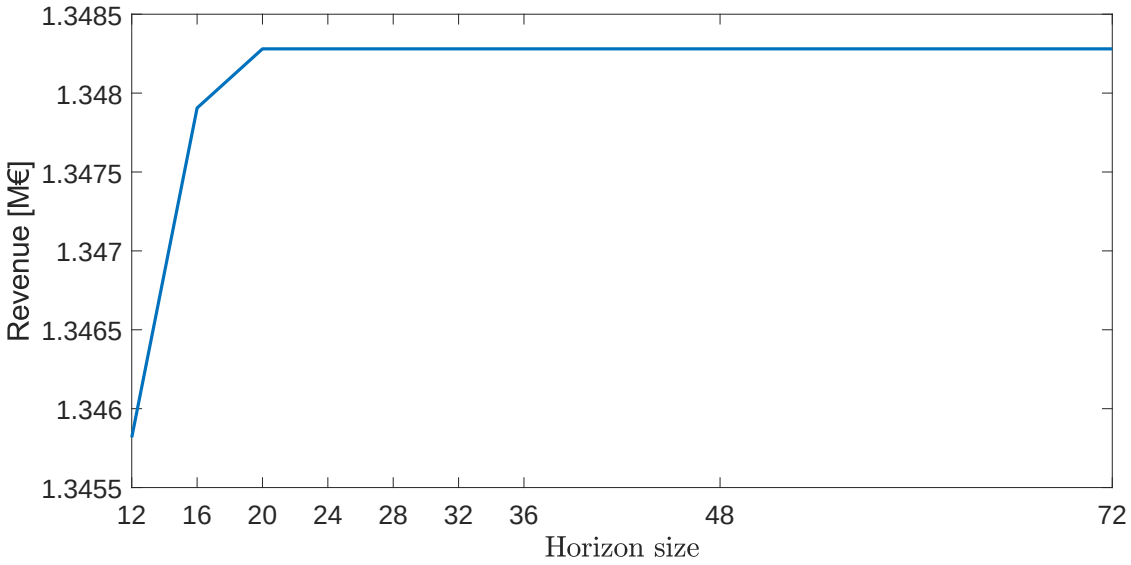

Figure 36: Revenue obtained by applying MIP-MPC with different horizon sizes. The revenue remains similar for horizons of 24 hours and up.

Since there is not a large difference in the revenue from 24 hours to 72 hours, the horizon size of 24 hours will be considered when applying model predictive control throughout the rest of this work, as the weather forecast becomes less accurate with increased time horizon. Another reason to keep the horizon size lower is the computation time, which rapidly increases with larger horizon size (above 72 hours).

Furthermore, it is important to notice that the optimal horizon size also depends on the starting time of the optimization, as well as the length of the optimization period (e.g. 30 days or one year). The mixed-integer linear programming formulation presented in Section 3.2.2 was solved using the Gurobi[4] solver.

To compare MIP-MPC with Pontryagin's maximum principle, the results are demonstrated for the objective function with and without the residual. The residual tariff of 45 €/MW_{el}h is considered. The resulting flows are almost identical, with the difference of MIP-MPC taking the "future" more into account, which results in a somewhat higher revenue. The strategy using Pontryagin's maximum principle during the night always tries to send maximum power out during a time step, as a result of bang-bang control. This sometimes results in not all energy from the storage being directly utilized because it is not sufficient to generate electricity. On the other hand, the MIP-MPC considers the next 24 hours, and decides not to send the maximum power to the power

[4]Gurobi optimization, `https://www.gurobi.com/`

block directly, but rather send less power at first in order to be able to empty out the storage and utilize more energy from it. After all, the stored energy is also influenced by the heat losses. Since the efficiency used for the power block is constant, the load does not influence the output electric power. The resulting flows for higher and lower irradiance weather conditions are presented in Figures 37 and 38, respectively.

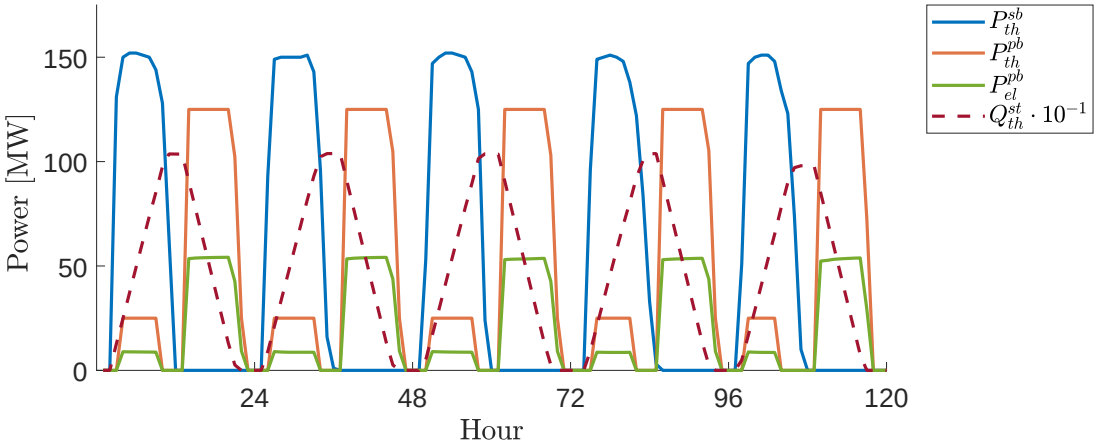

Figure 37: Power block output power and storage state based on the solar block power as a result of MIP-MPC with storage residual. A period of 5 days, starting on day 100 at 6 a.m. is depicted.

Compared to applying the Pontryagin's maximum principle on the objective function with residual, MIP-MPC results in a higher revenue, but also higher computational time of (ca. 187 s).

Furthermore, MIP-MPC is also executed without the residual in the objective function. The resulting power flows and revenue were the same as with residual tariff applied.

Comparison While buffer strategy is expectedly the most simple and computationally fast strategy, it is completely ineffective when the desire is to utilize the storage, which in the case of buffer strategy becomes unprofitable.

On the other hand, the Pontryagin's maximum principle and MIP-MPC expectedly shift the times of the power production to the hours with a higher tariff for energy production. While Pontryagin's maximum principle reduces the computational time for the optimization, the MIP-MPC deals better with distributing the power between the storage and turbine. The Pontryagin's bang-bang control disregards this fact and often ends up with extra power in the storage at the end of the day, which is too low to be used in the turbine.

However, both Pontryagin's maximum principle and MIP-MPC give very similar results and confirm each other, as well as the importance of the residual tariff. The lower residual tariff thus results in the strategies trying to maximize power output, while a higher tariff puts the emphasis on trying to store as much energy as possible.

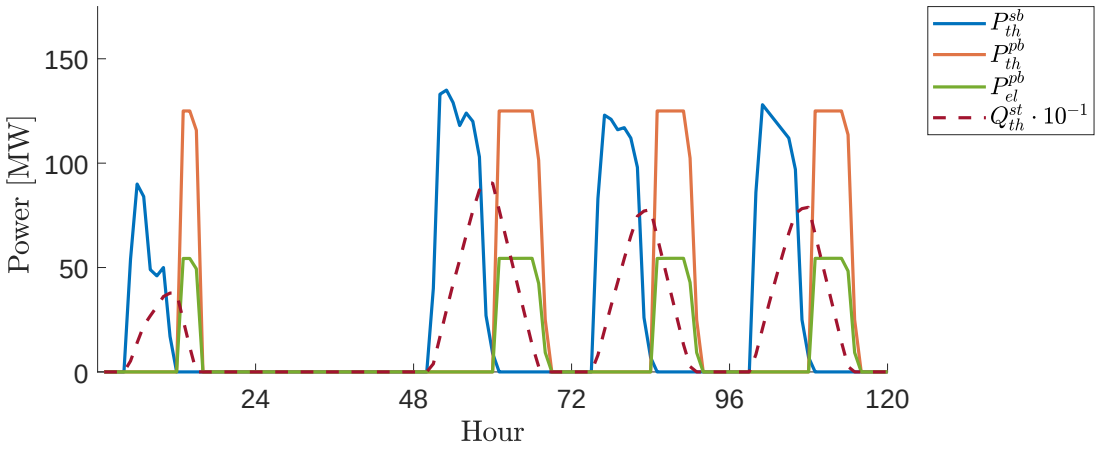

Figure 38: Power block output power and storage state based on the solar block power input as a result of MIP-MPC with storage residual. A period of 5 days, starting on day 10 at 6 a.m. is depicted. The solar block power input is mostly lower than the turbine limit.

The middle ground is the residual tariff that focuses on storing the energy during the day and generating it at night. Since there are only two tariff values, the values of the adjoining coefficient λ can be determined from (52) and (53), by setting up the storage price π_s higher than the day tariff and generation price π_g lower than the night tariff. For this particular test case, the value of residual tariff (i.e. adjoint coefficient) should be between 41.24 and 48.5 €/MW_{el}h. The storage heat loss needs to be also taken into account, because it influences the value of adjoint coefficient throughout the optimization window.

Applying the MIP-MPC to the test case confirms this theory, and the optimization without the residual in the objective function confirms that on the daily basis, to get the maximal revenue it is enough to focus on shifting the production times based on the tariff. However, for the given solar field size this often results in not producing enough, if any, power during the day, and not having enough energy in the storage to produce the energy during the night. An increase in the solar field size should thus be considered.

The computation time and revenue for the three strategies for the period of one year is given in Table 23.

6.2.3 Storage strategies for hybrid CSP-PV plant

The extended storage strategies from Section 5 are applied to the reference hybrid CSP-PV plant.

Extended buffer strategy When considering the extened buffer strategy, the PV stores the extra energy in the thermal storage to avoid just throwing it away when it cannot be released to the grid. The output power to the grid, as well as the storage fill

Strategy	Computation time [s]	Revenue [M€]
Buffer	3.274	14.646994
Pontryagin	155.548	16.961303
MIP-MPC	186.727	17.387386

Table 23: Computation time and annual revenue for all three strategies for the CSP plant. In case of Pontryagin's maximum principle and MIP-MPC, the objective function with residual is considered. The strategies were run with the residual $\pi_{\text{res}} = 45$ €/MW_{el}h and horizon window of 24 hours.

level for the period of five days, starting from day 100 at 6 a.m. is depicted in Figure 39.

At days with a lot of solar irradiance the extended buffer strategy fills the storage and utilizes it thanks to the power from the PV that is stored whenever it cannot be released to the grid. Since the PV power during sunny days is always above the grid limit it is successfully used for both generating power alongside the CSP and filling up the storage.

However, the days with sub-optimal weather conditions again have the problem of just generating the power when it's available and not utilizing the storage and shifting the production to when it's more profitable.

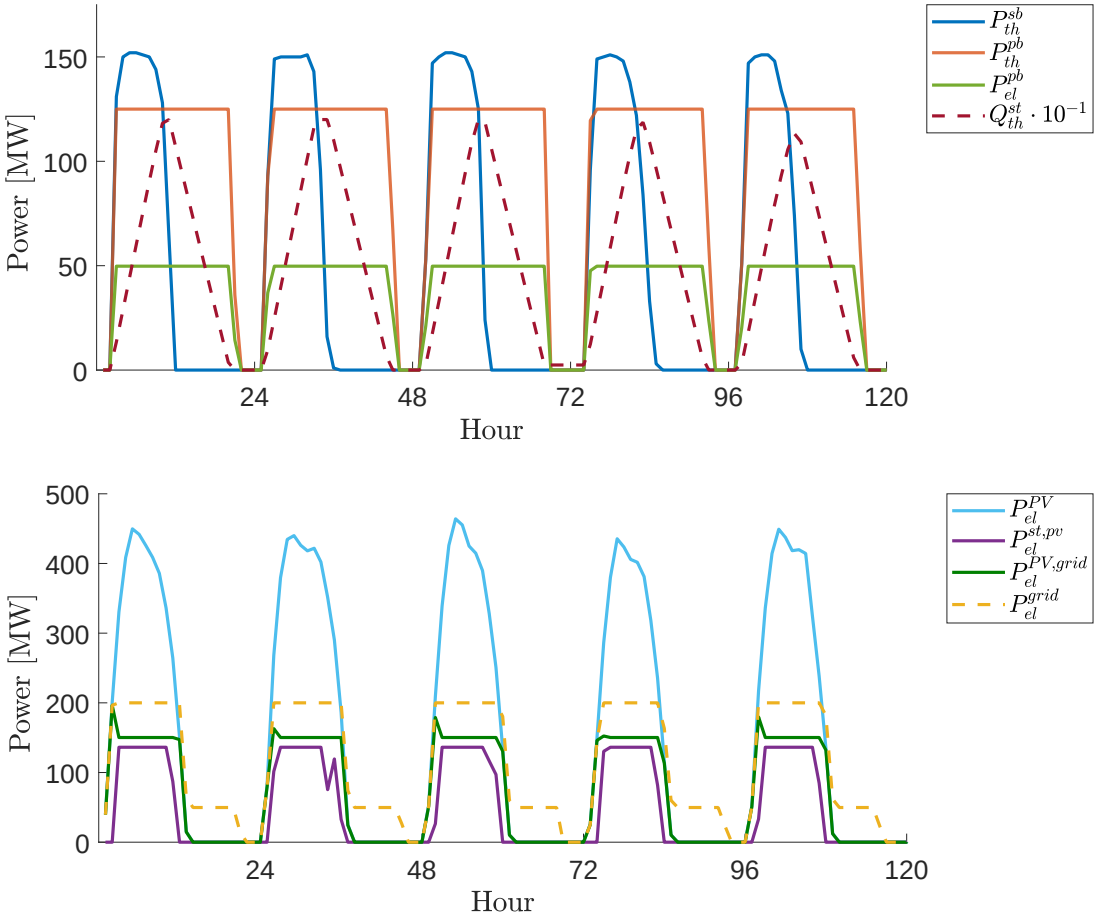

Figure 39: Extended buffer strategy power block output power and storage state (upper), followed by the electric power output (lower) based on the solar block power input and available PV power. A period of 5 days, starting on day 100 at 6 a.m. is depicted.

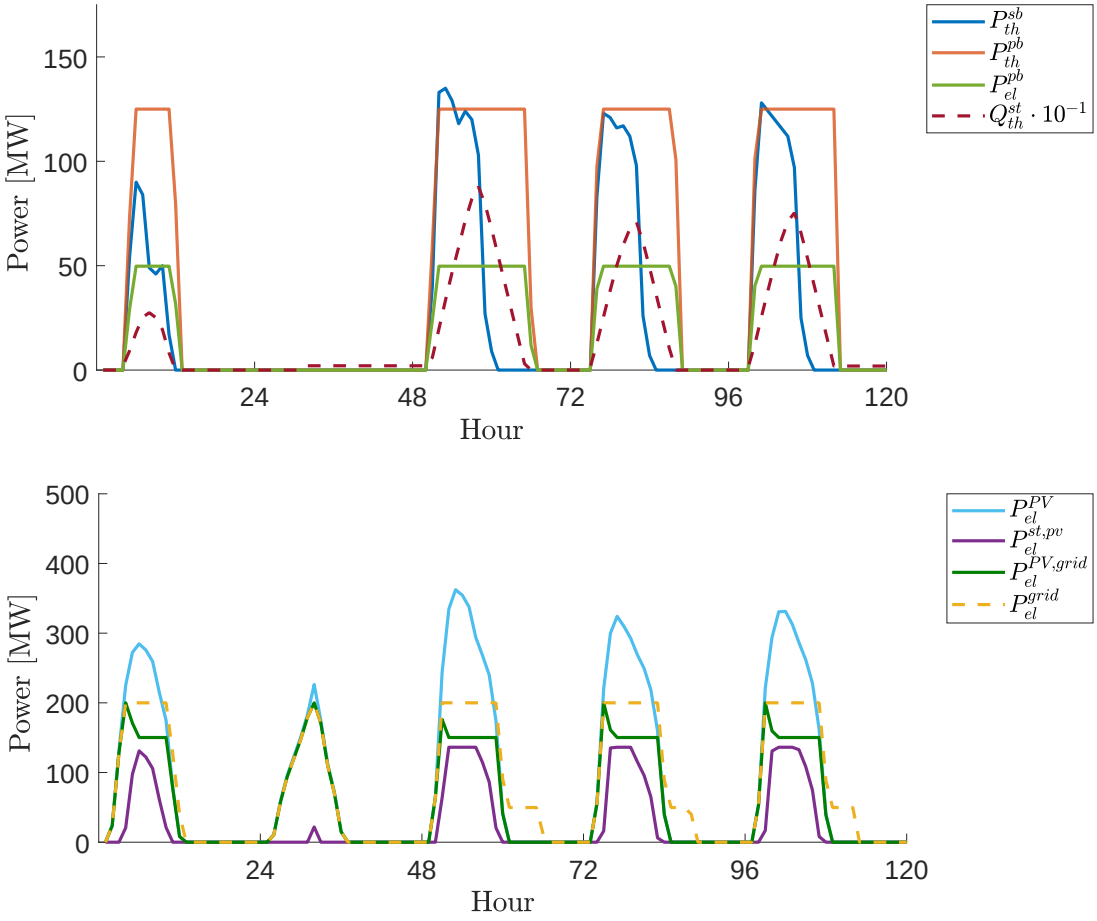

Figure 40: Extended buffer strategy power block output power and storage state (upper), followed by the electric power output (lower) based on the solar block power input and available PV power. A period of 5 days, starting on day 10 at 6 a.m. is depicted.

Model predictive control using Pontraygin's maximum principle Unlike the extended buffer strategy, extended Pontryagin's maximum principle (PMP) on the CSP side has the same behavior as introduced just for the CSP alone. The behavior is dependent on the tariff. During the day, the CSP is mostly used only for storing all the available energy, while PV sends all possible power to the grid. When it exceeds the grid limit, the PV sends the remaining power to the thermal storage. Expectedly, the PMP shifts the production to more profitable times (see Figure 41), however the days with a shortage of power still remain a problem, with not enough energy in the storage to produce the power (see Figure 42).

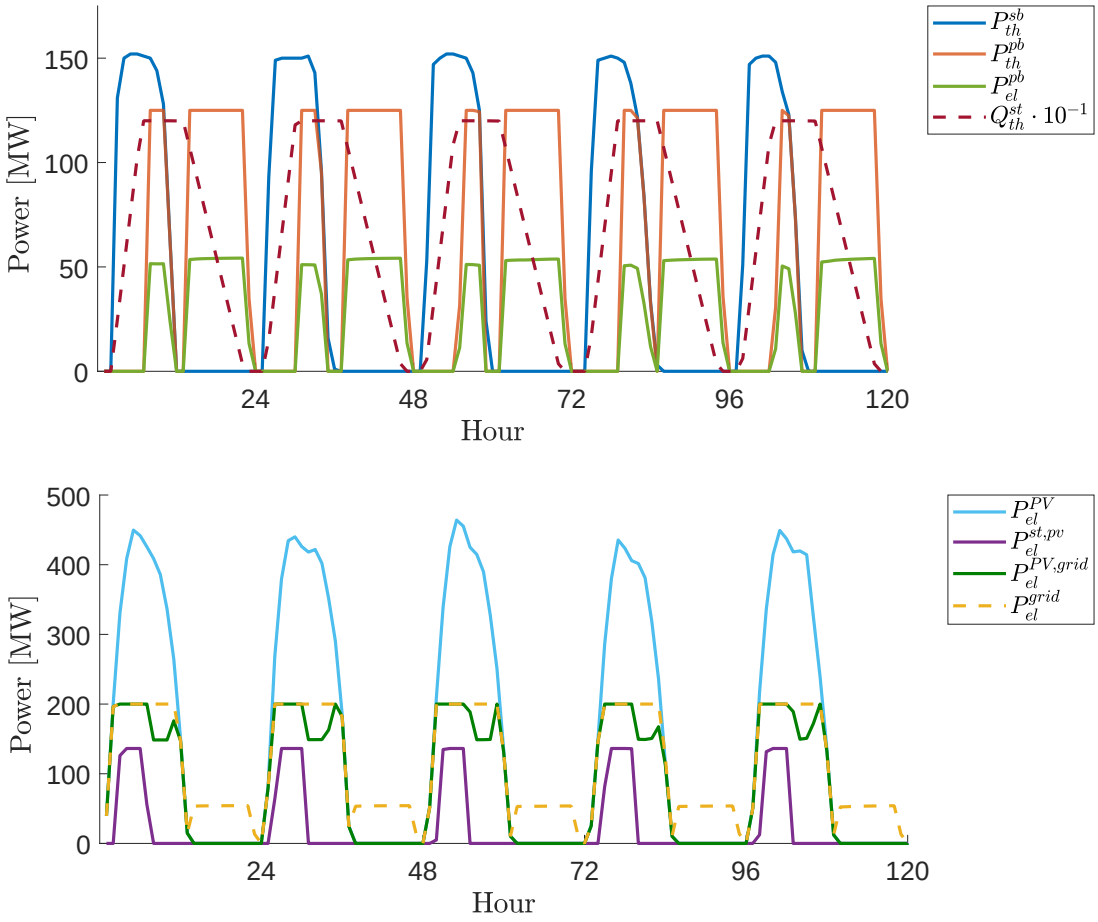

Figure 41: Extended PMP strategy power block output power and storage state (upper), followed by the electric power output (lower) based on the solar block power input and available PV power. A period of 5 days, starting on day 100 at 6 a.m. is depicted.

Another instance when PV would store the power is based on the tariff. However, for that to happen the tariff would need to be lower than the PV price π_{PV} introduced in Section 5. With the two values of tariffs used in this test case this would never happen unless the residual tariff became really high, which would result in the hybrid

plant only trying to store as much energy as possible. A sub-optimal solution indeed.

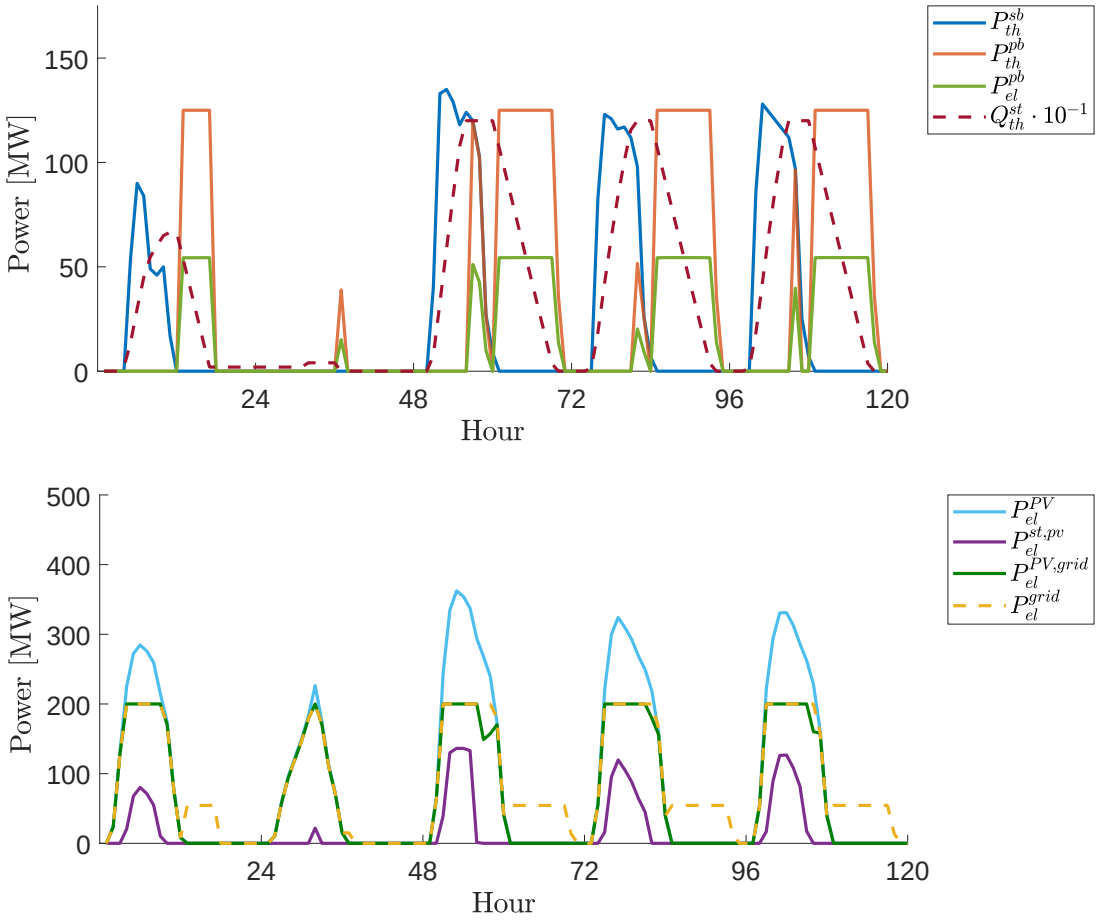

Figure 42: Extended PMP strategy power block output power and storage state (upper), followed by the electric power output (lower) based on the solar block power input and available PV power. A period of 5 days, starting on day 10 at 6 a.m. is depicted.

Model predictive control using Mixed-Integer Linear Programming The MIP solver again achieves a similar result to the PMP, while taking into account the future and not necessarily always putting an emphasis on maximum flows based on the current tariff, as is the case for the PMP.

Comparison Coupled with a PV system, all three strategies perform well and are able to utilize the storage. For the buffer strategy the computation time is again expectedly the lowest. However, as with the CSP buffer strategy, the problem is again that the production is not shifted according to the tariff and thus the revenue remains lower than for the other two strategies.

Since PMP performed well for a set residual tariff and the running time was significantly lower than in the case of defining the starting and final storage fill level, for the hybrid plant, the strategy was run only with the residual in the objective function. For PMP this resulted in lower computational cost, but not necessarily a greater revenue than MIP-MPC as the flows are rather limited by the current tariff and not taking into account the future as much as is the case with the MIP.

Furthermore, the decision on when to store the power from the PV is not as much driven by the current tariff, but rather with the limitation on the power that can be released to the grid from the hybrid plant. Compared to releasing the power directly to the grid with only the power losses caused by the inversion from DC to AC power, storing the power in the thermal storage and then using it later from the CSP introduces losses that are approximately 2.7 times higher. The losses are caused by the conversion from electrical DC to thermal power, and the losses for charging and discharging the storage, followed by the losses in the power block.

The computation time and revenue for the three strategies for the period of one year is given in Table 24.

Extended Strategy	**Computation time** [s]	**Revenue** [M€]
Buffer	5.619	89.9917735
Pontryagin	167.515	95.942417
MIP-MPC	231.943	95.990586

Table 24: Computation time and annual revenue for all three extended strategies for the hybrid CSP-PV plant. In case of Pontryagin's maximum principle and MIP-MPC, the objective function with residual is considered.

6.2.4 Comparison of a CSP and hybrid CSP-PV plant

A comparison of the gain rate for CSP and hybrid CSP-PV plants is done to determine how each of the plants performs. To consider the performance based on all three strategies used in this work, a mean value of revenue was taken for the CSP and hybrid CSP-PV plant. The values were taken from Tables 23 and 24, respectively. The mean value was then multiplied by the amount of years in lifetime period to obtain the total revenue for the lifetime.

The investment costs for each of the plants were taken from Table 18, where only the costs of the CSP solar field and power block were considered for the CSP plant.

The gain rate for each plant is described in Table 25.

Plant	Gain rate
CSP	1.481209
Hybrid CSP-PV	3.059604

Table 25: Gain rate for CSP and hybrid CSP plants, for the lifetime period of 25 years.

When comparing the gain rate between two plant types, combining the CSP and PV plants into a hybrid CSP-PV plant results in a greater gain.

Furthermore, to confirm the better performance of the hybrid CSP-PV plant, the net present value (NPV) is calculated, presented in (17).

The NPV values for both plants are displayed in Table 26.

Plant	Net present value
CSP	122.834491 M€
Hybrid CSP-PV	892.782127 M€

Table 26: Net present value for CSP and hybrid CSP plant.

These results indeed confirm that it is profitable to invest in a hybrid CSP-PV plant for a higher return.

The evaluation was done based on the test case data available for the period of one year.

6.2.5 Hybrid CSP-PV size optimization

To get the most profit out of the plant it is important that its size is set up in the way for it to be able to utilize the CSP field, PV and storage to its fullest potential. Thus, the NPV and gain rate taken from above as measures of plant performance were calculated for different CSP field, PV peak power and storage sizes of the hybrid plant. The costs for the components (see Table 18) are considered to scale linearly. The CSP power block capacity remains constant. The optimal plant configuration was separately calculated for all three strategies, with the initial investment costs from Table 18 considered as fixed. The comparison was done by considering the yearly revenues for the test case plant.

Buffer strategy For the buffer strategy, the maximal net present value, as well as the maximal gain rate, are achieved for the power plant set-up originally presented by the test case. The values of the parameters and evaluation results are presented in Table 27.

The NPV and gain rate depending on the storage size and PV peak power, along with the size of storage depending on the CSP field size and PV peak power are displayed in Figure 43. The storage size increases with the decrease in CSP field size and PV peak power as the total investment costs are fixed.

Pontryagin's maximum principle When using the Pontryagin's maximum principle, the optimal plant configuration favors an increase in PV peak power and storage size, while the CSP field size is decreased. The values of the parameters and evaluation parameters are presented in Table 27.

The NPV and gain rate depending on the storage size and PV peak power, along with the size of storage depending on the CSP field size and PV peak power are displayed in Figure 44.

MIP-MPC For the MIP-MPC, the maximal NPV and gain rate are achieved for the same plant configuration as in the case of Pontryagin's maximum principle. The values of the parameters and evaluation parameters are presented in Table 27.

The NPV and gain rate depending on the storage size and PV peak power, along with the size of storage depending on the CSP field size and PV peak power are displayed in Figure 45.

	Reference plant	**Buffer strategy**	**PMP**	**MIP-MPC**
CSP Solar field	150 MW_{th}	150 MW_{th}	100 MW_{th}	100 MW_{th}
Storage size	1200 $MW_{th}h$	1200 $MW_{th}h$	1500 $MW_{th}h$	1500 $MW_{th}h$
PV peak power	400 MW_{th}	400 MW_{th}	417.333 MW_{th}	417.333 MW_{th}
Yearly revenue	-	89.9917735 M€	95.942417 M€	95.990586 M€
NPV	-	864.467013 M€	967.611929 M€	977.050007 M€
Gain rate	-	2.935043	3.388786	3.430305

Table 27: Comparison of optimal CSP solar field, storage size and PV peak power for different strategies. The plant performance under different strategies and optimal configurations is furthermore compared based on the yearly revenue, net present value and gain rate.

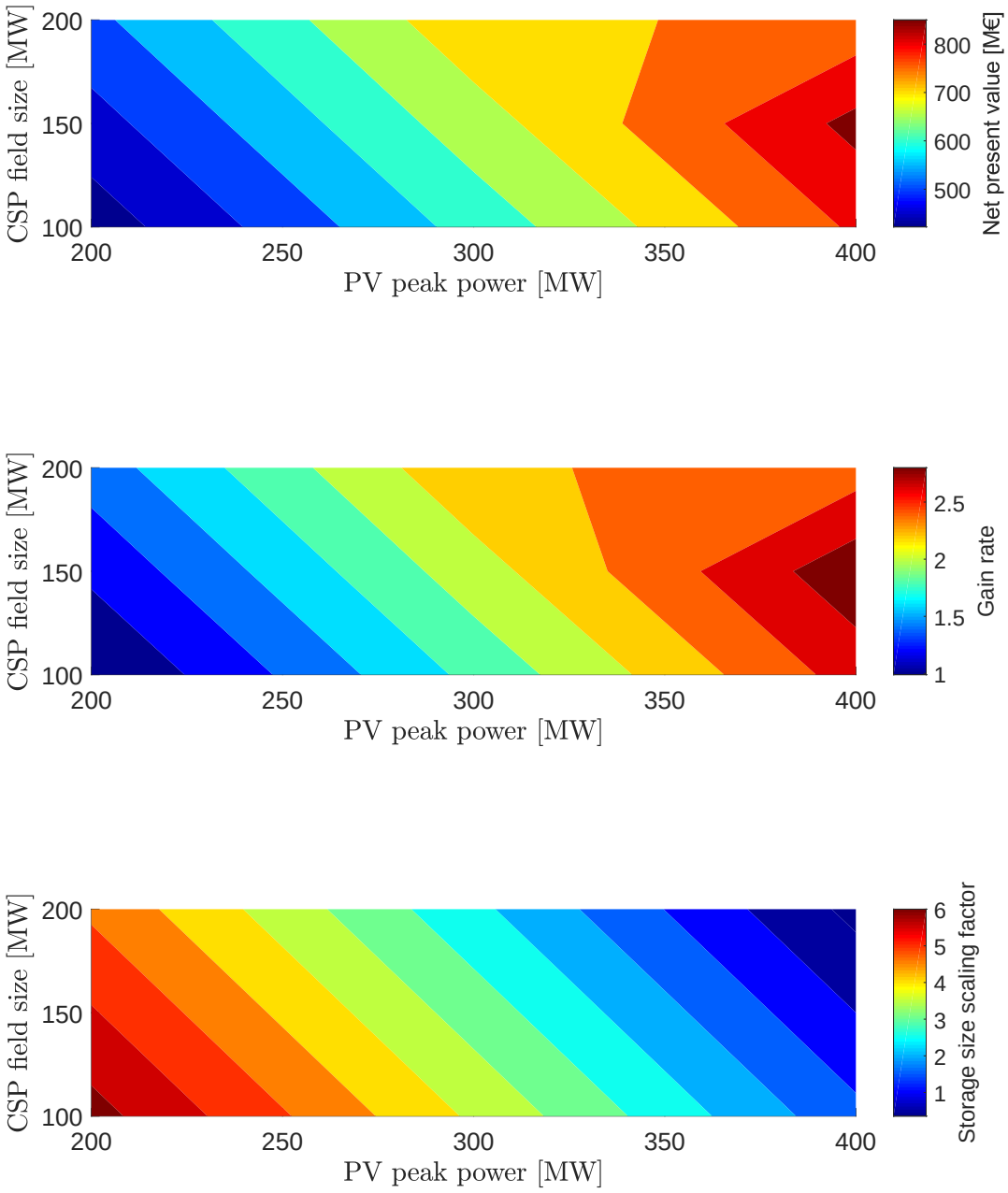

Figure 43: Net present value (top), gain rate (middle) and storage size (bottom) depending on the CSP field size and PV peak power, with buffer strategy as the storage strategy.

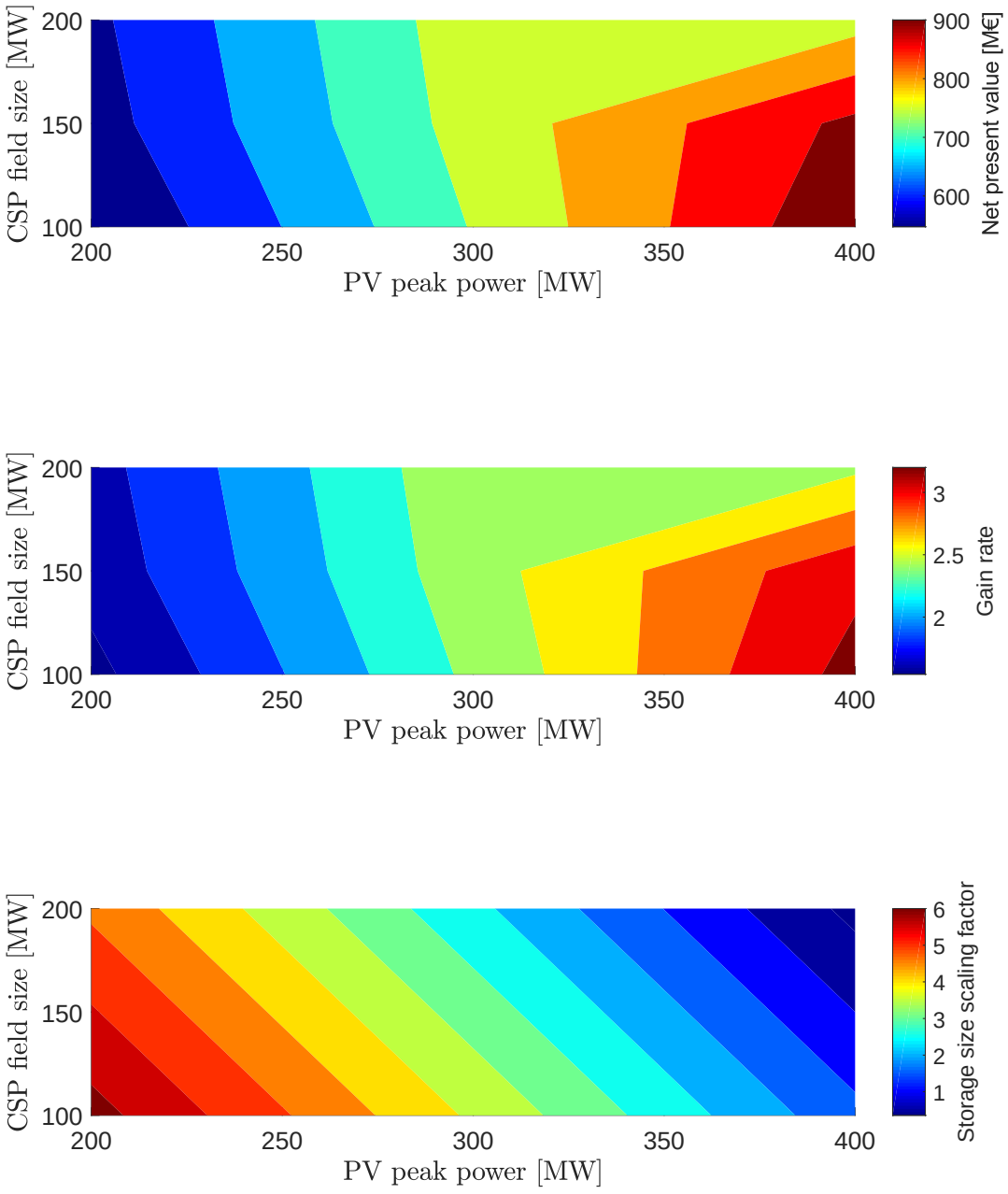

Figure 44: Net present value (top), gain rate (middle) and storage size (bottom) depending on the CSP field size and PV peak power, with PMP as the storage strategy.

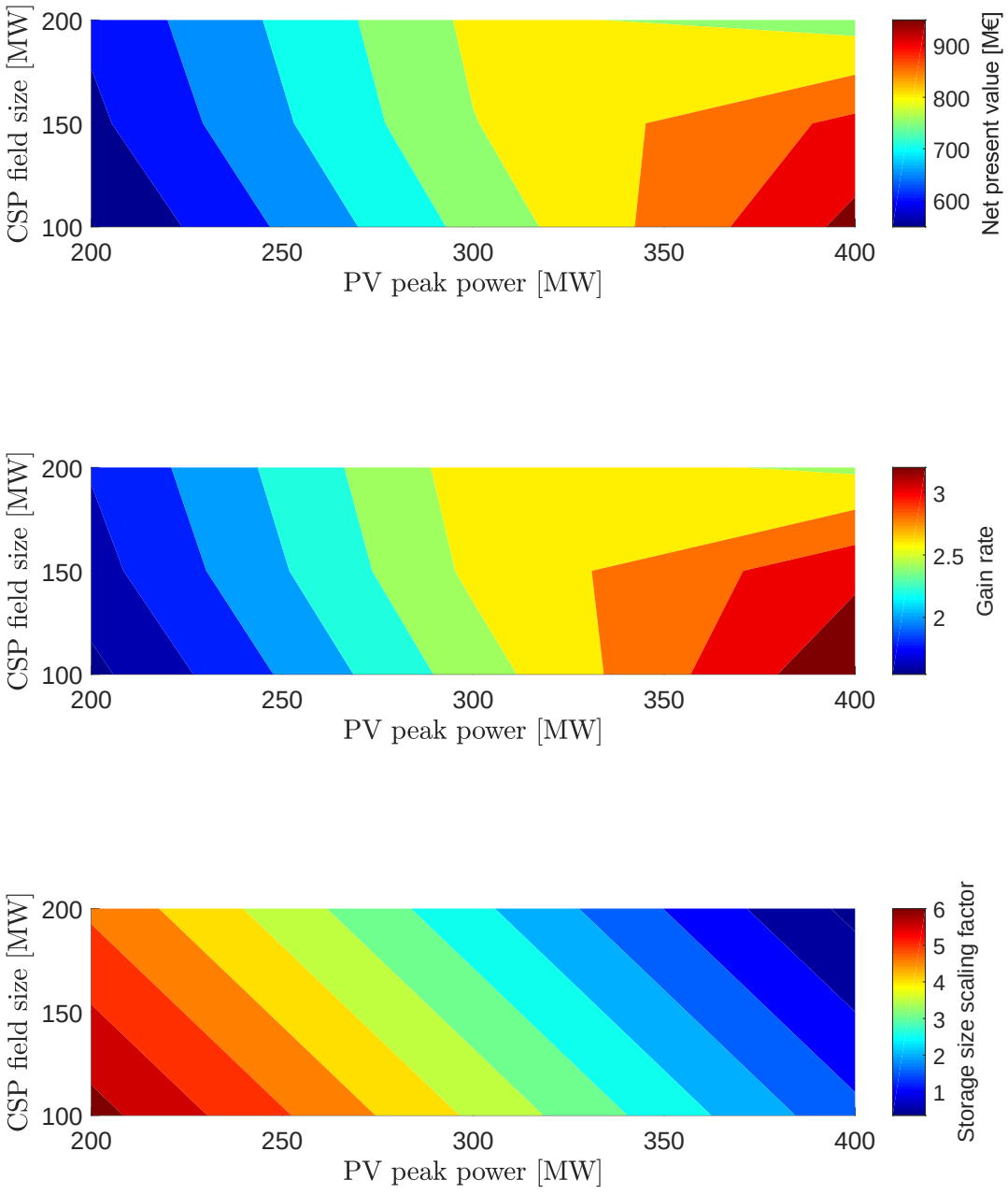

Figure 45: Net present value (top), gain rate (middle) and storage size (bottom) depending on the CSP field size and PV peak power, with MIP-MPC as the storage strategy.

The result in Table 27 confirms that the optimal configuration for the hybrid CSP-PV plant in case of revenue driven strategies (PMP and MIP-MPC) favors an increase in PV peak power and storage, with a decrease in CSP field size. With the tariff driven strategy the CSP is not able to contribute significantly to the power output during the day. On the other hand, an increase in PV peak power results in more energy production during the day, as well as potentially more energy in the storage. Thus, an increase in storage is favored in such a way that additional power can be accommodated. Since the turbine size in the power block stays fixed, it is not profitable to significantly increase the CSP field size.

Furthermore, the result above also demonstrates the significance of optimal storage strategy for plant layout optimization. After all, the storage strategy influences not only the plant revenue, but also the optimal configuration of the plant.

7 Conclusion

As a part of this work a PV plant and a hybrid CSP-PV plant models were introduced. Both models regarded the power flows in the system, with an emphasis on integration of a storage system.

Three different storage strategies were investigated, starting with the CSP plant. Though simple and computationally inexpensive, the buffer strategy, as an energy production maximization strategy, proved to be inefficient for power production during the periods of higher energy tariffs. On the other hand, the model predictive control with Pontryagin's maximum principle and mixed-integer programming successfully shifted the production times based on the tariff. However, this still led to the lack of produced power during the day.

The extended strategies for the hybrid CSP-PV plant model demonstrated a more successful power production both during the periods of higher and lower tariff. An expected result, given that the photovoltaic model would always produce additional energy during the day and, in the case of excess energy, fill the storage.

Considering the revenue and computation times of both strategies, the author of this work recommmends applying the Pontryagin's maximum principle and setting two thresholds for energy production and storage, when a fast computation time is relevant. Though the MIP-MPC regards the future, during the period of 24 hours, it often gives a rather similar power output to that of PMP. On the other hand, for the result of higher accuracy, where the computation time is not of such an importance, the usage of MIP-MPC is highly recommended, with a potentially larger horizon window, such that the shortages of solar power (in sub-optimal weather conditions) might also be accounted for.

When comparing the CSP and hybrid CSP-PV plant, the hybrid plant expectedly performs better. The cause of this result is also the ratio between the CSP field size and turbine size. Namely, the CSP solar field, as is, is rarely large enough to fill the storage during the day. Thus, during the last hours of a higher tariff period no energy is produced. One of the ways to solve this problem would be an increase in CSP field size.

When designing the hybrid CSP-PV plant, a plant design with higher PV peak power and storage generally results in a better plant performance. With a higher PV peak power more power is sent to the grid during the day, with more power potentially available for storing as well.

This work successfully investigated the optimization of strategies with the aim of maximizing the revenue. The resulting solution proves that, in case of a two-value tariff, even focusing just on storing and producing energy based on the tariff threshold is often enough to produce an acceptable solution. That is, storing the power when the tariff is below a fixed threshold and producing it when the tariff is above the threshold for energy production.

7.1 Outlook

Given the results of this work, there are several extensions and improvements to be regarded and implemented in the future.

Power block efficiency The power block efficiency is one of the modeling components that wasn't extensively studied in this work. To keep the models in optimization linear, a constant efficiency was applied. However, this creates a difference between the optimization result and the actual result. Thus, for a more accurate solution, a more precise efficiency approximation, such as the linear, quadratic or even the cubic approximation presented in this work, should be used.

Storage strategies On that note, the storage strategies that use the Pontryagin's maximum principle and mixed-integer programming should accommodate this change, by optimizing a non-linear model. In the case of Pontryagin's maximum principle, the optimal solution would then depend on the controls in the system and not just the current energy production tariff (as is the case for the current bang-bang control). For mixed-integer programming, another solver would be required to solve the non-linear approximation. For this purpose a tool such as APMonitor[5] could be used.

Furthermore, the strategies could be extended to consider other performance parameters than the tariff. Namely, despite the tariff for energy production, the potential amount of power that can be sent to the grid during the night is still less than during the day due to the limit on the power block. One of the ways to improve the general plant performance would be to focus on the energy demand, rather than designing the strategies and the plant (i.e. sizing of the components) with a single goal to maximize the revenue. The household energy demand often varies during the day and the strategy should accommodate this.

Moreover, only a two-value tariff was considered in this work. With an increase in number of different tariffs, the strategies should be modified to accommodate this change. For this purpose, the usage of residual tariff in this work should be reconsidered and an optimal and effective way of finding the price thresholds should be designed.

Weather data The weather data in this work is considered as perfect. To produce results closer to reality, the accuracy of predicted data should also be taken into account.

Hybrid CSP-PV model The hybrid CSP-PV model could be further improved by enabling the PV to draw the power from the thermal storage or increasing power limit on the turbine to increase the possible energy production at times with no sun or a higher tariff.

[5] APMonitor Optimization Suite, `https://apmonitor.com/`

Economic model The economic model could be further extended to consider the costs in more detail than was presented in this work.

References

[1] Eduardo F Camacho and Manuel Berenguel. Control of solar energy systems1. *IFAC Proceedings Volumes*, 45(15):848–855, 2012.

[2] Rafael Guedéz, Davide Ferruzza, Monica Arnaudo, Ivette Rodríguez, Carlos D Perez-Segarra, Zhor Hassar, and Björn Laumert. Techno-economic performance evaluation of solar tower plants with integrated multi-layered pcm thermocline thermal energy storage–a comparative study to conventional two-tank storage systems. In *AIP Conference Proceedings*, volume 1734, page 070012. AIP Publishing, 2016.

[3] Rafael Eduardo Guedez, Monika Topel, J Spelling, and Björn Laumert. Enhancing the profitability of solar tower power plants through thermoeconomic analysis based on multi-objective optimization. In *International Conference on Concentrating Solar Power and Chemical Energy Systems (SolarPACES), SEP 16-19, 2014, Beijing, PEOPLES R CHINA*, volume 69, pages 1277–1286, 2015.

[4] Sarada Kuravi, Jamie Trahan, D Yogi Goswami, Muhammad M Rahman, and Elias K Stefanakos. Thermal energy storage technologies and systems for concentrating solar power plants. *Progress in Energy and Combustion Science*, 39(4): 285–319, 2013.

[5] Luigi Rocco Cirocco, Martin Belusko, Frank Bruno, John Boland, and Peter Pudney. Maximising revenue via optimal control of a concentrating solar thermal power plant with limited storage capacity. *IET Renewable Power Generation*, 10 (5):729–734, 2016.

[6] Kody M Powell and Thomas F Edgar. Modeling and control of a solar thermal power plant with thermal energy storage. *Chemical Engineering Science*, 71:138–145, 2012.

[7] Gregor Heiming. Development of a techno-economic model for solar tower power plants. Master's thesis, MathCCES - RWTH Aachen, gregor.heiming@rwth-aachen.de, 11 2017.

[8] G Morin. Optimisation of concentrating solar power (csp) plant designs through integrated techno-economic modelling. In *Concentrating Solar Power Technology*, pages 495–535. Elsevier, 2012.

[9] Scott M Flueckiger, Brian D Iverson, and Suresh V Garimella. Economic optimization of a concentrating solar power plant with molten-salt thermocline storage. *Journal of Solar Energy Engineering*, 136(1):011015, 2014.

[10] K Nithyanandam and R Pitchumani. Cost and performance analysis of concentrating solar power systems with integrated latent thermal energy storage. *Energy*, 64:793–810, 2014.

[11] Luigi R Cirocco, Martin Belusko, Frank Bruno, John Boland, and Peter Pudney. Controlling stored energy in a concentrating solar thermal power plant to maximise revenue. *IET Renewable Power Generation*, 9(4):379–388, 2015.

[12] Rafael Guédez, James Spelling, Björn Laumert, and Torsten Fransson. Optimization of thermal energy storage integration strategies for peak power production by concentrating solar power plants. *Energy Procedia*, 49:1642–1651, 2014.

[13] J Usaola. Operation of concentrating solar power plants with storage in spot electricity markets. *IET renewable power generation*, 6(1):59–66, 2012.

[14] Francesco Casella, Emiliano Casati, and Piero Colonna. Optimal operation of solar tower plants with thermal storage for system design. *IFAC Proceedings Volumes*, 47(3):4972–4978, 2014.

[15] Michael Wittmann, Markus Eck, Robert Pitz-Paal, and Hans Müller-Steinhagen. Methodology for optimized operation strategies of solar thermal power plants with integrated heat storage. *Solar Energy*, 85(4):653–659, 2011.

[16] Eduardo F Camacho, Manuel Berenguel, and Antonio J Gallego. Control of thermal solar energy plants. *Journal of process control*, 24(2):332–340, 2014.

[17] Eduardo F Camacho and Antonio J Gallego. Model predictive control in solar trough plants: a review. *IFAC-PapersOnLine*, 48(23):278–285, 2015.

[18] Manuel Jesús Vasallo and José Manuel Bravo. A mpc approach for optimal generation scheduling in csp plants. *Applied Energy*, 165:357–370, 2016.

[19] Federico Dominio. Techno-economic analysis of hybrid pv-csp power plants. advantages and disadvantages of intermediate and peak load operation. Master's thesis, Universitat Politècnica de Catalunya, 2014.

[20] Rongrong Zhai, Ying Chen, Hongtao Liu, Hao Wu, and Yongping Yang. Optimal design method of a hybrid csp-pv plant based on genetic algorithm considering the operation strategy. *International Journal of Photoenergy*, 2018, 2018.

[21] Nils Ahlbrink, Boris Belhomme, Robert Flesch, Daniel Maldonado Quinto, Amadeus Rong, and Peter Schwarzbözl. Stral: Fast ray tracing software with tool coupling capabilities for high-precision simulations of solar thermal power plants. In *Proceedings of the SolarPACES 2012 conference*, 2012.

[22] Ioan Sarbu and Calin Sebarchievici. A comprehensive review of thermal energy storage. *Sustainability*, 10(1):191, 2018.

[23] Germain Augsburger. Thermo-economic optimisation of large solar tower power plants. 2013.

[24] Arthur Richards and Jonathan How. Mixed-integer programming for control. In *American Control Conference, 2005. Proceedings of the 2005*, pages 2676–2683. IEEE, 2005.

[25] Dennis Atabay. *Comparison of optimization methods for model predictive control: An application to a compressed air energy storage system.* PhD thesis, Technische Universität München, 2018.

[26] Donald E Kirk. *Optimal control theory: an introduction.* Courier Corporation, 2012.

[27] Richard F Hartl, Suresh P Sethi, and Raymond G Vickson. A survey of the maximum principles for optimal control problems with state constraints. *SIAM review*, 37(2):181–218, 1995.

[28] Zou Yuan, Liu Teng, Sun Fengchun, and Huei Peng. Comparative study of dynamic programming and pontryagin's minimum principle on energy management for a parallel hybrid electric vehicle. *Energies*, 6(4):2305–2318, 2013.

[29] L Bayón, JM Grau, MM Ruiz, and PM Suárez. An algorithm for bang–bang control of fixed-head hydroplants. *International Journal of Computer Mathematics*, 88(9):1949–1959, 2011.

[30] Ryozo Ooka and Shintaro Ikeda. A review on optimization techniques for active thermal energy storage control. *Energy and Buildings*, 106:225–233, 2015.

[31] Bhubaneswari Parida, S_ Iniyan, and Ranko Goic. A review of solar photovoltaic technologies. *Renewable and sustainable energy reviews*, 15(3):1625–1636, 2011.

[32] John A Duffie and William A Beckman. *Solar engineering of thermal processes.* John Wiley & Sons, 2013.

[33] Gilbert M Masters. *Renewable and efficient electric power systems.* John Wiley & Sons, 2013.

[34] C Parrado, A Girard, F Simon, and E Fuentealba. 2050 lcoe (levelized cost of energy) projection for a hybrid pv (photovoltaic)-csp (concentrated solar power) plant in the atacama desert, chile. *Energy*, 94:422–430, 2016.